

HYGROTHERMAL EFFECTS
ON COMPLEX MODULI OF COMPOSITE LAMINATES

BY

HACENE BOUADI

A DISSERTATION PRESENTED TO THE GRADUATE SCHOOL
OF THE UNIVERSITY OF FLORIDA IN
PARTIAL FULFILLMENT OF THE REQUIREMENTS
FOR THE DEGREE OF DOCTOR OF PHILOSOPHY

UNIVERSITY OF FLORIDA

1988

ACKNOWLEDGEMENTS

I would like to express my gratitude to Professor Chang-T. Sun, the chairman of my doctoral committee, for his guidance, time, and encouragement during this research.

Many thanks are owed to Professor Lawrence E. Malvern and Professor Martin A. Eisenberg for their teaching and financial support.

I also want to thank the other members of my doctoral committee, Dr. Charles E. Taylor and Dr. Robert E. Reed-Hill for their helpful comments, critique, and advice.

In addition, I gratefully recognize the assistance of Dr. David A. Jenkins for teaching me how to operate the material testing equipment that was indispensable for my work.

Finally, I appreciate Ms. Patricia Campbell's help in typing this manuscript.

TABLE OF CONTENTS

	<u>Page</u>
ACKNOWLEDGEMENTS	ii
LIST OF TABLES	vi
LIST OF FIGURES	vii
NOMENCLATURE	xiii
ABSTRACT	xvi
 CHAPTERS	
1 INTRODUCTION	1
1.1 General Introduction	1
1.2 Moisture Diffusion	2
1.3 Hygrothermal Effects.	2
1.4 Scope and Methodology	3
1.5 Dissertation Lay-Out	4
2 DIFFUSION OF MOISTURE	6
2.1 Introduction	6
2.2 Fickian Diffusion	6
2.3 Fickian Absorption in a Plate	8
2.3.1 Infinite Plate	8
2.3.2 Semi-Infinite Plate	10
2.3.3 Experimental Measurement of Moisture Content	11
2.3.4 Approximate Solutions of Moisture Content.	12
2.3.5 Edge Effects Corrections in a Finite Laminated Plate	13
2.4 Diffusivity and Maximum Moisture Content	15
3 COMPLEX MODULI OF UNIDIRECTIONAL COMPOSITES	21
3.1 Introduction	21
3.2 General Theory	21
3.3 Micromechanics Formulation of elastic Moduli	22
3.4 Complex Moduli	23

4	DAMPING	29
4.1	Damping Mechanisms	29
4.1.1	Nonmaterial Damping	29
4.1.2	Material Damping	30
4.2	Characterization of Damping	30
4.2.1	Free Vibration	30
4.2.2	Steady State Vibration	31
4.2.3	Complex Modulus Approach	32
5	DAMPING AND STIFFNESSES OF GENERAL LAMINATES . .	36
5.1	Introduction	36
5.2	Laminated Plate Theory Approach	36
5.3	Energy Method Approach	37
6	EXPERIMENTAL PROCEDURES	40
6.1	Introduction	40
6.2	Test Specimen	40
6.3	Environmental Conditioning	41
6.4	Four-Point Flexure Test Method	41
6.5	Impulse Hammer Technique	42
7	HYGROTHERMAL EXPANSION	48
7.1	Introduction	48
7.2	Coefficients of Thermal Expansion	49
7.3	Coefficients of Moisture Expansion	50
7.4	Experimental Data	51
7.4.1	Previous Investigations	51
7.4.2	Present Investigation	52
8	HYGROTHERMAL EFFECTS ON COMPOSITE COMPLEX MODULI	58
8.1	Literature Survey	58
8.2	Theoretical and Experimental Assumptions. . .	59
8.3	Modeling of Epoxy Properties	61
8.4	Results	63
8.4.1	Epoxy Complex Moduli	63
8.4.2	Composite Complex Moduli	65
9	HYGROTHERMAL EFFECTS ON STRESS FIELD	79
9.1	Introduction	79
9.2	Description of Study Cases	80
9.3	Numerical Results and Discussion	81
9.3.1	Glass/Epoxy	81
9.3.2	Graphite/Epoxy	82
9.3.3	Summary	82

10	HYGROTHERMAL EFFECTS ON COMPLEX STIFFNESSES . . .	95
10.1	Introduction	95
10.2	Numerical Results and Discussion	95
10.2.1	Glass/Epoxy	95
10.2.2	Graphite/Epoxy.	96
10.2.3	Summary	97
11	CONCLUSION	111
APPENDICES		
A	COMPLEX STIFFNESSES OF COMPOSITES	115
A.1	Elastic Stiffnesses	115
A.2	Complex Stiffnesses	117
B	DEVELOPMENT OF THE FINITE ELEMENT METHOD	119
B.1	Equilibrium Equations	119
B.2	Program Organization	122
B.3	Shape Functions, Jacobian and Strain Matrix	123
B.4	Elasticity Matrix	125
B.5	Element stiffness Matrix	128
B.6	Equivalent Nodal Loadings	128
B.6.1	Element Edge Loadings	128
B.6.2	Hygrothermal Loadings	129
B.7	Element Stresses	130
REFERENCES		133
BIOGRAPHICAL SKETCH		137

LIST OF TABLES

<u>Tables</u>	<u>Page</u>
6.1 Initial properties of Magnolia 2026 epoxy, 3M Scotchply Glass/Epoxy, and a typical Graphite/epoxy composite.	45
7.1 Coefficients of moisture and thermal expansion of epoxy and graphite and glass fibers.	54
7.2 Properties of Glass and Graphite Fibers . . .	54
9.1 Description of cases in Figure 9.2.	84
9.2 Typical strengths of Glass/Epoxy and Graphite/Epoxy.	84

LIST OF FIGURES

<u>Figures</u>		<u>Page</u>
2.1	Plate subjected to a constant humid. environment on both sides.	18
2.2	Moisture distribution across a plate. The numbers on the curves are the values of $(\bar{c} - c_i)/(c_\infty - c_i)$	18
2.3	Semi-infinite plate in a humid environment.	19
2.4	Comparison of the exact specific moisture concentration equation with some approximate solutions.	19
2.5	Geometry of a plate.	20
2.6	Moisture content versus square root of time. On the curve $\sqrt{t_1} < \sqrt{t_2} < \sqrt{t_L}$ and the slope is constant for $\sqrt{t} < \sqrt{t_L}$	20
4.1	Schematic drawing of a free-clamped beam under free vibration and plot of its deflection versus time.	35
4.2	Schematic drawing of a free-clamped beam under forced vibration and plots of the deflection versus time and deflection amplitude versus frequency.	35
6.1	Schematic drawing of environmental and testing chambers.	46
6.2	Loading configuration of the 4-point flexure test.	46

6.3	Schematic drawing of the impulse hammer technique apparatus and a typical display of the Fourier Transform.	47
7.1	Transverse moisture strain of Magnolia epoxy and 3M Scotchply Glass/Epoxy.	55
7.2	Plot of the thermal expansion coefficients in terms of fiber volume fraction of a dry S Glassfiber/Epoxy at 20°C.	56
7.3	Plot of the thermal expansion coefficients in terms of fiber volume fraction of a dry Graphite/Epoxy at 20°C.	56
7.4	Plot of the moisture expansion coefficients in terms of fiber volume fraction of a dry S Glassfiber/Epoxy at 20°C.	57
7.5	Plot of the moisture expansion coefficients in terms of fiber volume fraction of a dry Graphite/Epoxy at 20°C.	57
8.1	Schematic variation of the storage modulus of epoxy with temperature.	67
8.2	Schematic variation of Poisson's ratio of epoxy with temperature.	67
8.3	Schematic variation of damping of epoxy with temperature.	68
8.4	Glass transition temperature of epoxy. From Delasi and Whiteside [6].	68
8.5	Experimental data of the storage modulus of epoxy as a function of temperature at diverse constant moisture contents	69
8.6	Experimental data of the storage modulus of epoxy as a function of moisture content at diverse constant temperatures	69
8.7	Experimental data of the storage modulus of epoxy as a function of normalized temperature $(T - T_o)/(T_g - T_o)$	70
8.8	Experimental data of damping of epoxy as a function of temperature at diverse constant moisture contents	71

8.9	Experimental data of damping of epoxy as a function of moisture content at diverse constant temperatures	71
8.10	Experimental data of the storage modulus of epoxy as a function of normalized temperature $(T - T_o)/(T_g - T_o)$	72
8.11	Experimental data of Poisson's ratio of epoxy in term of temperature.	73
8.12	Experimental data of Poisson's ratio of epoxy in term of moisture content.	73
8.13	Experimental data of Poisson's ratio in term of the normalized temperature $T_n = (T - T_o)/(T_g - T_o)$	74
8.14	Longitudinal storage modulus (E'_{11}) of Glass/Epoxy versus $T_n = (T - T_o)/(T_g - T_o)$. . .	75
8.15	Transverse (E'_{22}) and shear (G'_{12}) storage moduli of Glass/epoxy versus $T_n = (T - T_o)/(T_g - T_o)$	75
8.16	Longitudinal (η_{11}), transverse (η_{22}), and shear (η_G) damping of Glass/Epoxy versus $T_n = (T - T_o)/(T_g - T_o)$	76
8.17	Poisson's ratio (ν'_{12}) of Glass/Epoxy versus $T_n = (T - T_o)/(T_g - T_o)$	76
8.18	Longitudinal storage modulus (E'_{11}) of Graphite/Epoxy versus $T_n = (T - T_o)/(T_g - T_o)$	77
8.19	Transverse (E'_{22}) and shear (G'_{12}) storage moduli of Graphite/epoxy versus $T_n = (T - T_o)/(T_g - T_o)$	77
8.20	Longitudinal (η_{11}), transverse (η_{22}), and shear (η_G) damping of Graphite/Epoxy versus $T_n = (T - T_o)/(T_g - T_o)$	78

8.21	Poisson's ratio (ν'_{12}) of Graphite/Epoxy versus $T_n = (T - T_o)/(T_g - T_o)$	78
9.1	Geometry of a laminate and finite mesh of a 1/4 cross-section area.	85
9.2	Description of the applied moisture gradients.	86
9.3	Profile of the hygrothermal stress σ_y across a $[(90/0)_2]_s$ Glass/Epoxy laminate at $y/b = 0.472$	87
9.4	Profile of the hygrothermal stress σ_z across a $[(90/0)_2]_s$ Glass/Epoxy laminate at $y/b = 0.472$	88
9.5	Profile of the hygrothermal stress σ_x across a $[(90/0)_2]_s$ Glass/Epoxy laminate at $y/b = 0.472$	89
9.6	Profile of the hygrothermal stress σ_{yz} across a $[(90/0)_2]_s$ Glass/Epoxy laminate at $y/b = 0.993$	90
9.7	Profile of the hygrothermal stress σ_y across a $[(90/0)_2]_s$ Graphite/Epoxy laminate at $y/b = 0.472$	91
9.8	Profile of the hygrothermal stress σ_z across a $[(90/0)_2]_s$ Graphite/Epoxy laminate at $y/b = 0.472$	92
9.9	Profile of the hygrothermal stress σ_x across a $[(90/0)_2]_s$ Graphite/Epoxy laminate at $y/b = 0.472$	93
9.10	Profile of the hygrothermal stress σ_{yz} across a $[(90/0)_2]_s$ Graphite/Epoxy laminate at $y/b = 0.993$	94
10.1	Line style legend of Figures 10.2-13.	98

10.2	Complex in-plane stiffness A_{11}^* of Glass/Epoxy. a) Non-dimensional Real part; b) corresponding damping.	99
10.3	Complex in-plane stiffness A_{12}^* of Glass/Epoxy. a) Non-dimensional Real part; b) corresponding damping.	100
10.4	Complex in-plane stiffness A_{66}^* of Glass/Epoxy. a) Non-dimensional Real part; b) corresponding damping.	101
10.5	Complex bending stiffness D_{11}^* of Glass/Epoxy. a) Non-dimensional Real part; b) corresponding damping.	102
10.6	Complex bending stiffness D_{12}^* of Glass/Epoxy. a) Non-dimensional Real part; b) corresponding damping.	103
10.7	Complex bending stiffness D_{66}^* of Glass/Epoxy. a) Non-dimensional Real part; b) corresponding damping.	104
10.8	Complex in-plane stiffness A_{11}^* of Graphite/Epoxy. a) Non-dimensional Real part; b) corresponding damping.	105
10.9	Complex in-plane stiffness A_{12}^* of Graphite/Epoxy. a) Non-dimensional Real part; b) corresponding damping.	106
10.10	Complex in-plane stiffness A_{66}^* of Graphite/Epoxy. a) Non-dimensional Real part; b) corresponding damping.	107
10.11	Complex bending stiffness D_{11}^* of Graphite/Epoxy. a) Non-dimensional Real part; b) corresponding damping.	108

10.12	Complex bending stiffness D_{12}^* of Graphite/Epoxy.	
	a) Non-dimensional Real part;	
	b) corresponding damping.	109
10.13	Complex bending stiffness D_{66}^* of Graphite/Epoxy.	
	a) Non-dimensional Real part;	
	b) corresponding damping.	110
B.1	Organization of the F.E.M. program.	131
B.2	Local axes ξ and η , Gauss point numbers and local node numbers of an eight-node isoparametric element.	132

NOMENCLATURE

A_{ij}^*	complex in-plane stiffness.
B_{ij}^*	complex coupling stiffness
B^*	complex modulus
B'	storage modulus
B''	loss modulus
c	moisture concentration
\bar{c}	average specific moisture
c_∞	equilibrium moisture concentration
C_v	specific heat
D_{ij}^*	complex bending stiffness
D_x, D_{xx}	moisture diffusivities
$[D]$	diffusivity matrix, elasticity matrix
E_{11}	longitudinal Young modulus
E_{22}	transverse Young modulus
G_{12}	in-plane shear modulus
K_x	thermal conductivity
m	weight of absorbed moisture
M	percent moisture content

M_i	initial percent moisture content
M_∞	equilibrium percent moisture content
\bar{Q}_{ij}	transformed stiffness
\bar{Q}_{ij}^*	complex transformed stiffness
s	specific gravity
t	time
T	temperature
v_f	fiber volume fraction
v_m	matrix volume fraction
w	weight
α_i	coefficient of thermal expansion
β_i	coefficient of moisture expansion
ϵ	strain
η	damping or loss factor
ν_{12}	major Poisson's ratio
θ_j	fiber orientation of j-th layer
ρ	density
σ	stress

Subscripts

1, 2, 3	principal directions of the fibers
f	fiber
i	initial
j	layer number

L	longitudinal direction
m	matrix
x, y, z	Cartesian coordinates
∞	maximum or equilibrium

Superscripts

H	moisture
o	initial
T	transpose, thermal
*	complex value
'	real part
"	imaginary part

Abstract of Dissertation Presented to the Graduate School
of the University of Florida in Partial Fulfillment
of the Requirements for the Degree of Doctor of Philosophy

HYGROTHERMAL EFFECTS
ON THE COMPLEX MODULI OF COMPOSITE LAMINATES

By

Hacene Bouadi

April 1988

Chairman: Dr. Chang-T. Sun

Major Department: Engineering Sciences

The effects of absorbed moisture and temperature on the complex moduli of composite laminates are investigated and the mechanisms of moisture diffusion in a lamina are also analyzed.

First, the variation of the complex moduli of epoxy in terms of temperature and moisture content are experimentally determined. Then, the hygrothermal effects on the complex moduli of composites are derived by using the complex moduli of the matrix, micromechanical formulas and experimental data. Only the hygrothermal effects on the complex moduli of pure epoxy need to be experimentally determined since these effects on the fibers' properties are negligible.

In addition, the effects of hygrothermal environment on the stress field and material damping of general laminated composite plates are analyzed. It is shown that hygrothermal stresses induced directly by moisture and indirectly by material property changes can be very high, but the effects on damping are less pronounced.

CHAPTER 1 INTRODUCTION

1.1 General Introduction

The introduction of advanced composites in aerospace applications has led to an extensive study of their mechanical behavior. The amount of experimental and theoretical findings of composite material researchers made during the 1960's was so vast that Broutman and Krock [1] needed eight volumes to edit a summary of the resulting knowledge.

The interest in composite materials arose from their ideal characteristics for aerospace structures. Replacement of the commonly used aircraft material, aluminum, by high strength/density ratio and versatile composites can lead to a theoretical 60% weight reduction [2, p. 22]. Due to such benefits, lower costs and better understanding of their mechanisms, the use of composite materials has been increasing slowly but steadily.

Exposure of aircraft structures to high temperature and humidity in the environment and the tendency of composites to absorb moisture gave rise to concern about their performances under adverse operating conditions.

Therefore, considerable work has been done to understand the effects of hygrothermal environment on the mechanical behavior of composite materials.

1.2 Moisture Diffusion

In a 1967 study on the effects of water on glass reinforced composites, Fried hypothesized that water can penetrate the resin phase by two general processes, by diffusion through the resin and by capillary or Poiseuille type of flow through cracks and pinholes [3]. But no mathematical theory was presented. Later, investigators established that the primary mechanism for the transfer of moisture through composites is a diffusion process and adapted the general theory of mass diffusion in a solid medium to moisture diffusion in composite materials. The transfer of moisture through cracks is a secondary effect [4, 5]. Experimental data indicate that for most composite materials, the diffusion of moisture can be adequately described by a concentration dependent form of Fick's law [4-10].

1.3 Hygrothermal Effects

The degradation of mechanical properties of glass reinforced plastics exposed to water has long been

recognized by marine engineers who use "wet" strengths in the design of naval structures [3]. Requirements in aircraft structures are more stringent. The mechanical properties of materials used in aerospace applications must be completely characterized. Therefore, the effects of hygrothermal environment on the elastic, dynamic, and viscoelastic responses of composites have been studied. To date, the effects of moisture and/or temperature on the following performances have been investigated: tensile strength, shear strength, elastic moduli [3, 11-14], fatigue behavior [15-17], creep, relaxation, viscoelastic responses [18-20], dimensional changes [21], dynamic behavior [22], glass transition temperature [23], etc.

Only tensile and shear strengths and elastic moduli have been thoroughly studied by many researchers. But data on the other properties are more limited and hence inadequate to constitute a good design data-base.

1.4 Scope and Methodology

The present investigation is a combined theoretical and experimental work and is concerned with predicting the hygrothermal effects (below the glass transition temperature) on the complex moduli of composite materials.

This program is undertaken by carrying out the following steps:

i) The complex moduli of epoxy matrix in terms of temperature and moisture concentration are obtained by using experimental tests and theoretical expressions.

ii) The effects of temperature and moisture on the complex moduli of unidirectional composites can be derived by using the complex moduli of the matrix, micromechanics formulas, and experimental observations. In addition, we neglect the hygrothermal effects on the fibers.

iii) The effects of hygrothermal conditions on the stress field and the material damping of some general laminated composite plates undergoing simple hygrothermal loadings are analysed.

1.5 Dissertation Lay-Out

Right after the introduction, the mechanism of moisture diffusion is described in Chapter 2, where the absorption of moisture through thin composite laminae is analyzed in detail.

The complex moduli of unidirectional composites are defined in Chapter 3. Sections 3.3 and 3.4 give the micromechanics formulations of the elastic and complex moduli in terms of the constituent material properties. The damping of composites based on the dynamic and complex modulus approaches is characterized and the equivalence of both approaches is proven in Chapter 4. In Chapter 5, the damping and complex stiffnesses of general laminates are

derived by using the laminated plate theory, the energy approach, and the preceding derivations. The complex stiffnesses are completely expressed in Appendix A.

The environmental conditioning of the test specimens, the static flexure test, and the impulse hammer techniques are presented in Chapter 6. These experimental methods, although simple, are very versatile and are adequate in determining the necessary data for the purpose of this investigation.

The theoretical and experimental results are given in Chapters 7-10. The moisture and thermal expansions of composites are quantified in Chapter 7. The current experimental results and data and conclusions of previous investigators are used in Chapter 8 to model the complex moduli of epoxy as functions of temperature and moisture content. In Chapters 9 and 10, the hygrothermal effects on the stress field across laminates and on damping of composites are investigated with the help of the results in the preceding Chapters. The Finite Element Method (F.E.M.) used in determining the stresses is summarized in Appendix B.

CHAPTER 2 DIFFUSION OF MOISTURE

2.1 Introduction

The mechanism of moisture absorption and desorption in most fiber reinforced composites is adequately described by Fick's law [4]. Fick recognized that heat transfer by conduction is analogous to the diffusion process. Therefore, he adopted a mathematical formulation similar to Fourier's heat equation to quantify the diffusion process [24, 25].

2.2 Fickian Diffusion

The Fourier and Fick's equations, describing the one-dimensional temperature and moisture concentration, are respectively given by

$$\rho C_v \frac{\partial T}{\partial t} = \frac{\partial}{\partial x} \left[K_x \frac{\partial T}{\partial x} \right] \quad (2.1)$$

$$\frac{\partial c}{\partial t} = \frac{\partial}{\partial x} \left[D_x \frac{\partial c}{\partial x} \right] \quad (2.2)$$

where ρ is the density of the material, C_v is the

specific heat, T is the temperature, t and x are the time and spatial coordinates, respectively, K_x is the thermal conductivity, c is the moisture concentration, and D_x is the moisture diffusivity.

The moisture diffusivity, D_x , and the thermal diffusivity, $K_x/(\rho C_v)$, are the rate of change of the moisture concentration and the temperature, respectively. In general, both parameters depend on temperature and moisture concentration. But experimental data show that, for most composites, moisture diffusivity does not depend strongly on moisture concentration [4]. Hence, Eq (2.2) becomes

$$\frac{\partial c}{\partial t} = D_x \frac{\partial^2 c}{\partial x^2} \quad (2.3)$$

and is solved independently of Eq (2.1).

The three-dimensional diffusion in an anisotropic medium is obtained by generalization of Eq (2.2) as follows

$$\frac{\partial c}{\partial t} = \vec{\nabla} \cdot ([D] \cdot \vec{\nabla} c) \quad (2.4)$$

where the diffusivity matrix is

$$[D] = \begin{bmatrix} D_{xx} & D_{xy} & D_{xz} \\ D_{yz} & D_{yy} & D_{yz} \\ D_{zx} & D_{zy} & D_{zx} \end{bmatrix} \quad (2.5)$$

Expansion of Eq (2.4) results in an equation of the form

$$\begin{aligned} \frac{\partial c}{\partial t} = & D_{xx} \frac{\partial^2 c}{\partial x^2} + D_{yy} \frac{\partial^2 c}{\partial y^2} + D_{zz} \frac{\partial^2 c}{\partial z^2} + (D_{yz} + D_{zy}) \frac{\partial^2 c}{\partial y \partial z} \\ & + (D_{zx} + D_{xz}) \frac{\partial^2 c}{\partial x \partial z} + (D_{xy} + D_{yx}) \frac{\partial^2 c}{\partial x \partial y} \end{aligned} \quad (2.6)$$

if the coefficients D_{ij} 's are considered to be constant.

2.3 Fickian Diffusion in a Plate

Laminated plates are widely used in the experimental characterization of composites. Hence, being of practical interest, the problem of moisture absorption in a plate is thoroughly discussed in this section.

2.3.1 Infinite Plate

The case of moisture absorption through a material bounded by two parallel planes is considered. The initial and boundary conditions of an infinite plate exposed on both sides to the same constant environment (Figure 2.1) are given by

$$\left. \begin{array}{l} T = T_i \\ c = c_i \end{array} \right\} \text{ for } 0 \leq z \leq h \text{ and } t \leq 0 \quad (2.7)$$

$$\left. \begin{array}{l} T = T_i \\ c = c_\infty \end{array} \right\} \text{ for } z = 0, z = h \text{ and } t > 0$$

where T_i is a constant temperature, c_i is the initial moisture concentration inside the material, and c_∞ is the maximum moisture concentration. It is assumed that the moisture concentration on the exposed sides of the plate reaches c_∞ instantly.

The solution of Eq (2.3) in conjunction with the conditions of Eqs. (2.7) is given by Jost [25]

$$\frac{c - c_i}{c_\infty - c_i} = 1 - \frac{4}{\pi} \sum_{j=0}^{\infty} \frac{1}{(2j+1)} \sin \frac{(2j+1)\pi z}{h} \exp \left[- \frac{(2j+1)^2 \pi^2 D_z t}{h^2} \right] \quad (2.8)$$

Equation (2.8) is plotted in Figure 2.2.

The average moisture concentration is given by

$$\bar{c} = \frac{1}{h} \int_0^h c \, dz \quad (2.9)$$

Substitution of Eq. (2.8) into Eq. (2.9) and integration result in

$$\frac{\bar{c} - c_i}{c_\infty - c_i} = 1 - \frac{8}{\pi^2} \sum_{j=0}^{\infty} \frac{1}{(2j+1)^2} \exp \left[- (2j+1)^2 \pi^2 \frac{D_z t}{h^2} \right] \quad (2.10)$$

This analysis can be applied to the case of diffusion of

moisture into a laminated composite plate so thin that moisture enters predominantly through the plane faces.

2.3.2 Semi-Infinite Medium

In the early stages of moisture diffusion into a plate, there is no interaction between moisture entering through different faces. Therefore, the solution of moisture absorption into a semi-infinite half-plane is applicable to a plate for short time.

The initial and boundary conditions of a semi-infinite plane (Figure 2.3) exposed to a constant moist environment are

$$\left. \begin{array}{l} T = T_i \\ c = c_i \end{array} \right\} \text{ for } 0 \leq z < \infty \text{ and } t \leq 0$$

$$\left. \begin{array}{l} T = T_i \\ c = c_\infty \end{array} \right\} \text{ for } z = 0 \text{ and } t > 0$$
(2.11)

The solution of Eq (2.3) in this case is [24, 25]

$$\frac{c - c_i}{c_\infty - c_i} = 1 - \operatorname{erf} \left[\frac{z}{2 \sqrt{D_z t}} \right]$$
(2.12)

The rate at which the total specific mass of moisture, m , is diffusing into the half-plane is

$$\frac{dm}{dt} = - D_z \left[\frac{\partial c}{\partial z} \right]_{z=0} \quad (2.13)$$

Thus, the total mass of moisture entering through an area A in time t is

$$m = - \int_0^t \rho A D_z \left[\frac{\partial c}{\partial z} \right]_{z=0} dt = 2 \rho A (c_\infty - c_i) \sqrt{\frac{D_z t}{\pi}} \quad (2.14)$$

Equation (2.14) shows that the mass of diffusing substance is proportional to the square root of time.

2.3.3 Experimental Measurement of Moisture Content

In the case of a finite plate, the total moisture content is

$$m = \rho V \bar{c} \quad (2.15)$$

where V is the volume of the test piece. The total moisture content is experimentally measured by subtracting the dry weight, w_d , from the current weight, w, of the plate, i.e.,

$$m = w - w_d \quad (2.16)$$

A parameter of practical interest is the percent moisture content defined as

$$M = 100 \frac{w - w_d}{w_d} \quad (2.17)$$

Since

$$\frac{M - M_i}{M_\infty - M_i} = \frac{\bar{c} - c_i}{c_\infty - c_i} ; \quad M = 100c \quad (2.18)$$

the experimentally measured M of Eq (2.18) can be compared to the analytical value given by Eq (2.10).

2.3.4 Approximate Solution of Moisture Content

Approximate solutions of the specific moisture distribution in a plate subjected to the conditions given by Eqs (2.7) are useful, since the difficulty of dealing with infinite series can be avoided.

Small time. As discussed in section 2.3.2, Eq (2.14) can be applied during the early stages of absorption. It yields

$$\frac{\bar{c} - c_i}{c_\infty - c_i} = \frac{M - M_i}{M_\infty - M_i} = 4 \sqrt{\frac{D_z t}{\pi h^2}} \quad (2.19)$$

Large time. Tsai and Hahn [26, p. 338] suggest that, for sufficiently large t , Eq. (2.10) can be approximated by using the first term of the series, i.e.,

$$\frac{\bar{c} - c_i}{c_\infty - c_i} = 1 - \frac{8}{\pi^2} \exp \left[- \pi^2 \frac{D_z t}{h^2} \right] \quad (2.20)$$

Shen and Springer formulation. These researchers have derived in Ref. [4] the following approximation

$$\frac{\bar{c} - c_i}{c_\infty - c_i} = 1 - \exp \left[- 7.3 \left[\frac{D_z t}{h^2} \right]^{0.75} \right] \quad (2.20)$$

Figure 2.4 shows a comparison of Eqs (2.19-21) with the exact solution.

2.3.5 Edge-Effect Corrections in a Finite Laminated Plate

A plate exposed to a humid environment absorbs moisture through all its six sides. At small time, the interaction of moisture entering through different sides is negligible. Therefore, Eq. (2.19) can be applied to such cases. It yields

$$m = 4\rho(c_\infty - c_i) \left[bL \sqrt{D_z} + bh \sqrt{D_x} + hL \sqrt{D_y} \right] \sqrt{t/\pi} \quad (2.22)$$

where D_x , D_y , and D_z are the diffusivities in the x, y, and z directions, respectively. The geometry of the plate is shown in Figure 2.5. Rewriting Eq. (2.22) in terms of the percent moisture content gives

$$M = 4M_{\infty} \sqrt{\frac{Dt}{\pi h^2}} \quad (2.23a)$$

where the effective diffusivity D is

$$D = D_z \left[1 + \frac{h}{L} \sqrt{\frac{\overline{D}_x}{D_z}} + \frac{h}{b} \sqrt{\frac{\overline{D}_y}{D_z}} \right] \quad (2.23b)$$

The micromechanics formulation for diffusivities proposed by Shen and Springer [4] and modified by Hahn [26] for impermeable, circular cross-section, fiber-reinforced composites is

$$D_L = D_m \quad (2.24)$$

$$D_T = \left[1 - 2 \sqrt{\frac{v_f}{\pi}} \right] \frac{D_m}{v_m}$$

where D_m , D_T and D_L are the matrix, transverse, and longitudinal diffusivities, respectively. Equation (2.23b) for a unidirectional lamina with all fibers parallel to the x -direction can be written as

$$D = D_z \left[1 + \frac{h}{b} + \frac{h}{L} \sqrt{\frac{v_m}{1 - 2 \sqrt{\frac{v_f}{\pi}}}} \right] \quad (2.25)$$

For a general laminated plate consisting of N layers with fiber orientations θ_j , the diffusivities are

$$D_z = D_T$$

$$D_x = \frac{D_L \sum_{j=1}^N h_j \cos^2 \theta_j + D_T \sum_{j=1}^N h_j \sin^2 \theta_j}{\sum_{j=1}^N h_j} \quad (2.26)$$

$$D_y = \frac{D_L \sum_{j=1}^N h_j \sin^2 \theta_j + D_T \sum_{j=1}^N h_j \cos^2 \theta_j}{\sum_{j=1}^N h_j}$$

where h_j is the thickness of the j -th layer. The effective diffusivity of a general laminate is obtained by substituting Eqs. (2.26) into Eq (2.23b).

2.4 Diffusivity and Maximum Moisture Content

The diffusivity D_z and the maximum moisture content M_∞ must be experimentally determined in order to predict the moisture content and distribution in a lamina. These parameters are obtained by the following procedures:

- a thin, unidirectional composite plate is completely dried and its weight is recorded,

- the specimen is then placed in a constant temperature and constant relative humidity environment, and its weight as function of time is recorded,

- the moisture content, M , versus the square root of time, \sqrt{t} , is plotted as shown in Figure 2.6.

The maximum moisture content is determined from the plot and the diffusivity from the following equation

$$\frac{M_2 - M_1}{\sqrt{t_2} - \sqrt{t_1}} = 4M_\infty \sqrt{\frac{D_z}{\pi h^2}} \quad (2.27)$$

The subscripts 1 and 2 are defined in Figure 2.6.

The diffusivity depends only on the material and temperature as follows

$$D_z = D_o \exp \left[- \frac{E_d}{RT} \right] \quad (2.28)$$

where R is the gas constant, D_o and E_d are the pre-exponential factor and the activation energy, respectively.

Experimental research has shown that the maximum moisture content depends on environment humidity content and material. For a material exposed to humid air [4], the equilibrium moisture content can be expressed as

$$M_\infty = a\phi^b \quad (2.26)$$

where ϕ is the relative humidity, a and b are material constants.

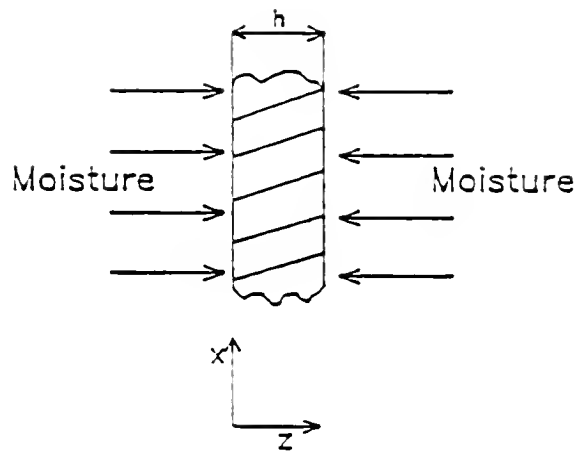


Fig. 2.1 Plate subjected to a constant humid environment on both sides.

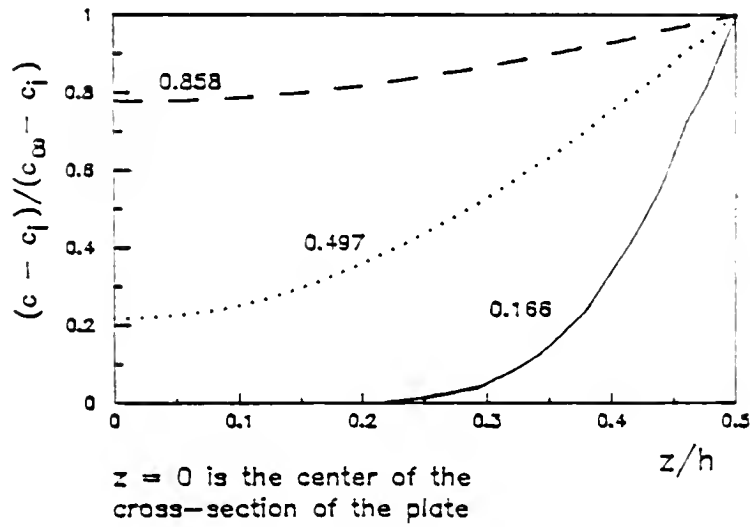


Fig. 2.2 Moisture distribution across a plate. The numbers on the curves are the values of $(\bar{c} - c_i)/(c_\infty - c_i)$.

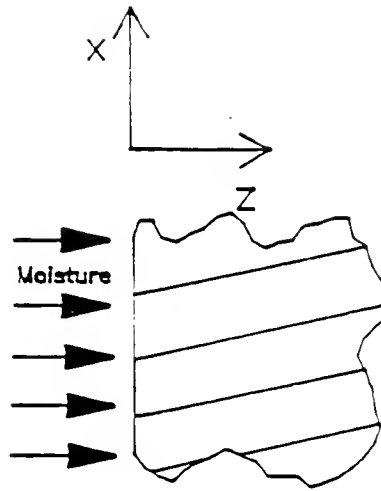


Fig. 2.3 Semi-infinite plate in a humid environment.

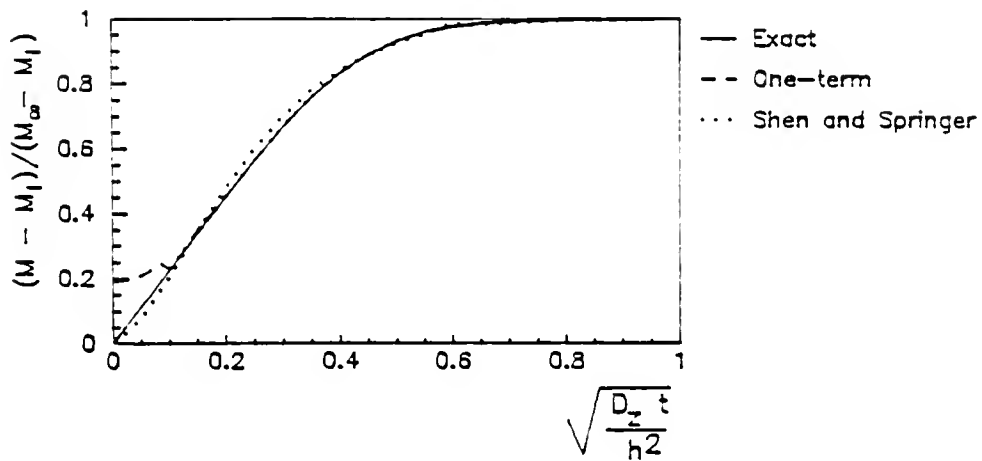


Fig. 2.4 Comparison of the exact specific moisture concentration equation with some approximate solutions.

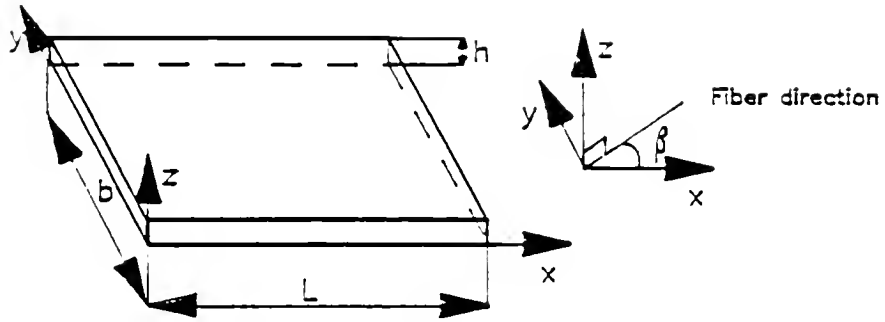


Fig. 2.5 Geometry of a plate

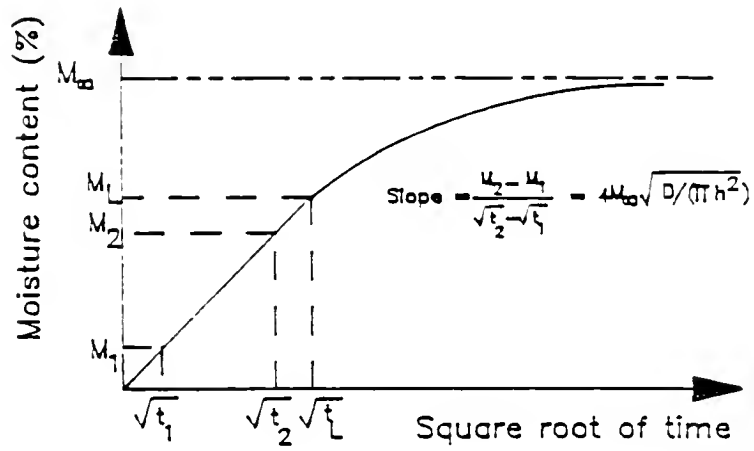


Fig. 2.6 Moisture content versus square root of time. On the curve $\sqrt{t_1} < \sqrt{t_2} < \sqrt{t_L}$ and the slope is constant for $\sqrt{t} < \sqrt{t_L}$.

CHAPTER 3 COMPLEX MODULI OF UNIDIRECTIONAL COMPOSITES

3.1 Introduction

Composite materials, such as Glass/Epoxy and Graphite/Epoxy, have a polymeric matrix. Therefore, they display viscoelastic behavior. Some of the effects of this time-dependent phenomenon are: stress relaxation under constant deformation, creep under constant load, damping of dynamic response, etc.

This chapter is an introduction to the dynamic behavior of viscoelastic composites in terms of complex moduli.

3.2 General Theory

A usual representation of the one-dimensional stress-strain relation of a viscoelastic material subjected to a harmonic strain history of the form

$$\epsilon(t) = \epsilon^0 e^{i\omega t} \quad (3.1)$$

is given by

$$\sigma(t) = B^*(i\omega)\epsilon^0 e^{i\omega t} = B^*(i\omega)\epsilon(t) \quad (3.2)$$

The complex modulus B^* can be decomposed into its real and imaginary parts as follows

$$B^*(i\omega) = B'(\omega) + iB''(\omega) \quad (3.3)$$

The terms B' and B'' are called the storage and loss moduli, respectively, and the ratio of the loss over the storage modulus

$$\eta = \frac{B''}{B'} \quad (3.4)$$

is referred to as either the loss factor or damping. The loss modulus is a measure of the energy dissipated or lost as heat per cycle of harmonic deformation.

3.3 Micromechanics Formulation of Elastic Moduli

The longitudinal modulus E_{11} , the transverse modulus E_{22} , the in-plane shear modulus G_{12} , and the major Poisson's ratio ν_{12} can be obtained by using the rule of mixtures and the Halpin-Tsai equations, viz.,

$$E_{11} = \nu_f E_{f11} + \nu_m E_m \quad (3.5)$$

$$E_{22} = E_m \frac{1 + 2n_1 v_f}{1 - n_1 v_f} \quad (3.6)$$

$$G_{12} = G_m \frac{1 + n_2 v_f}{1 - n_2 v_f} \quad (3.7)$$

$$\nu_{12} = v_f \nu_{f12} + v_m \nu_m \quad (3.8)$$

where

$$n_1 = \frac{(E_{f22}/E_m) - 1}{(E_{f22}/E_m) + 2} \quad (3.9)$$

$$n_2 = \frac{(G_{f12}/G_m) - 1}{(G_{f12}/G_m) + 1} \quad (3.10)$$

The subscripts f and m stand for fiber and matrix, respectively, and v_f and v_m are the volume fractions.

3.4 Complex Moduli

The micromechanics formulations of the complex moduli are obtained by applying the elastic-viscoelastic correspondence principle [27-29], i.e., by undertaking the following steps:

i) determining the elastic moduli of composites in terms of the constituent material properties,

ii) replacing the elastic moduli of fibers and matrix by corresponding complex expressions.

For a viscoelastic composite, the properties of the constituent materials are

$$E_{f11}^* = E_{f11}' + iE_{f11}''$$

$$E_{f22}^* = E_{f22}' + iE_{f22}''$$

$$G_{f1}^* = G_{f1}' + iG_{f1}''$$

$$E_m^* = E_m' + iE_m'' \quad (3.11)$$

$$G_m^* = G_m' + iG_m''$$

$$\nu_m^* = \nu_m' + i\nu_m''$$

$$\nu_{f12}^* = \nu_{f12}'$$

The bulk modulus of epoxy matrix, K_m , is real and independent of frequency [2S]. It is given by

$$K_m = \frac{E_m}{3(1 - 2\nu_m)} \quad (3.12)$$

while the viscoelastic bulk modulus is obtained from the correspondence principle

$$K_m^* = \frac{E_m' + iE_m''}{3[1 - 2(\nu_m' + i\nu_m'')] } \quad (3.13)$$

Separation of the real and imaginary parts of Eq. (3.13) yields

$$K_m^* = \frac{(1 - 2\nu_m')E_m' - 2\nu_m''E_m'' + i[2E_m''\nu_m'' + E_m'(1 - 2\nu_m'')]}{3[(1 - 2\nu_m')^2 + 4\nu_m''^2]} \quad (3.14)$$

Since the dilatation bulk modulus is real, the imaginary part of Eq. (3.14) is equal to zero; hence

$$2E_m''\nu_m'' + E_m''(1 - 2\nu_m'') = 0 \quad (3.15)$$

Equation (3.15) results in

$$\nu_m'' = \frac{E_m''}{E_m'}(\nu_m' - 0.5) \quad (3.16)$$

The shear modulus of the matrix is given by

$$G_m^* = \frac{E_m^*}{2(1 + \nu_m^*)} = \frac{3K_m E_m^*}{9K_m - E_m^*} \quad (3.17a)$$

Separating the real and imaginary parts and neglecting the terms of the form $(E_m'')^2$ yield

$$G_m^* = \frac{3K_m E_m'}{9K_m - E_m'} \left[1 + i \frac{9K_m}{9K_m - E_m'} \frac{E_m''}{E_m'} \right] \quad (3.17b)$$

Introduction of the material properties

$$\eta_m = \frac{E_m''}{E_m'}$$

$$\eta_{f11} = \frac{E_{f11}''}{E_{f11}'} \quad (3.18)$$

$$\eta_{f22} = \frac{E_{f22}''}{E_{f22}'}$$

$$\eta_{Gm} = \frac{G_m''}{G_m'} = \frac{9K_m}{9K_m - E_m'} \eta_m$$

into Eqs. (3.11) results in

$$E_{f11}^* = E_{f11}' (1 + i\eta_{f11})$$

$$E_{f22}^* = E_{f22}' (1 + i\eta_{f22})$$

$$G_{f12}^* = G_{f12}' (1 + i\eta_{f12})$$

$$E_m^* = E_m' (1 + i\eta_m) \quad (3.19)$$

$$G_m^* = G_m' (1 + i\eta_{Gm})$$

$$\nu_m^* = \nu_m' + i\eta_m(\nu_m' - \frac{1}{2})$$

$$\nu_{f12}^* = \nu_{f12}' = \nu_{f12}$$

There are no satisfactory data on the shear and transverse damping of fibers. Fibers have damping with a magnitude order ten times smaller than epoxy. The dampings η_{f11} , η_{f22} , and η_{f12} are assumed to be equal and are replaced by η_f in subsequent equations. Since the fiber damping, η_f , is much smaller than the matrix damping, η_m , the imaginary part of the fiber Poisson's ratio is neglected. The preceding assumptions have a negligible effect on the complex moduli of composites.

Application of the elastic-viscoelastic correspondence principle to Eqs. (3.5)-(3.10) and substituting them into Eqs (3.19) yield the following complex material properties

$$E_{11}^* = \nu_f E_{f11}' (1 + i\eta_f) + \nu_m E_m' (1 + i\eta_m)$$

$$E_{22}^* = E_m' (1 + i\eta_m) \frac{1 + 2n_1^* \nu_f}{1 - n_1^* \nu_f} \quad (3.20)$$

$$G_{12}^* = G_m' (1 + i\eta_{Gm}) \frac{1 + n_2^* \nu_f}{1 - n_2^* \nu_f}$$

$$\nu_{12}^* = (\nu_f \nu_{f12} + \nu_m \nu_m') + i\eta_m(\nu_m' - \frac{1}{2})\nu_m$$

where

$$n_1^* = \frac{E_{f22}'(1 + i\eta_f) - E_m'(1 + i\eta_m)}{E_{f22}'(1 + i\eta_f) + 2E_m'(1 + i\eta_m)}$$

$$n_2^* = \frac{G_{f12}'(1 + i\eta_f) - G_m'(1 + i\eta_{Gm})}{G_{f12}'(1 + i\eta_f) + G_m'(1 + i\eta_{Gm})}$$

The elastic moduli given by Eqs. (3.5)-(3.8) model experimental results with a good accuracy [2]. Therefore, they are used instead of mathematically exact micromechanics formulas, such as those derived by Hashin [27, 29].

CHAPTER 4 DAMPING

4.1 Damping Mechanisms

Any vibrational energy introduced in a structure tends to decay in time. This phenomenon is called damping. There are two types of damping mechanisms, external or nonmaterial and internal or material.

4.1.1 Nonmaterial Damping.

Two common types of external damping are

- Accoustic damping: a vibrating structure always interacts with the surrounding fluid medium (air, water, etc.). This effect can lead to noise emission and even to changes of the natural frequencies and mode shapes. Thus, mechanical responses might be modified.

- Coulomb friction damping: two contacting surfaces in relative motion dissipate energy through frictional forces.

4.1.2 Material Damping

There are many damping mechanisms that dissipate vibrational energy inside the volume of a material. Damping phenomena include thermal effects, magnetic effects, stress relaxation, phase processes in solid solutions [30, p. 61], etc.

The internal damping of polymeric matrix composites, such as Glass/Epoxy and Graphite/Epoxy, is dominated by viscoelastic damping.

4.2 Characterization of Damping

4.2.1 Free Vibration

A cantilever under free vibration oscillates regularly with an amplitude that decreases from one oscillation to the next one (Figure 4.1). A measure of damping is the logarithmic decrement defined as

$$\delta = \frac{1}{N} \ln \left[\frac{A_n}{A_{n+N}} \right] \quad (4.1)$$

where

A_n = amplitude of the n-th cycle

A_{n+N} = amplitude of the (n+N)-th cycle

The damping defined in Eq (4.1) is applicable to viscous

damping and for hysteretic damping that is represented by a complex modulus approach.

4.2.2 Steady State Vibration

Damping also influences the dynamic equilibrium amplitude of structures (e.g. beams) that undergo harmonic oscillation. A resonance usually occurs (Figure 4.2). The following measure of damping is used

$$\eta = \frac{\omega_2 - \omega_1}{\omega_0} \quad (4.2)$$

where

ω_0 = resonant frequency
 ω_1, ω_2 = frequencies on either sides of ω_0 such that the amplitude is $1/\sqrt{2}$ times the resonant amplitude.

In the case of a vibration induced by the force

$$f(t) = F \sin(\omega t)$$

the response (deflection), $w(t)$, is out of phase with $f(t)$ by an angle ϵ such that

$$w(t) = W \sin(\omega t + \epsilon)$$

The work done per cycle is

$$D = \int_0^{2\pi/\omega} f(t) \frac{dw}{dt} dt = \pi W F \sin(\epsilon) \quad (4.3)$$

The strain energy stored in the system at the maximum displacement is half the product of the maximum displacement by the corresponding value of the force, i.e.,

$$U = \frac{1}{2} F W \cos(\epsilon) \quad (4.4)$$

There is no damping if the work done per cycle is zero, i.e., if $\sin(\epsilon) = 0$.

The ratio of energy dissipated in a cycle to energy stored at the maximum displacement is another measure of damping. Therefore, the damping is

$$\eta = \frac{D}{2\pi U} = \tan(\epsilon) \quad (4.5)$$

The definitions of damping given by Eqs. (4.2) and (4.5) are equivalent [33].

4.2.3 Complex Modulus Approach

The one-dimensional stress-strain relation of a viscoelastic material undergoing harmonic motion has been shown to be (Eq. (3.2))

$$\sigma^*(t) = E^*(\omega)\epsilon_0 e^{i\omega t} = (E'(\omega) + iE''(\omega))\epsilon_0 e^{i\omega t} \quad (4.6)$$

Noting that $i|\omega|\epsilon = d\epsilon/dt$, Eq. (4.6) can be written as

$$\sigma^*(t) = \epsilon_0 e^{i\omega t} + \frac{E''}{|\omega|} i\omega e^{i\omega t} \epsilon_0 \quad (4.7)$$

The real part is given by (after algebraic manipulation)

$$\sigma(t) = E'\epsilon_0 \sin(\omega t + \epsilon) \sqrt{1 + \eta^2} \quad (4.8)$$

where $\eta = \tan(\epsilon) = E''/E'$

The energy dissipated during a cycle per unit volume is

$$D = \oint \sigma d\epsilon_x = \int_0^{2\pi/\omega} \sigma \frac{d\epsilon_x}{dt} dt = \pi \eta E' \epsilon_0^2 \quad (4.9)$$

The maximum energy stored is

$$U = \frac{1}{2} E' \epsilon_0^2 \quad (4.10)$$

Therefore,

$$\eta = \frac{E''}{E'} = \frac{D}{2\pi U} \quad (4.11)$$

Hence, the definitions of damping given by Eq. (3.4) and Eq. (4.5) are equivalent. This conclusion is also valid for general cases of structural vibration.

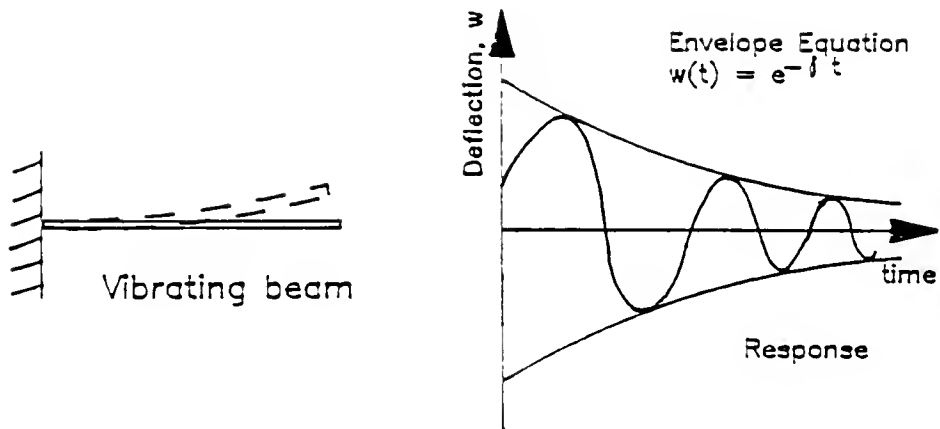


Fig. 4.1 Schematic drawing of a free-clamped beam under free vibration and plot of its deflection versus time.

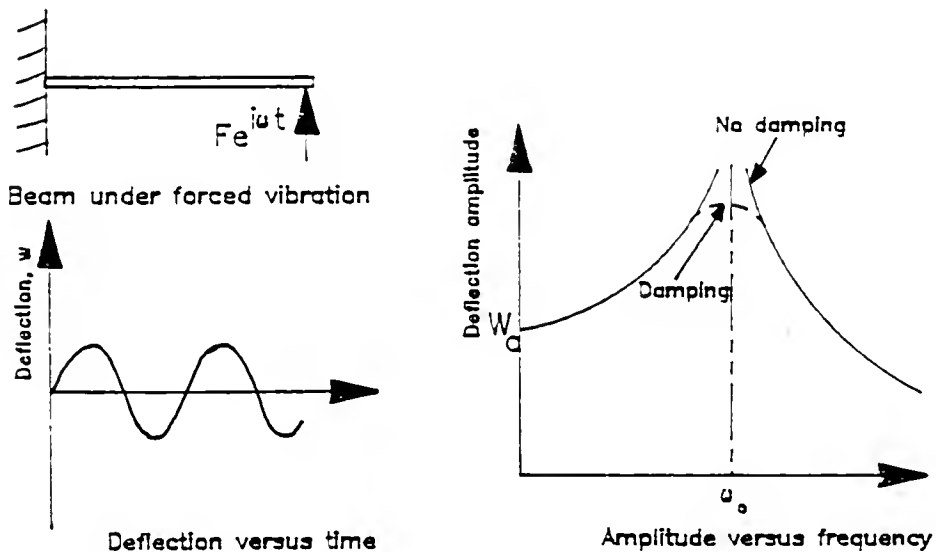


Fig. 4.2 Schematic drawing of a free-clamped beam under forced vibration and plots of the deflection versus time and deflection amplitude versus frequency.

CHAPTER 5 DAMPING AND STIFFNESSES OF GENERAL LAMINATES

5.1 Introduction

Both the laminated plate theory and the energy method approaches for analyzing the damping and the stiffnesses of general laminates are presented in this chapter.

5.2 Laminate Plate Theory Approach

Four independent parameters are needed to determine completely the damping of a unidirectional composite. But, the analysis of the material damping of a general laminated composite requires the use of eighteen parameters. These quantities are the ratios of the imaginary over the real parts of the complex in-plane stiffnesses A_{ij}^* 's, the complex coupling stiffnesses B_{ij}^* 's, and the complex bending stiffnesses D_{ij}^* 's (see Appendix A).

The terms A_{ij}^* 's, B_{ij}^* 's, and D_{ij}^* 's are defined as

$$A_{ij}^* = \int_{-h/2}^{+h/2} \bar{Q}_{ij}^* dz$$

$$B_{ij}^* = \int_{-h/2}^{+h/2} z \bar{Q}_{ij}^* dz \quad (5.1)$$

$$D_{ij}^* = \int_{-h/2}^{+h/2} z^2 \bar{Q}_{ij}^* dz$$

where the complex transformed stiffness \bar{Q}_{ij}^* 's depend on E_{11}^* , E_{22}^* , G_{12}^* , ν_{12}^* and the orientation of each layer of the laminate.

The in-plane, coupling, and flexural material damping are defined as

$$I^{\eta}_{ij} = \frac{A''_{ij}}{A'_{ij}}$$

$$C^{\eta}_{ij} = \frac{B''_{ij}}{B'_{ij}} \quad (5.2)$$

$$F^{\eta}_{ij} = \frac{D''_{ij}}{D'_{ij}}$$

respectively.

5.3 Energy Method Approach

The energy method can be used to determine the damping of laminated composite materials under certain loading and boundary conditions. The damping of a laminated

composite material in the first mode of vibration can be defined as

$$\eta = \frac{\sum_{k=1}^N ({}_kU_d)_{cyc.}}{\sum_{k=1}^N 2\pi {}_kU_s} \quad (5.3)$$

where N is the total number of layers, $({}_kU_d)_{cyc.}$ is the energy dissipated in the k -th layer during a cycle, and ${}_kU_s$ is the maximum energy stored in the k -th layer. The storage and the dissipated energy are given by

$${}_kU_s = \frac{1}{2} \int_{V_k} \epsilon_j C'_{ji} \epsilon_i \, dV \quad (5.4)$$

$${}_kU_d = \pi \int_{V_k} \epsilon_j C''_{ji} \epsilon_i \, dV$$

where i and j are the material principal axes, C'_{ji} and C''_{ji} are the real and imaginary parts of the complex stiffnesses and V_k is the volume of each layer. Hence, the "total" damping of an N -layered laminate is given by

$$\eta = \frac{\sum_{k=1}^N \int_{V_k} \{\epsilon\}^T [C''] \{\epsilon\} \, dV}{\sum_{k=1}^N \int_{V_k} \{\epsilon\}^T [C'] \{\epsilon\} \, dV} \quad (5.5)$$

The maximum strain vector $\{\epsilon\}$ can be determined by the finite element method first. Then, the damping can be deduced. Equation (5.5) is used to determine the damping of a beam with variable thickness or of more general structures.

CHAPTER 6 EXPERIMENTAL PROCEDURES

6.1 Introduction

A description of the test specimens and the experimental procedures of the present investigation is given in this chapter.

6.2 Test Specimens

The test specimens used to determine the complex moduli of epoxy and of composite materials are thin strips of approximate dimensions, 150mm by 25mm by 2mm. The only materials tested are Magnolia 2026 laminating epoxy and 3M Scotchply Glass/Epoxy. The curing temperatures of the epoxy and the Glass/Epoxy are 175°C and 170°C, respectively. The initial properties of these materials (at 20°C and without moisture), as well as those of a typical Graphite/Epoxy, are given in Table 6.1.

6.3 Environmental Conditioning

The specimens are conditioned in a Thermotron environment chamber at a constant temperature and constant relative humidity. The weight gain of the test pieces as a function of time is monitored. Right after moisture equilibrium is reached, the specimens undergo all tests at diverse temperatures inside a testing chamber connected to the environment chamber (Figure 6.1). The range of temperature achieved inside the environment chamber is 4°C to 90°C and the range of relative humidity is 4% to 99% for temperatures below 75°C. As temperature increases, the highest relative humidity that can be obtained decreases steadily to 75% at 90°C.

6.4 Four-Point Flexure Test Method

The Young's modulus and the Poisson's ratio can be determined with the four-point flexure test method. The loading configuration of this test is shown in Figure 6.2. The elastic flexural analysis yields [31]

$$\bar{E} = \frac{Pl^3}{8bh^3w} \quad (6.1)$$

where \bar{E} is the effective modulus, P is the applied load, l is the length of the specimen, b is the specimen width, h

is the thickness, and w is the deflection at quarter-point. Poisson's ratio is expressed as

$$\nu = - \frac{\epsilon_y}{\epsilon_x} = - \frac{l^2}{6hw} \epsilon_y \quad (6.2)$$

where the transverse strain ϵ_y is measured with a transverse strain gage cemented in the middle of the specimen.

6.5 Impulse Hammer Technique

The material damping and the storage modulus of a one-dimensional thin beam are determined with the impulse hammer technique. This technique was pioneered by Halvorsen and Brown [32]. The equipment set-up is shown in Figure 6.3. The specimen is clamped inside the testing chamber. A force impulse is applied to the test piece by a force transducer. The end displacement of the specimen is recorded with a non-contacting motion transducer. Both responses from the force and motion transducers go through signal conditioning equipments (filters, amplifiers). These responses are digitized in a Fast Fourier Transform analyzer (FFT) to obtain the transfer function in terms of the frequency. The transfer function is defined as the ratio of the Fourier Transform of the output (displacement

$v(t)$) over the Fourier Transform of the input (force impulse $u(t)$); that is,

$$H(f) = \frac{V(f)}{U(f)} \quad (6.3)$$

where

t = time

f = frequency

$V(f)$ = Fourier Transform of $v(t)$

$U(f)$ = Fourier Transform of $u(t)$

The real and imaginary parts of $H(f)$ are displayed on the FFT analyser CRT (Figure 6.3). The material damping defined by Eq. (4.11) is experimentally obtained by the following expression

$$\eta = \frac{(f_a/f_b)^2 - 1}{(f_a/f_b)^2 + 1} \quad (6.4)$$

where the frequencies f_a and f_b are defined in Figure 6.3. The storage modulus is expressed as [33, p.464]

$$E' = 38.32 f_r^2 \rho \frac{l^4}{h^2} \quad (6.5)$$

where f_r is the resonant frequency in Hz., ρ is the material density, l is the length of the specimen and h is the thickness of the specimen. Equation (6.5) is valid only

for the case of the first mode free vibration of a clamped-free beam. A complete description and analysis of the impulse hammer technique are presented in Lee's dissertation [34].

Table 6.1 Initial properties of Magnolia 2026 epoxy, 3M Scotchply Glass/Epoxy, and a typical Graphite/Epoxy composite.

Properties	Epoxy	Glass/Epoxy	Graphite/Epoxy
v_f		0.50	0.70
ρ (g/cm ³)	1.25	1.93	1.6
E_{11} (GPa.)	4.0	37.00	155.23
E_{22} (GPa.)	4.0	11.54	10.81
G_{12} (GPa.)	1.52	3.46	4.35
ν_{12}	0.32	0.285	0.217
η_{11}	0.018	0.0023	0.0019
η_{22}	0.018	0.015	0.0078

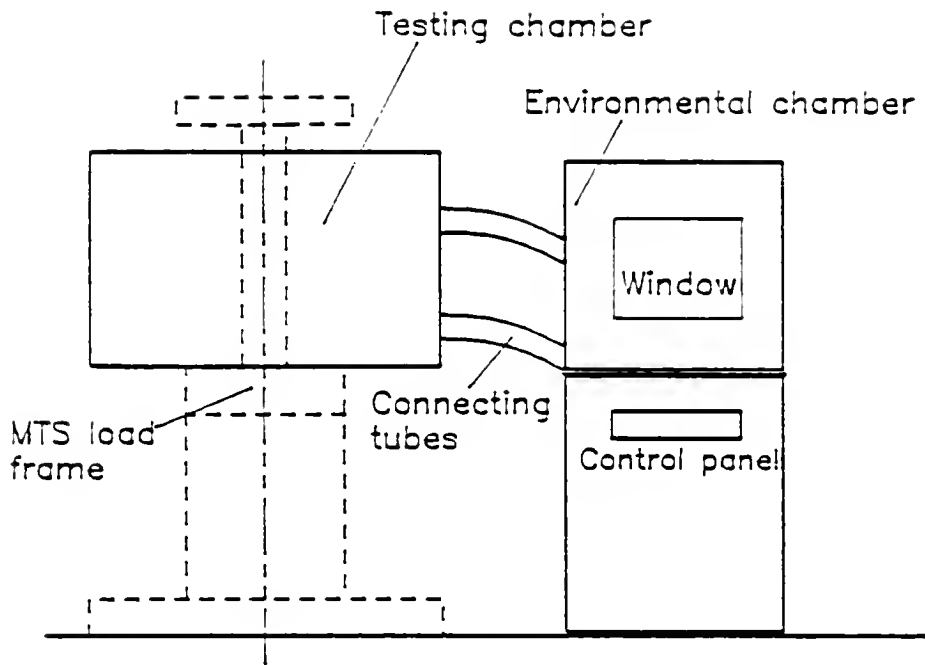


Fig. 6.1 Schematic drawing of environmental and testing chambers.

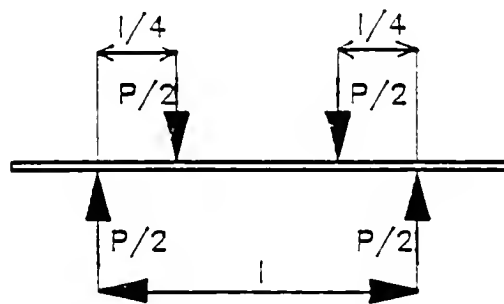
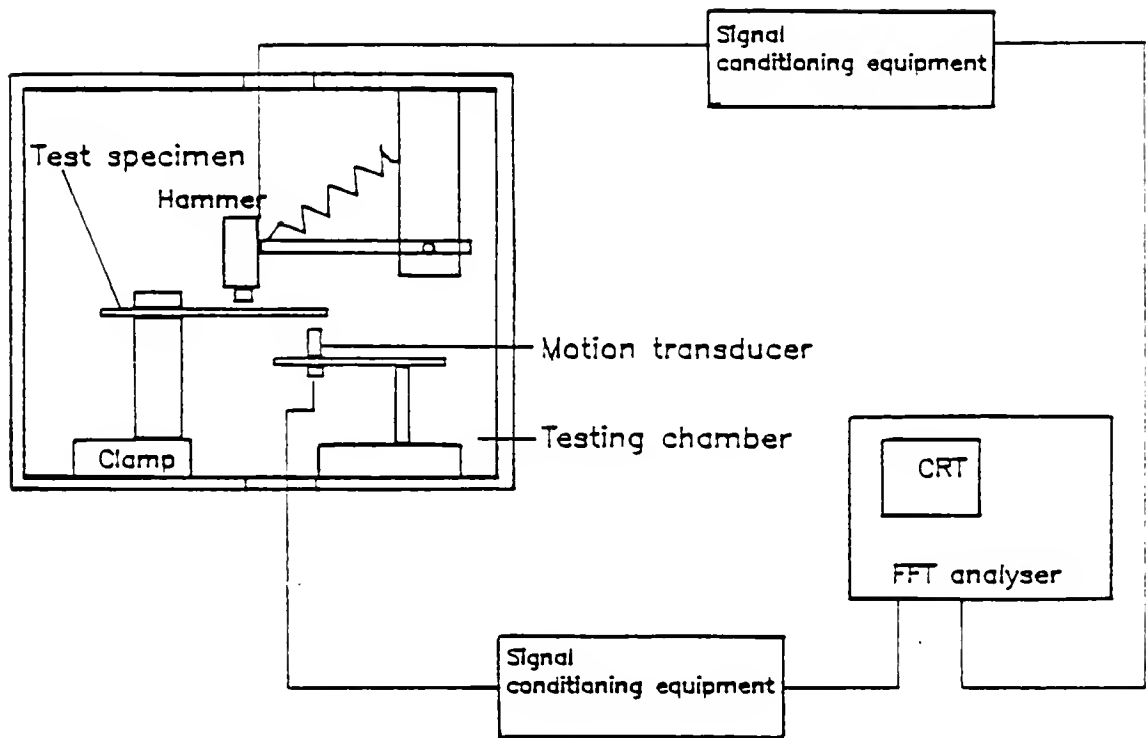
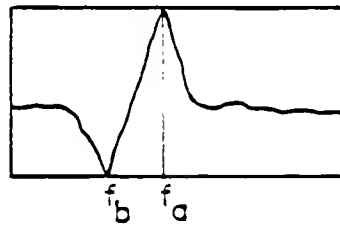


Fig. 6.2 Loading configuration of the 4-point flexure test.



Fourier Transform

Real part



Im. part

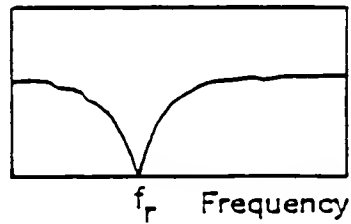


Fig. 6.3 Schematic drawing of the impulse hammer technique apparatus and a typical display of the Transfer Fourier Transform.

CHAPTER 7 HYGROTHERMAL EXPANSION

7.1 Introduction

When a metallic or composite structure is subjected to a change of temperature, there are dimensional variations and there may be stress development. For a one-dimensional case, it is assumed that the thermal strain is given by

$$\epsilon_i^T = \alpha_i (T - T_o) = \alpha_i \Delta T \quad (7.1)$$

where

α_i = coefficient of thermal expansion

T = actual temperature

T_o = reference temperature.

A polymer matrix composite exposed to a humid environment absorbs moisture. Hence, it increases in weight and dimensions. This situation produces a moisture strain that varies linearly with moisture concentration [26]. In the one-dimensional case, the hygrostrain is given by

$$\epsilon_i^H = \beta_i (c - c_o) = \beta_i \Delta c \quad (7.2)$$

where c_o is the initial moisture concentration and β_i is the coefficient of moisture expansion.

7.2 Coefficients of Thermal Expansion

In the case of laminated composite plates, three coefficients of thermal expansion are used in determining the thermal strains. These parameters can be written in terms of fiber and matrix properties. The micromechanics formulas for a unidirectional orthotropic lamina are given by (see Refs. [35, p. 24], and [36, p. 405] for a detailed derivation)

$$\alpha_1 = \frac{v_f \alpha_f E_f + v_m \alpha_m E_m}{E_{11}}$$

$$\alpha_2 = v_f \alpha_f + v_m \alpha_m + v_f v_f \alpha_f + v_m v_m \alpha_m - v_{12} \alpha_1 \quad (7.3)$$

$$\alpha_{12} = 0$$

where the subscripts 1 and 2 represent the fiber and the transverse directions. The thermal expansion coefficients of an orthotropic lamina whose fibers make an angle θ with the x-direction (Figure 2.5) are given by

$$\alpha_x = \alpha_1 \cos^2 \theta + \alpha_2 \sin^2 \theta$$

$$\alpha_y = \alpha_1 \sin^2 \theta + \alpha_2 \cos^2 \theta \quad (7.4)$$

$$\alpha_{xy} = 2(\alpha_1 - \alpha_2) \cos \theta \sin \theta$$

7.3 Coefficients of Moisture Expansion

Similarly, the coefficients of moisture expansions of an orthotropic lamina with impermeable fibers can be expressed as [36, p. 406]

$$\beta_1 = \frac{s E_m}{s_m E_{11}} \beta_m$$

$$\beta_2 = \frac{s}{s_m} (1 + \nu_m) \beta_m - \nu_{12} \beta_1 \quad (7.5)$$

$$\beta_{12} = 0$$

where s and s_m are the specific gravities of the composite material and the matrix. The moisture expansion coefficients expressed in an axis system such that the x -direction makes an angle θ with the fibers are given by Eqs. (7.4) after replacement of α_i 's by β_i 's.

7.4 Experimental Data

7.4.1 Previous Investigations

Hahn and coworkers' investigations [21, 26, 37] of swelling of composites are outlined in this section. Some of the typical results of the transverse strain versus percent moisture gain are obtained by conducting the following tests: absorption is conducted in moisture saturated air such that Eqs (2.2) and (2.7) are satisfied; while desorption takes place in vacuum at the same temperature. Their data show a hysteretic nature of swelling in this case.

But, when swelling of composites is given in terms of moisture concentration, the average behavior of S2-Glass/Epoxy, Kevlar 49/Epoxy and Graphite/Epoxy can be approximated by

$$\epsilon_2^H \simeq 0.43c = \beta_2 c \quad (7.6)$$

Since the data presented in their publications display a wide scatter, Hahn et al. suggest that Eq. (7.6) can be used to estimate the moisture strains for most composite materials.

7.4.2 Present Investigation

Epoxy and Glass/Epoxy specimens are conditioned at a constant relative humidity until the absorbed moisture reaches equilibrium. The changes in transverse dimensions are measured. This procedure is repeated at diverse values of relative humidity. The results are plotted in Figure 7.1. The longitudinal swelling strains could not be measured since the micrometer calipers used were not sufficiently accurate. These data yield the following experimental values

$$\beta_m(\text{epoxy}) = 0.25 \quad (7.7)$$

$$\beta_2(\text{Glass/Epoxy}) = 0.48 \quad (7.8)$$

Substitution of Eq. (7.7) and the parameters given in Table 6.1 into Eqs. (7.5) yields the following empirical values

$$\beta_1 = 0.042 \quad (7.9a)$$

$$\beta_2 = 0.47 \quad (7.9b)$$

for the 3M Glass/Epoxy composite. The experimental and empirical values of β_2 are practically equal. Hence, the

present results differ slightly from the approximation given by Eq. (7.6).

The above coefficients and the typical coefficients of expansion of graphite are quantified in Table 7.1, while the storage moduli and the density of glass and graphite fibers are listed in Table 7.2. These properties are used to plot the thermal and moisture expansion coefficients versus the fiber volume fraction of Glass/Epoxy and Graphite/Epoxy in Figures 7.2 through 7.5.

The values in these plots are valid for dry composites at room temperature. Since the storage modulus of epoxy varies with temperature and moisture content, this additional effect is investigated in Chapter 8.

In general, the thermal expansion coefficients are functions of temperature, but this temperature effect is negligible below 100°C . Therefore, in the subsequent chapters, the thermal expansion coefficients are assumed to be independent of temperature.

Table 7.1 Coefficients of moisture and thermal expansion of epoxy and graphite and glass fibers.

	Epoxy	Glass	Graphite
α ($\mu\text{m}/\text{m}$)/K	54.0	5.0	0.2
β	0.25	0.0	0.0

Table 7.2 Properties of Glass and graphite Fibers.

	Glass	Graphite
E'_{f11} (GPa)	70.0	220.0
E'_{f22} (GPa)	70.0	16.6
G'_{f12} (GPa)	28.7	8.27
η_f	0.0015	0.0015
ν_{f12}	0.22	0.16
ρ (g/cm^3)	2.60	1.75

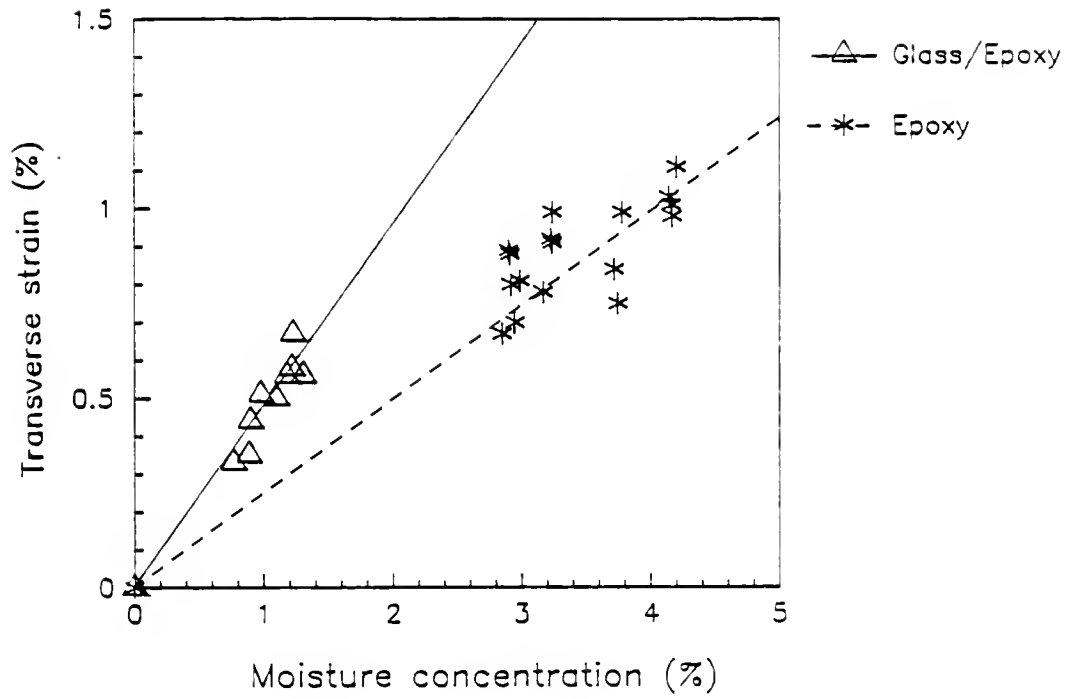


Fig. 7.1 Transverse moisture strain of Magnolia epoxy and 3M Scotchply Glass/epoxy.

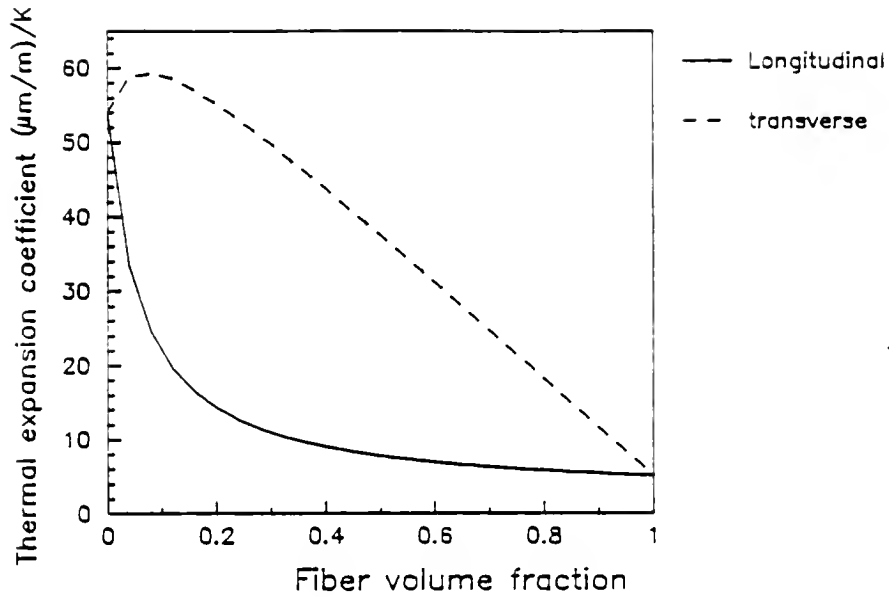


Fig. 7.2 Plot of the thermal expansion coefficients in terms of fiber volume fraction of a dry S Glassfiber/Epoxy at 20°C.

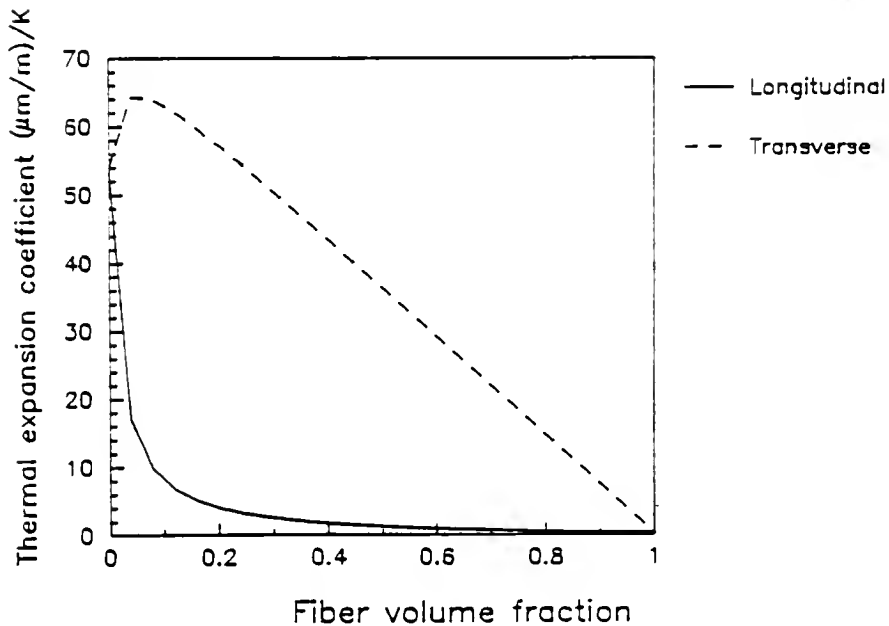


Fig. 7.3 Plot of the thermal expansion coefficients in terms of fiber volume fraction of a dry Graphite/Epoxy at 20°C.

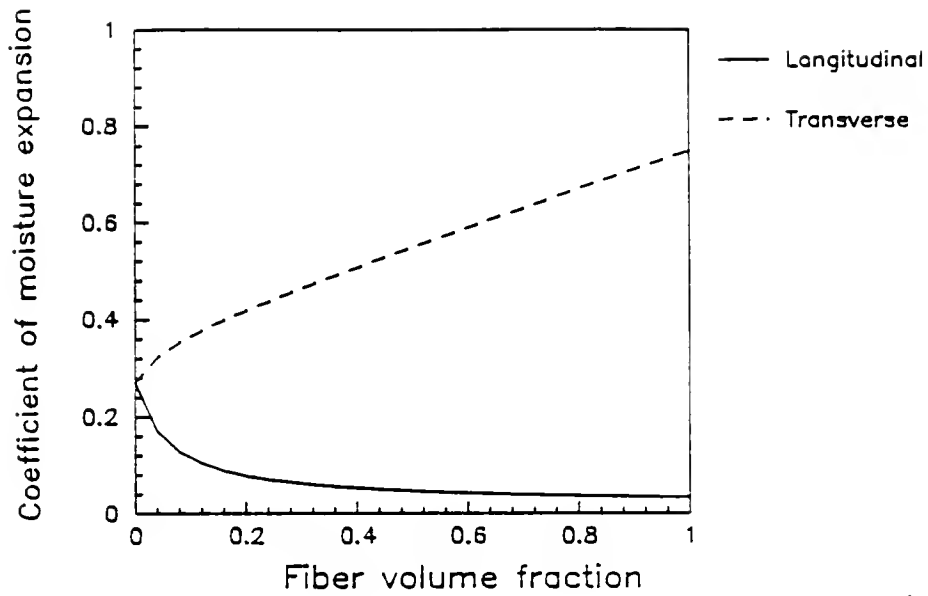


Fig. 7.4 Plot of the moisture expansion coefficients in terms of fiber volume fraction of a dry S Glassfiber/Epoxy at 20°C.

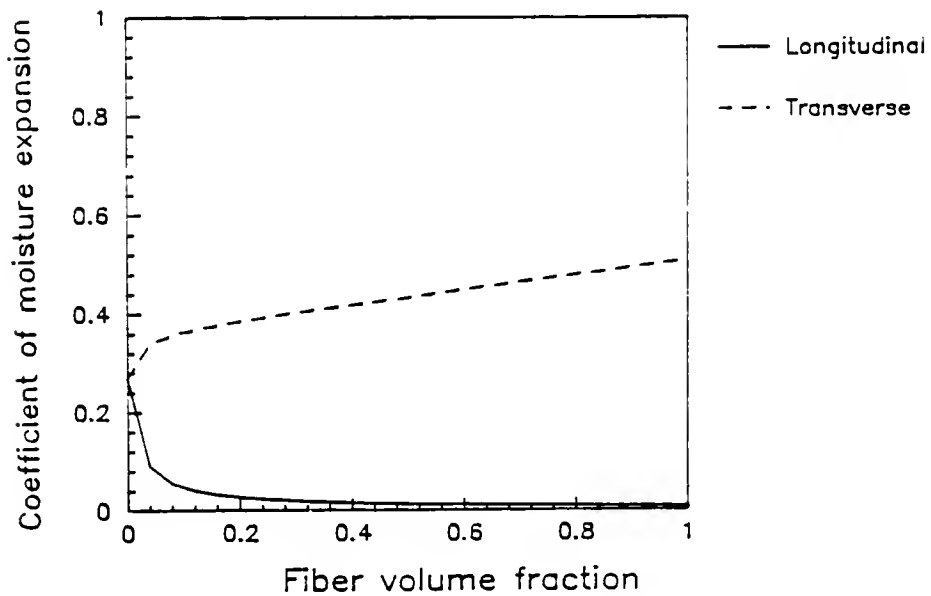


Fig. 7.5 Plot of the moisture expansion coefficients in terms of fiber volume fraction of a dry Graphite/Epoxy at 20°C.

CHAPTER 8 HYGROTHERMAL EFFECTS ON COMPOSITE COMPLEX MODULI

8.1 Literature Survey

The storage moduli (real parts of Eqs. (3.11)) of composites are usually determined by dynamic testings, such as the technique described in section 6.5. They can be approximated by using static tests [38].

Shen and Springer [12] investigated the environmental effects on the elastic moduli of a Graphite/Epoxy composite and made a survey of existing data showing the effects of temperature and moisture on the elastic modulus of several composites. Their conclusions are listed below.

i) The hygrothermal effects on the 0° fiber direction laminates are negligible.

ii) For 90° fiber direction laminates, the hygrothermal effects on the modulus are insignificant in the 200K to 300K temperature range. But, between 300K and 450K, the hygrothermal effects on the modulus are important.

Putter et al. [38] investigated the influence of frequency and environmental conditions on the dynamic

behavior of Graphite/Epoxy composites. Their overall conclusions are

i) The effects of frequency on the modulus and damping are quite small in all cases.

ii) The effects of frequency on the modulus and damping are relatively greater for matrix-controlled laminates at higher frequencies (above 400 Hz.).

iii) At the same temperature, damping increases with moisture saturation. But for dry laminates, damping decreases slightly as temperature increases.

From all these experimental works, a general summary can be drawn: the influence of hygrothermal conditions on the elastic modulus, dynamic modulus and damping of composites is matrix dominated.

8.2 Theoretical and Experimental Assumptions

Since the hygrothermal influence on composite properties is matrix controlled [12, 38], the fiber properties are assumed to be constant at any temperature below the glass transition temperature and at any moisture content. Therefore, to obtain the values of the complex moduli of composites, it is sufficient to know how temperature and moisture affect the complex moduli of the epoxy matrix, and then use the micromechanics formulations given by Eqs. (3.20). Thus, only the following functions

$$E'_m = E'_m(T, c)$$

$$\nu'_m = \nu'_m(T, c) \quad (8.1)$$

$$\eta_m = \eta_m(T, c)$$

need to be experimentally evaluated. The constant fiber properties are given in Table 7.2. The effects of frequency are negligible below 400 Hz. The results of this investigation are not accurate for higher frequencies since their effects have not been taken into account.

The qualitative influence of temperature only on the storage modulus, real part of Poisson's ratio, and damping of epoxy is illustrated in Figures 8.1-8.3. There are three distinct regions. At room temperature (in the glassy region), the storage modulus, Poisson's ratio, and damping of epoxy are equal to about 4.0 GPa, 0.35, and 0.018, respectively. In the glassy region, the storage modulus decreases slowly, while Poisson's ratio and the damping increase as temperature increases. In the next region (transition region), the storage modulus decreases rapidly, and both Poisson's ratio and damping reach their maximum values. The last region is the rubbery region where the modulus takes a very low value, and all three parameters stay relatively constant.

Typical values of the modulus in the rubbery region could be 10^{-2} times the glassy modulus or lower. The damping

can reach a value of 1 or even 2 in the transition region [30, p. 90]. Poisson's ratio reaches the limiting value of 0.5, which is approximated by incompressible rubbers [39, p. 293].

The position of the transition region depends on the moisture concentration. The effects of moisture on the glass transition temperature, T_g , of six epoxy resins have been determined by DeLasi and Whiteside [6]. These results are plotted in Figure 8.4. They are compatible with the data of McKague [40] and satisfy the theoretical relation derived in Ref. [41, p. 69].

8.3 Modeling of Epoxy Properties

The observations of the preceding section are used for modeling the material properties of epoxy that are given by Eq. (8.1).

The glass transition region of epoxy resin is not broad [6], therefore, a glass transition temperature is used instead. The temperature T_g is usually obtained by measuring the expansion of a specimen as function of temperature. The point where the epoxy stops expanding as temperature increases corresponds to the first deviation from the glassy state and is termed T_g .

According to the experimental data plotted in Figure 8.4, T_g is strongly dependent on absorbed moisture. These results show that, as the moisture content of epoxy

increases, the transition temperature moves to the left in Figures 8.1-8.3. Hence, the abrupt change of the material properties starts at a lower temperature as the moisture content increases. This fact and the conclusions reached by previous investigators [12] suggest that the following modelings of E'_m , ν'_m , and η'_m are appropriate,

$$E'_m = E'_o \, f \left[\frac{T - T_o}{T_g - T_o} \right] \quad (8.2)$$

$$\nu'_m = \nu'_o \, g \left[\frac{T - T_o}{T_g - T_o} \right] \quad (8.3)$$

$$\eta'_m = \eta'_o \, h \left[\frac{T - T_o}{T_g - T_o} \right] \quad (8.4)$$

where the temperature T_o is equal to 273K. The moisture concentration appears implicitly in T_g . The glass transition temperature is represented by

$$T_g = 210 \exp(-9c) \quad (^\circ\text{C}) \quad (8.5)$$

where c is the moisture concentration.

This modeling has been chosen so that it does not represent the material properties beyond T_g , since the study of epoxy in the rubbery stage is not within the scope of this research. Equations (8.2)-(8.4) are valid only for

the continuous parts of the curves plotted in Figures 8.1-8.3. •

8.4 Results

All test specimens are conditioned in a constant relative humidity environment until moisture equilibrium is reached. Then, the test pieces undergo the impulse hammer technique and the four-point flexure tests to determine the storage moduli, the material damping, and Poisson's ratio at several temperature and moisture contents.

8.4.1 Complex Moduli of Epoxy

Storage modulus. The experimental data on the storage modulus of epoxy in term of temperature at three different equilibrium moisture concentrations are plotted in Figure 8.5. It can be concluded that increase in either temperature or moisture content or both results in a decrease in the storage modulus. Plotting these data in terms of moisture content in Figure 8.6 does not lead to any additional insight. But, representing these results in term of the following normalized non-dimensional temperature

$$T_n = \frac{T - T_o}{T_g - T_o} \quad (8.5)$$

in Figure 8.7 shows a clear trend. Experimental studies have shown that the modulus of polymer is very low at the glass transition temperature, therefore, adding the value $E_m = 0$ for $T = T_g$ to the data yields the following modeling

$$E'_m = 4.0(1 - T_n^2) \quad (\text{GPa}) \quad (8.6)$$

Material damping. Similarly, the experimental data of the hygrothermal effects on the damping of epoxy are plotted in three Figures (8.8-8.10). There is very little change in damping for all the considered conditions. Therefore, it is proposed to let

$$\eta_m = 0.018 \quad (8.7)$$

for temperatures up to 80°C and moisture contents up to 5%. The conclusion that the hygrothermal effects on the damping of epoxy is negligible is qualitatively corroborated by Putter et al. [38]. A quantitative comparison cannot be made since these researchers have not included in their publication the values of the fiber volume fraction and moisture content of the test specimens.

Poisson's ratio. The experimental values of the Poisson's ratio in terms of temperature at two different

moisture contents, are plotted in Figure 8.11. These results show that Poisson's ratio increases at a negligible rate as temperature varies from 0 to 80°C. Representing the same data in terms of the moisture content up to $M = 4.5\%$ (Figure 8.12) shows that the moisture effect is also negligible. Therefore,

$$\nu'_m = 0.32 \quad (8.8)$$

for temperatures up to 80°C and moisture contents up to 5%. Since ν'_m equals 0.5 at the glass transition temperature ($T_n = 0$), the plot of Poisson's ratio versus the normalized temperature has been extrapolated as shown in Figure 8.13. The extrapolation displays a qualitative trend only.

8.4.2 Complex Moduli of Composites

The complex moduli of Glass/Epoxy and Graphite/Epoxy in terms of moisture content and temperature can be determined by using the fibers' properties given in Table 7.2, Eqs. (8.6) through (8.8) and the micromechanics formulas (Eqs. (3.20)).

This procedure is illustrated by determining the storage moduli and the damping of a Glass/Epoxy lamina with a fiber volume fraction of 0.5 and a Graphite/Epoxy lamina with a fiber volume fraction of 0.7.

Glass/Epoxy. The parameters E'_{11} , E'_{22} , G'_{12} , η_{11} , η_{22} , η_G , and ν'_{12} versus the normalized temperature are plotted in Figures 8.14-17. The experimental data substantiate the theoretical results.

Graphite/Epoxy. Similarly, E'_{11} , E'_{22} , G'_{12} , η_{11} , η_{22} , η_G , and ν'_{12} versus the normalized temperature of Graphite/Epoxy are plotted in Figures 8.18-21.

For both Glass/Epoxy and Graphite/Epoxy, the results show that the matrix-dominated parameters (E'_{22} and G'_{12}) are strongly affected by moisture and temperature, while the fiber-dominated parameters (E'_{11} , ν'_{12}) stay practically constant.

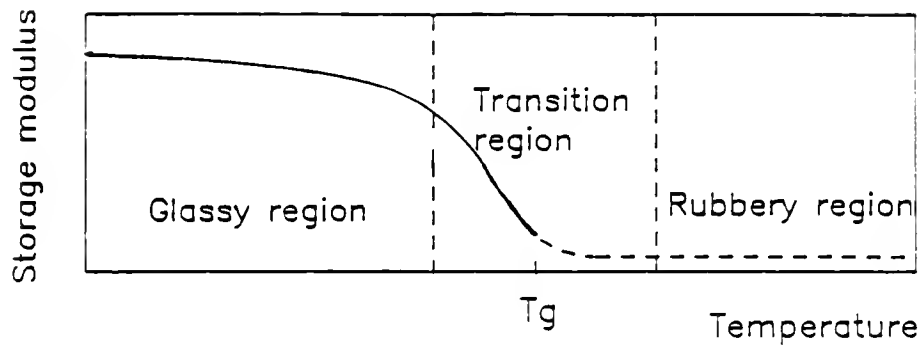


Fig. 8.1 Schematic variation of the storage modulus of epoxy with temperature.

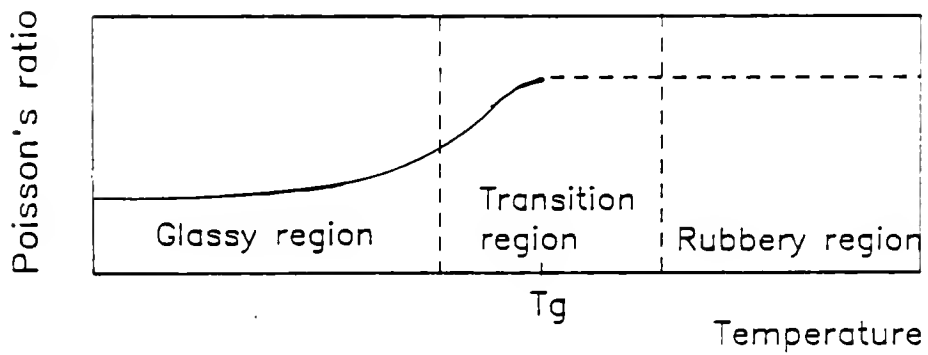


Fig. 8.2 Schematic variation of Poisson's ratio of epoxy with temperature.

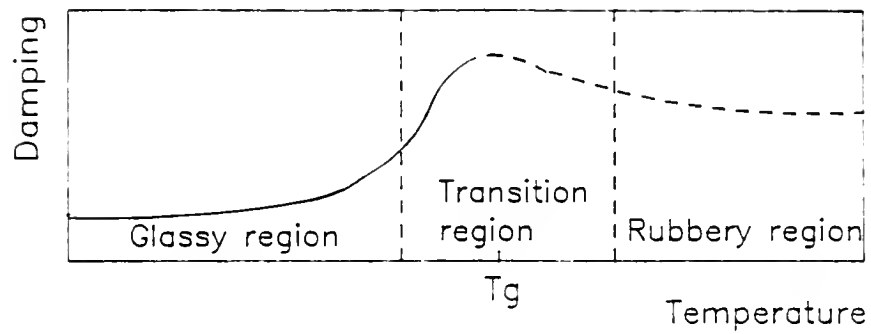


Fig. 8.3 Schematic variation of damping of epoxy with temperature.

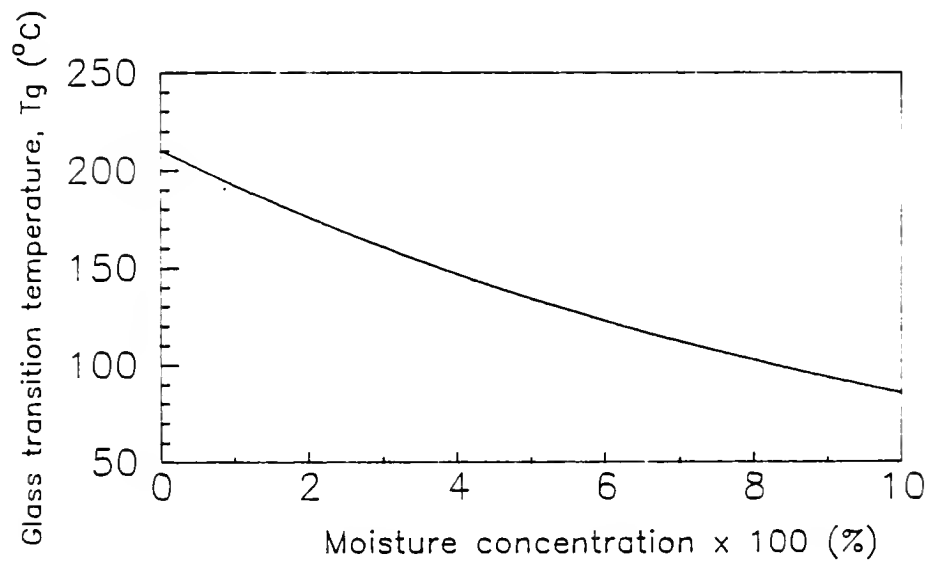


Fig. 8.4 Glass transition temperature of epoxy. From DeIasi and Whiteside [6].

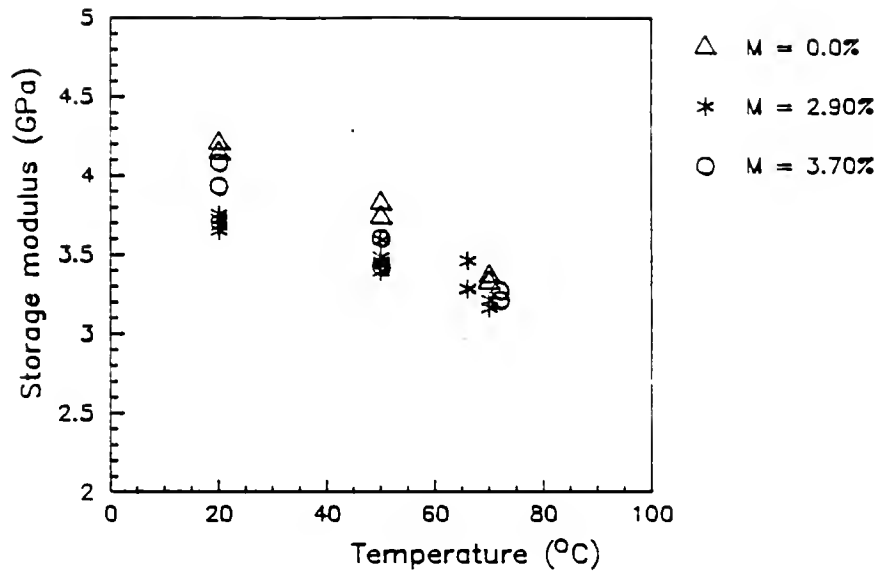


Fig. 8.5 Experimental data of the storage modulus of epoxy as a function of temperature at diverse constant moisture contents.

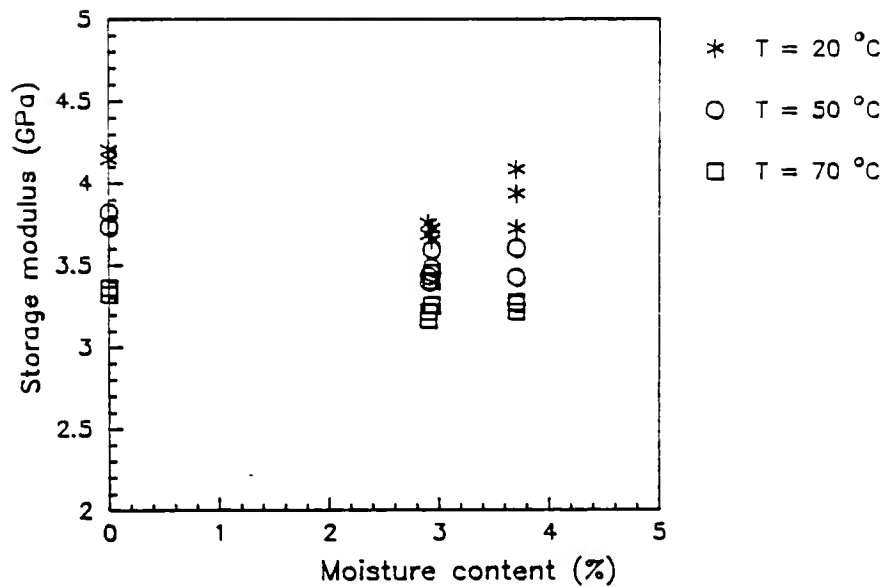


Fig. 8.6 Experimental data of the storage modulus of epoxy as a function of moisture content at diverse constant temperatures.

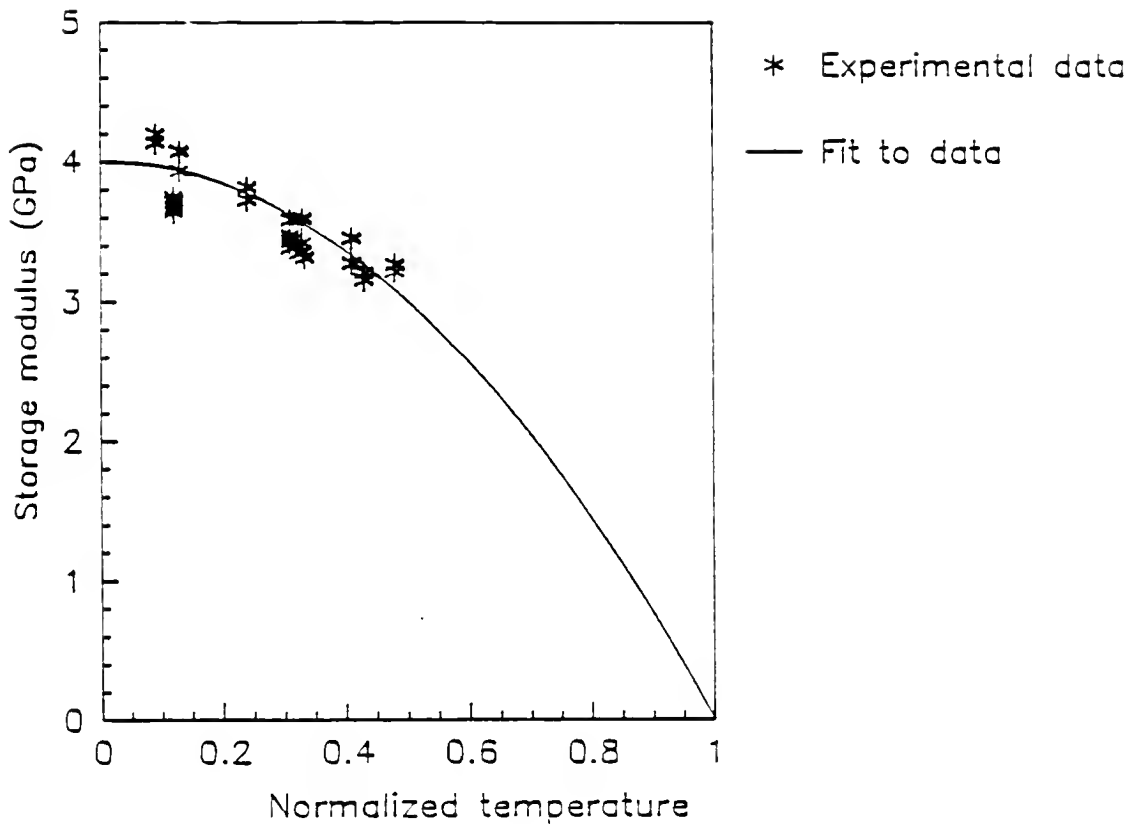


Fig. 8.7 Experimental data of the storage modulus of epoxy as a function of normalized temperature $(T - T_o)/(T_g - T_o)$

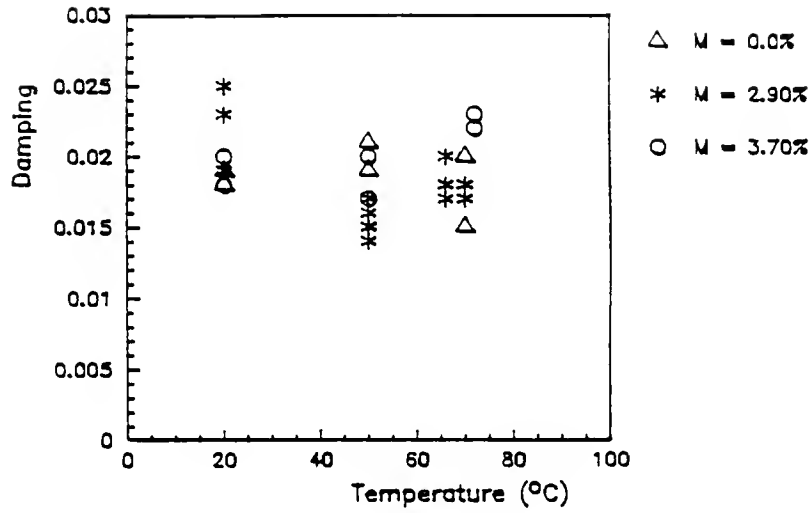


Fig. 8.8 Experimental data of damping of epoxy as a function of temperature at diverse constant moisture contents.

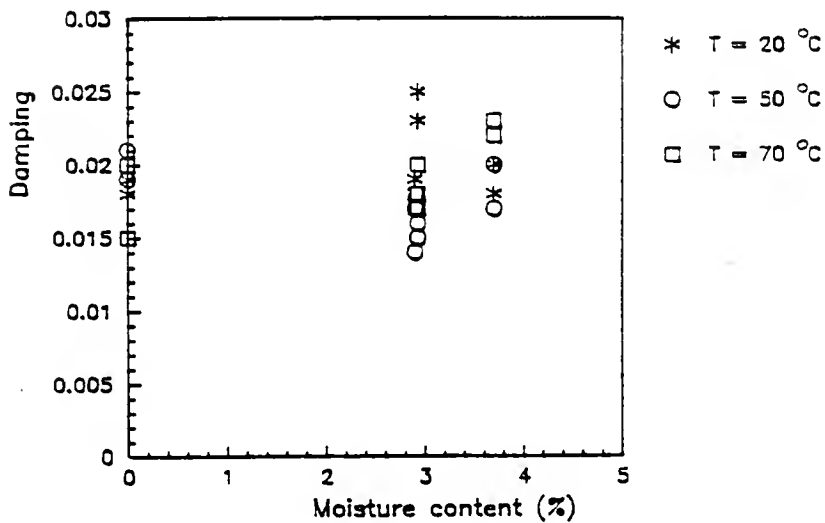


Fig. 8.9 Experimental data of damping of epoxy as a function of moisture content at diverse constant temperatures.

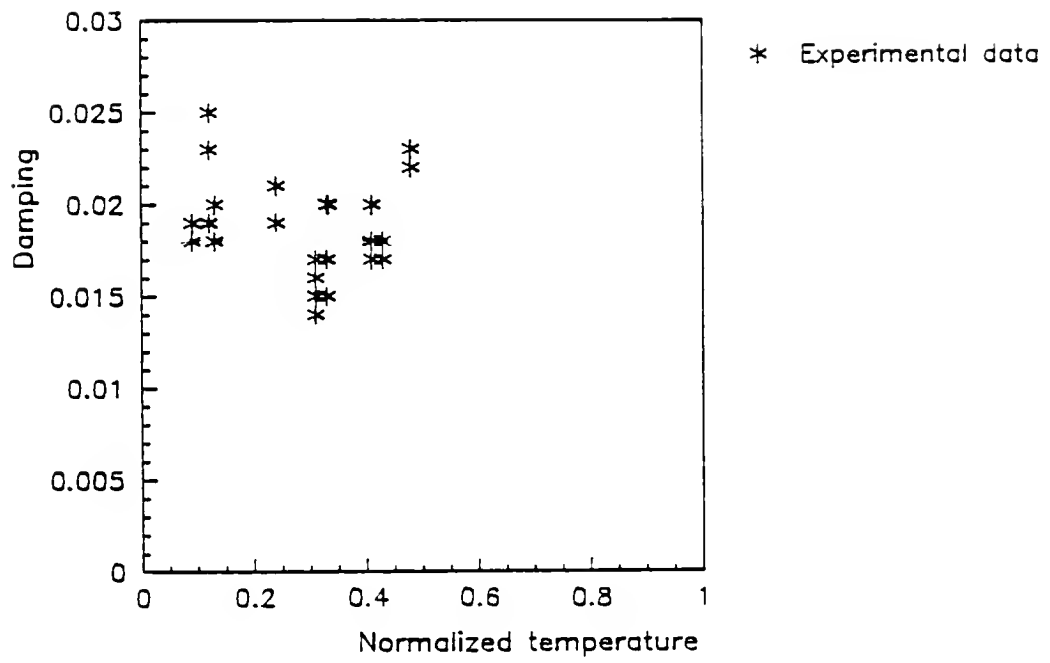


Fig. 8.10 Experimental data of the storage modulus of epoxy as a function of normalized temperature $(T - T_o)/(T_g - T_o)$

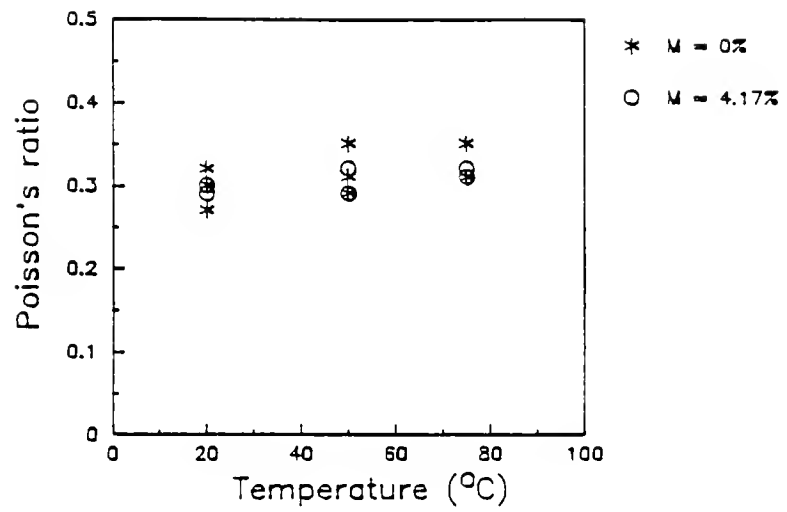


Fig. 8.11 Experimental data of Poisson's ratio of epoxy in term of temperature

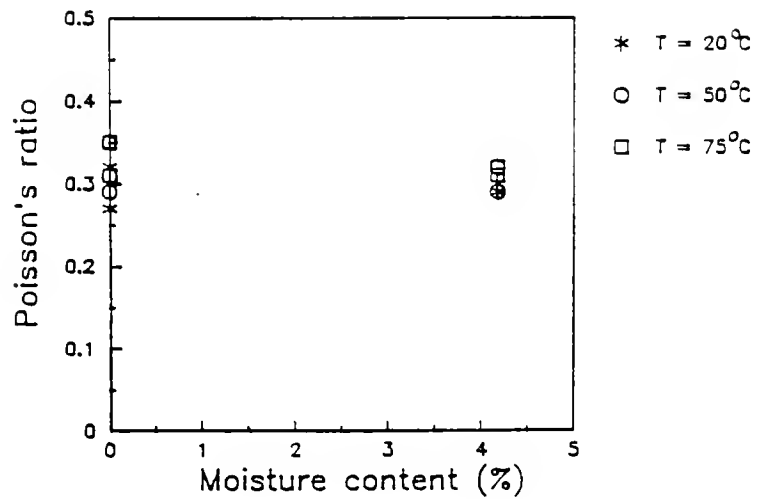


Fig. 8.12 Experimental data of Poisson's ratio of epoxy in term of moisture content.

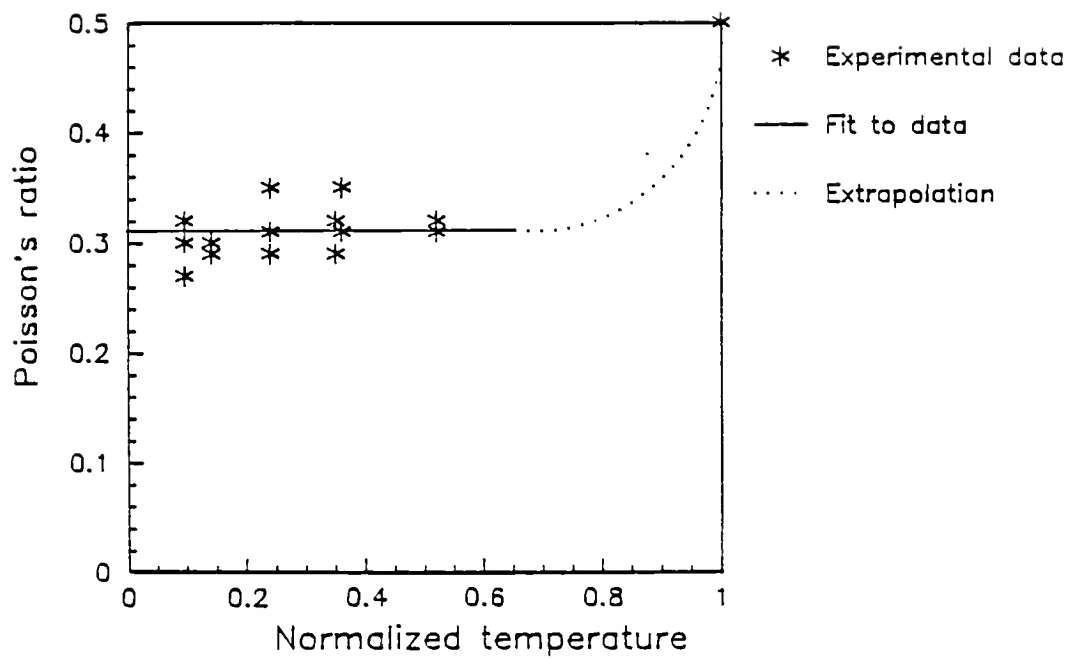


Fig. 8.13 Experimental data of Poisson's ratio in term of the normalized temperature $T_n = (T - T_o)/(T_g - T_o)$.

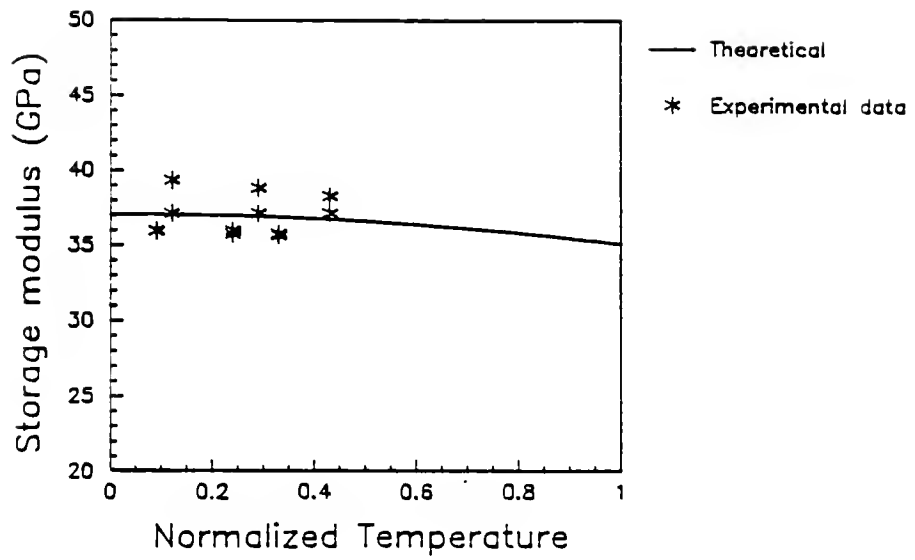


Fig. 8.14 Longitudinal storage modulus (E'_{11}) of Glass/Epoxy versus $T_n = (T - T_o)/(T_g - T_o)$.

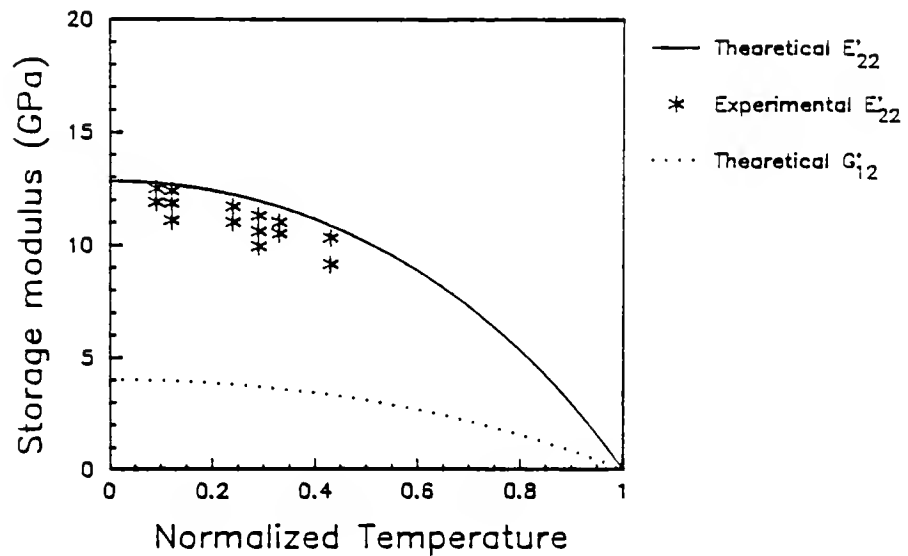


Fig. 8.15 Transverse (E'_{22}) and shear (G'_{12}) storage moduli of Glass/epoxy versus $T_n = (T - T_o)/(T_g - T_o)$.

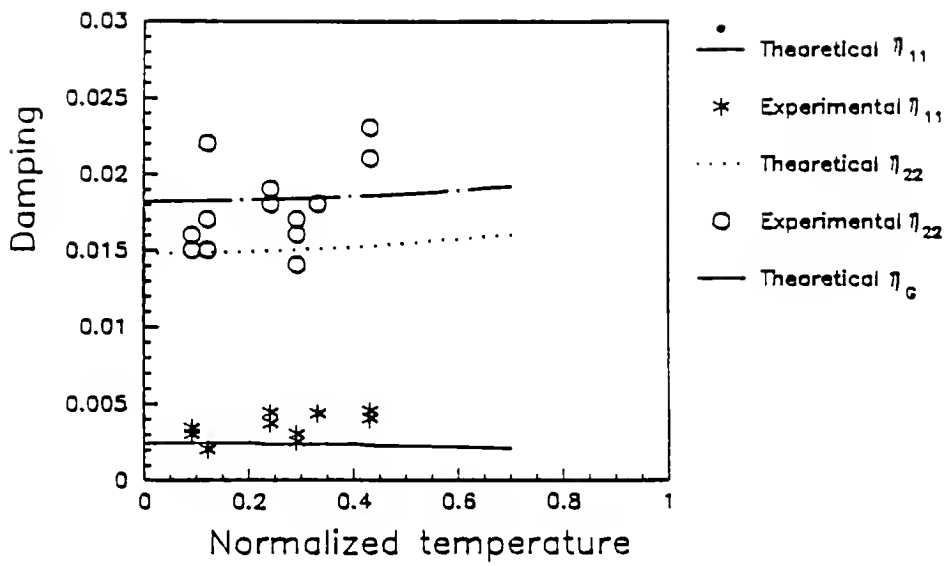


Fig. 8.16 Longitudinal (η_{11}), transverse (η_{22}), and shear (η_G) damping of Glass/Epoxy versus $T_n = (T - T_o)/(T_g - T_o)$.

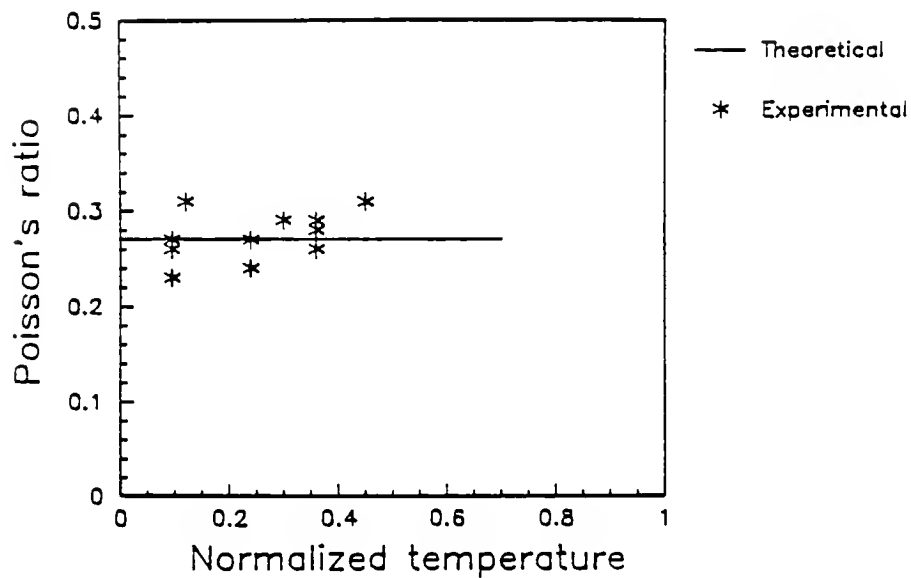


Fig. 8.17 Poisson's ratio (ν'_{12}) of Glass/Epoxy versus $T_n = (T - T_o)/(T_g - T_o)$.

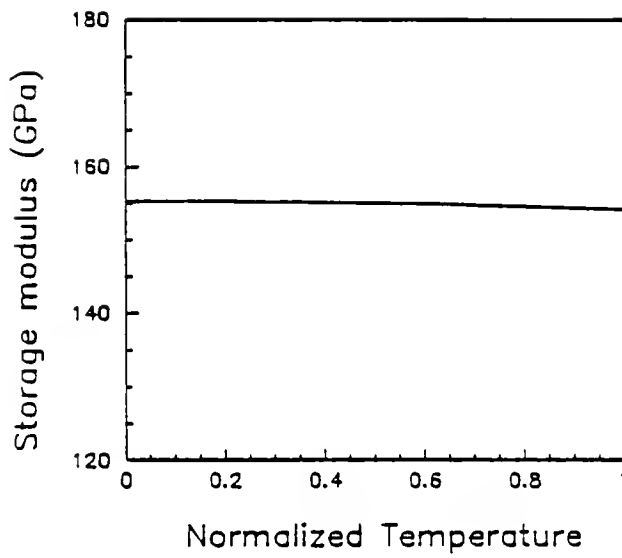


Fig. 8.18 Longitudinal storage modulus (E'_{11}) of Graphite/Epoxy versus $T_n = (T - T_o)/(T_g - T_o)$.

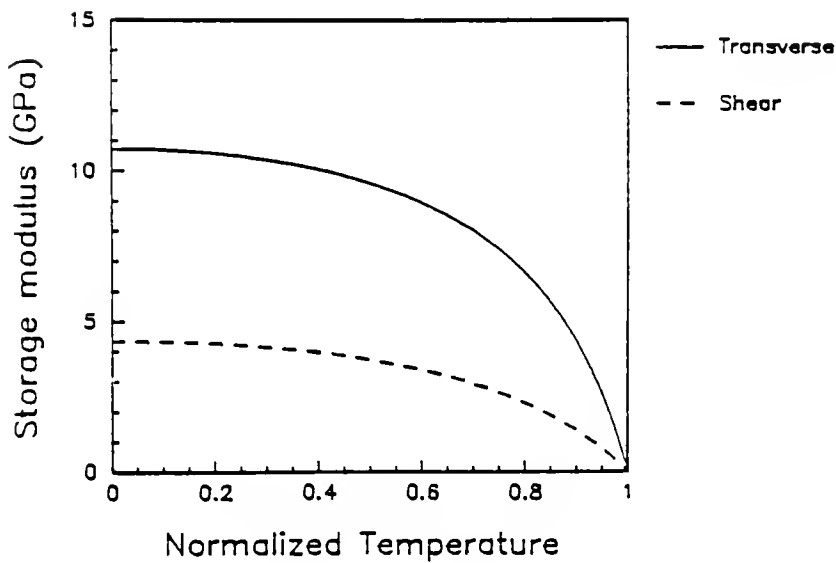


Fig. 8.19 Transverse (E'_{22}) and shear (G'_{12}) storage moduli of Graphite/epoxy versus $T_n = (T - T_o)/(T_g - T_o)$.

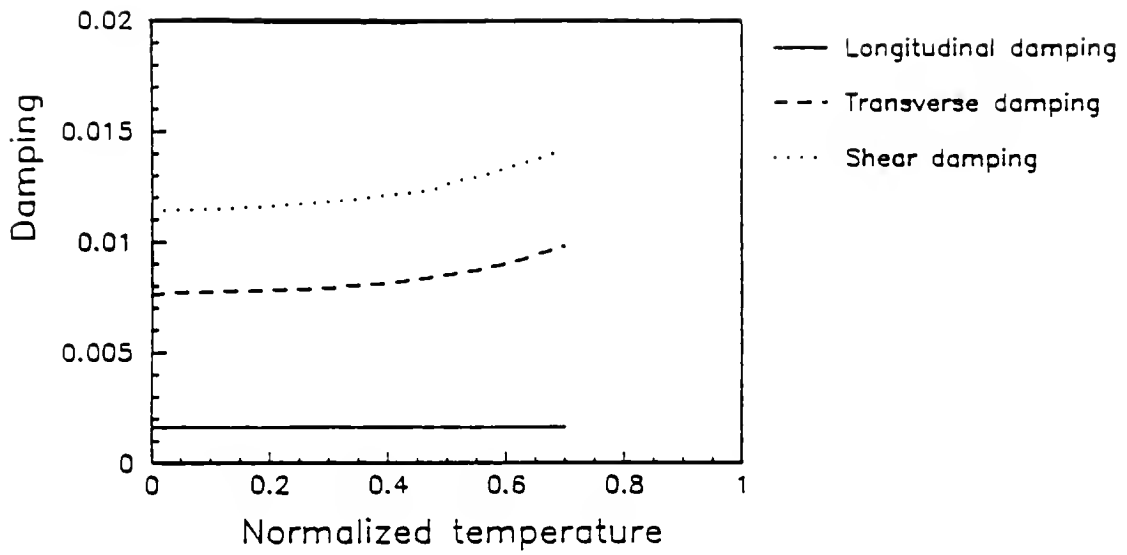


Fig. 8.20 Longitudinal (η_{11}), transverse (η_{22}), and shear (η_G) damping of Graphite/Epoxy versus $T_n = (T - T_o)/(T_g - T_o)$.

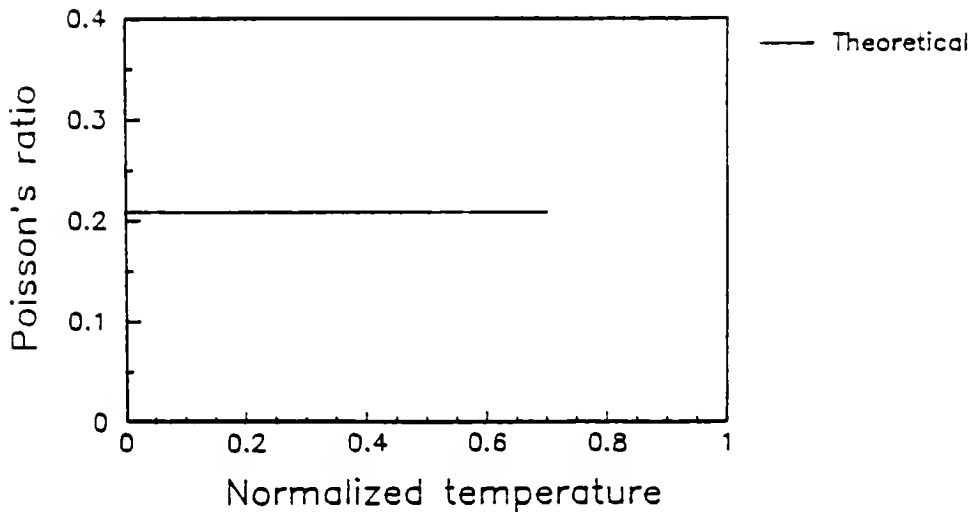


Fig. 8.21 Poisson's ratio (ν'_{12}) of Graphite/Epoxy versus $T_n = (T - T_o)/(T_g - T_o)$.

CHAPTER 9 HYGROTHERMAL EFFECTS ON STRESS FIELD

9.1 Introduction

The hygrothermal effects on the stress field are investigated by considering an infinitely long, finite width and symmetric composite laminate undergoing hygrothermal loadings. The Finite Element Method is used in order to estimate the magnitude of hygrothermal stresses in laminated composites (see Appendix B). The geometry of a laminate and the finite mesh of a quarter cross-section are shown in Figure 9.1 and the boundary conditions are given by

$$v = 0 \quad \text{for } (y,z) = (0,z)$$

(9.1)

$$w = 0 \quad \text{for } (y,z) = (y,0)$$

where v and w are the displacements in the y and z directions, respectively. The grid consists of 24 eight node isoparametric elements and 93 nodes. Only 24 elements

are used since increasing the number of elements to 48 results in a relatively small change in the stress magnitudes. The material properties in terms of temperature and moisture content have been derived in the preceding chapter. The constitutive equations are given by Eq. (B.12) and can be written in matrix form as

$$\{\sigma\} = [\bar{Q}](\{\epsilon\} - \{\alpha\}\Delta T - \{\beta\}c) \quad (9.2)$$

where $\{\alpha\}$ and $\{\beta\}$ are the vectors of thermal and moisture expansion coefficients.

9.2 Description of Study Cases

The considered stacking sequence is the $[(90/0)_2]_S$ lay-up. The cross-ply laminate is preferred over other laminate since hygrothermal loadings induce very high stresses in this case. The volume fiber fractions of the Glass/epoxy and the Graphite/Epoxy are 0.5 and 0.7, respectively. The thickness and the width of the laminates are assumed to be 2 mm and 20 mm, respectively.

Three cases of moisture gradients are applied. They are described in Figure 9.2 and Table 9.1. Cases A and C correspond to the dry and moisture saturated states, respectively. While the non-uniform moisture gradient (case B) corresponds to a moisture profile as derived in section 2.3. Two uniform temperatures (20°C and 80°C) are

used. All laminates are assumed to be initially (dry at 20°C) free of stress. Hence, residual stresses are not taken into account. The elastic moduli used in computing the stresses are approximated by the real parts of the complex moduli. Therefore, the hygrothermal effects on the elastic properties can be deduced from the results given in Chapter 8

9.3 Numerical Results and Discussion

For all considered cases, the following remarks can be drawn: at $z/h = \text{constant}$, the stresses away from the free edge stay constant and the shear stress (σ_{yz}) is zero, but, as y/b approaches 1, σ_{yz} takes significant non-zero values and there are small variations in the values of the other stresses. Hence, the stresses σ_y , σ_z and σ_x are plotted across the section of the laminate at $y/b = 0.472$ and the shear stress σ_{yz} is plotted across the section at $y/b = 0.993$ (close to the free edge).

The stresses are compared to typical strengths of Glass/Epoxy and Graphite/Epoxy that are provided in Table 9.2.

9.3.1 Glass/Epoxy

The equilibrium moisture concentration, c_∞ , of the Glass/Epoxy material is 0.025.

The stress σ_y is plotted in Figure 9.3. It reaches a maximum magnitude of 166 MPa. for case C at 20°C. It is compressive for the 0° layer and tensile for the 90° layer.

The stress σ_z is shown in Figure 9.4. It is compressive everywhere and reach a magnitude of 288 MPa. for the case C at 20°C. The stress σ_x is also compressive (Figure 9.5) and reaches a maximum of 245 MPa.. The free edge shear stress σ_{yz} (Figure 9.6) is very significant since its maximum magnitude is about 80 MPa..

9.3.2 Graphite/Epoxy

The equilibrium moisture concentration c_∞ for these cases is 0.015. The stresses σ_y , σ_z , σ_x , and σ_{yz} are plotted in Figures 9.7-10. These results show the same trend as for the Glass/Epoxy cases. However, since the moisture concentration is lower and graphite fibers have stiffer moduli and lower coefficient of thermal expansion, the magnitude of the stresses is smaller.

9.3.3 Summary

The hygrothermal conditions used in the preceding sections are practically achieved only under very adverse conditions. Hence, the induced stresses can be considered

an upper bound for hygrothermal stresses. The results yield the following observations:

1) The stresses induced by temperature only (dry at 80°C) are much smaller than those induced by high moisture content.

2) The stresses due to a non-uniform moisture gradient can be as high as those induced by the saturated moisture case.

3) Since the hygrothermal conditions degrade the modulus of the epoxy matrix, the stresses caused by the most severe hygrothermal condition (moisture case C at 80°C) are lower than for some of the other cases.

4) The hygrothermal stresses of the cross-ply laminates are very significant since their magnitude is of the same order of those of the strengths given in Table 9.2.

Table 9.1 Description of cases in Figure 9.2.

Case	Description
A	Dry
B	$(M - M_i)/(M_\infty - M_i) = 0.5$ (absorption cycle)
C	$(M - M_i)/(M_\infty - M_i) = 1.0$ (fully saturated)

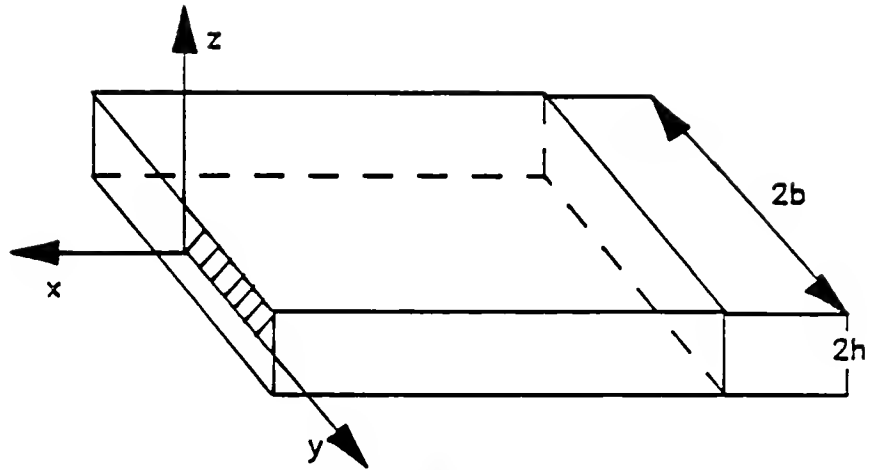
Table 9.2 Typical strengths of Glass/Epoxy and Graphite/Epoxy

Strengths (MPa.)	Glass/Epoxy	Graphite/Epoxy
X_t	1000.0	1200.0
X_c	1000.0	700.0
Y_t	30.0	40.0
Y_c	140.0	70.0
S	40.0	70.0

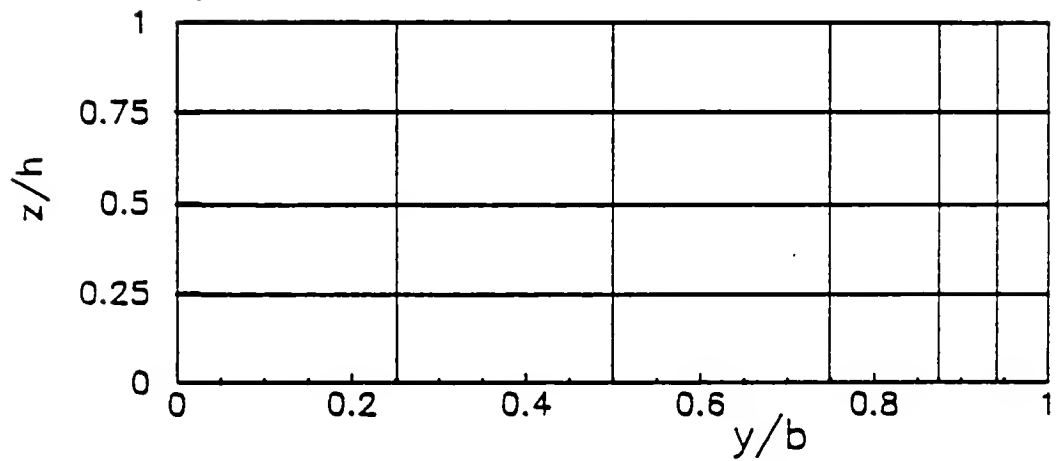
X_t (X_c) = Longitudinal strength in tension (compression)

Y_t (Y_c) = Transverse strength in tension (compression)

S = Shear strength.



Geometry of laminate



Finite element mesh of shaded area

Fig. 9.1 Geometry of a laminate and finite mesh of a 1/4 cross-section area.

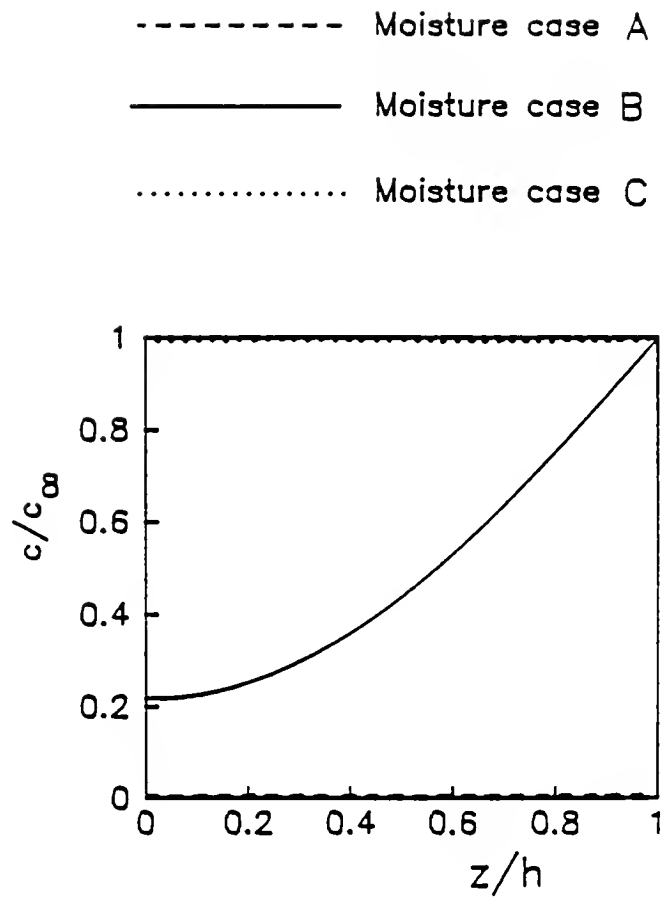


Fig. 9.2 Description of the applied moisture gradients.

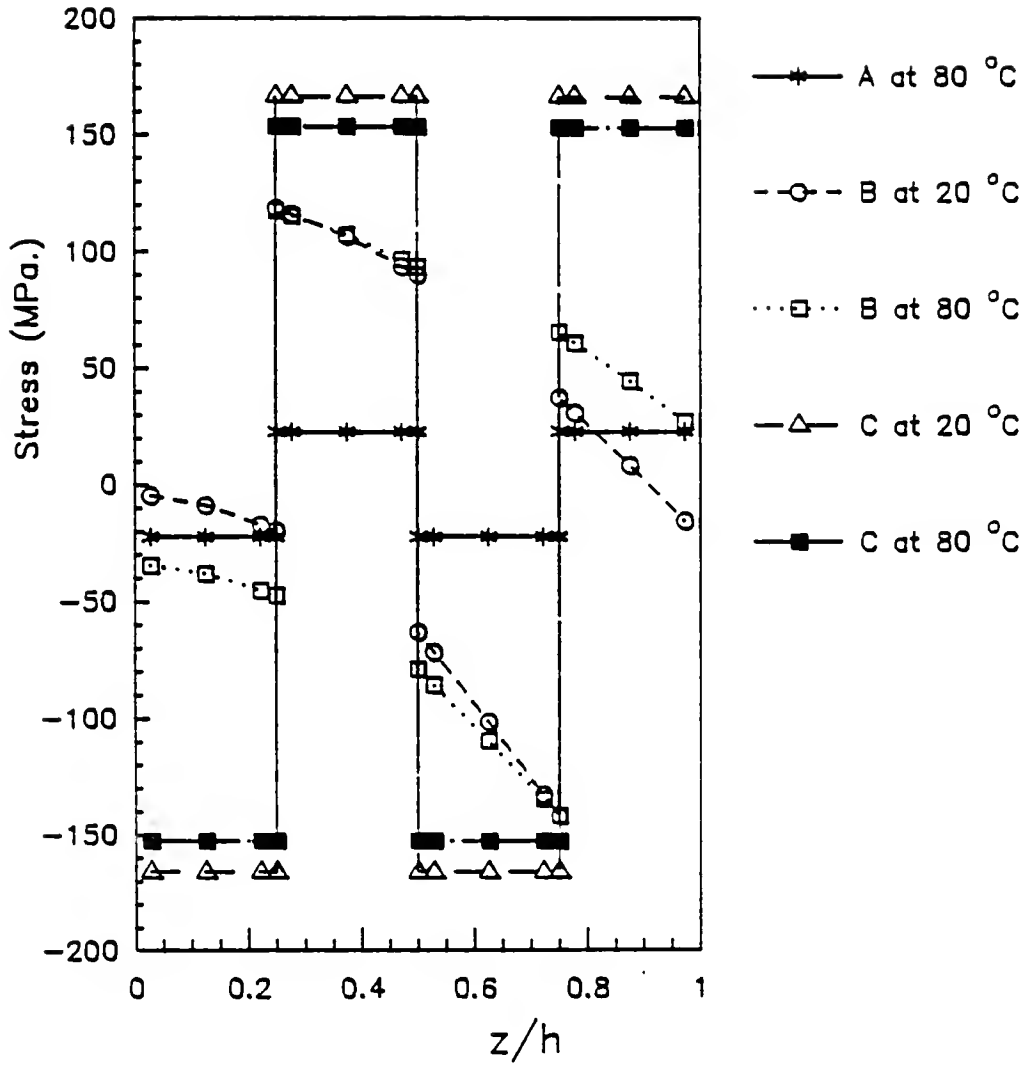


Fig. 9.3 Profile of the hygrothermal stress σ_y across a $[(90/0)_2]_s$ Glass/Epoxy laminate at $y/b = 0.472$.

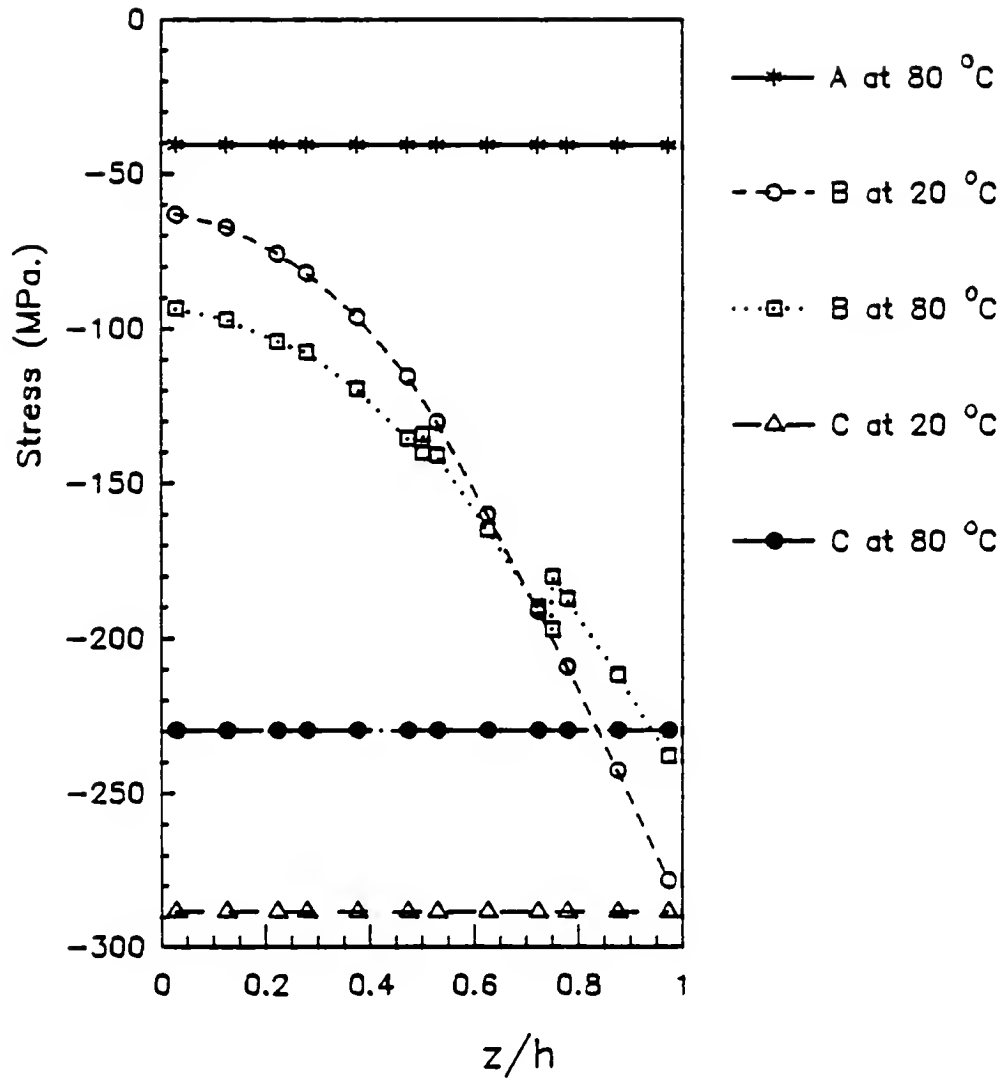


Fig. 9.4 Profile of the hygrothermal stress σ_z across a $[(90/0)_2]_s$ Glass/Epoxy laminate at $y/b = 0.472$.

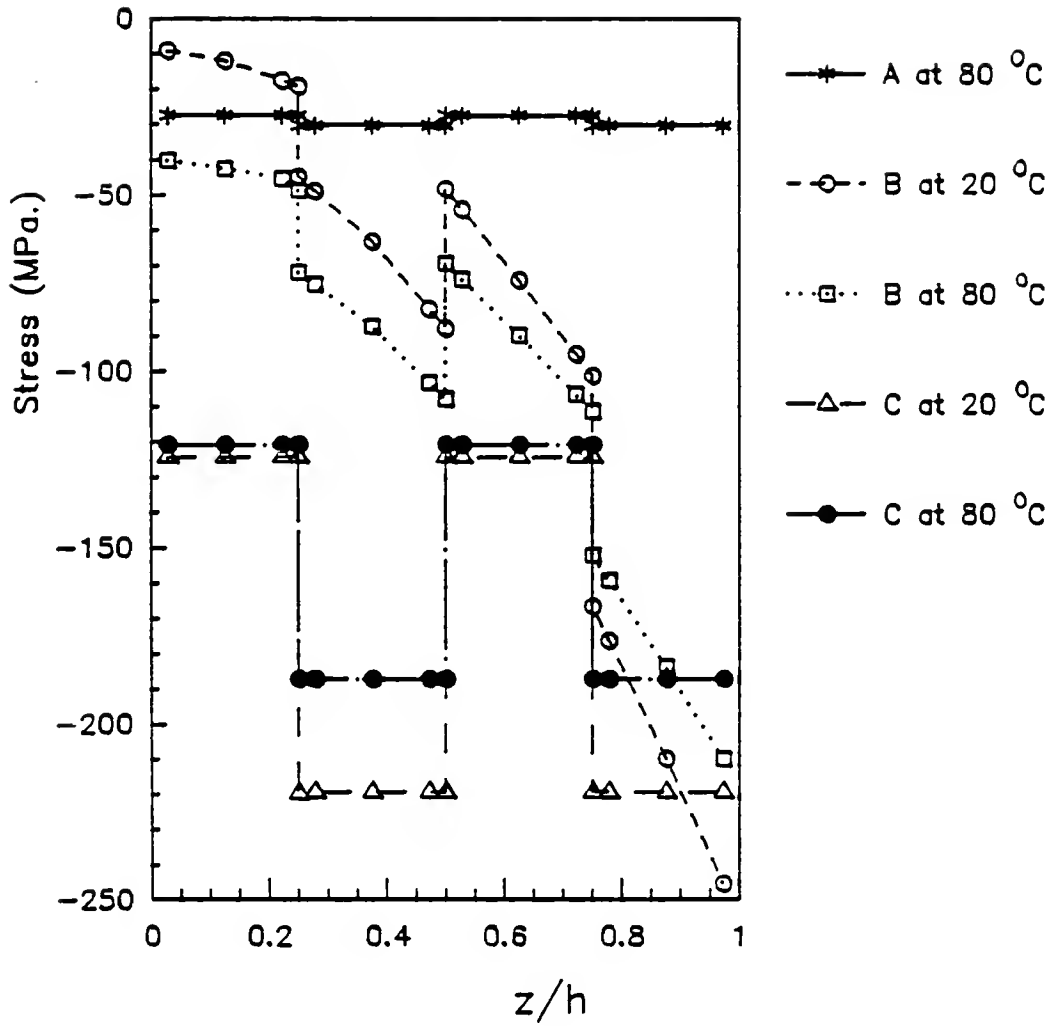


Fig. 9.5 Profile of the hygrothermal stress σ_x across a $[(90/0)_2]_s$ Glass/Epoxy laminate at $y/b = 0.472$.

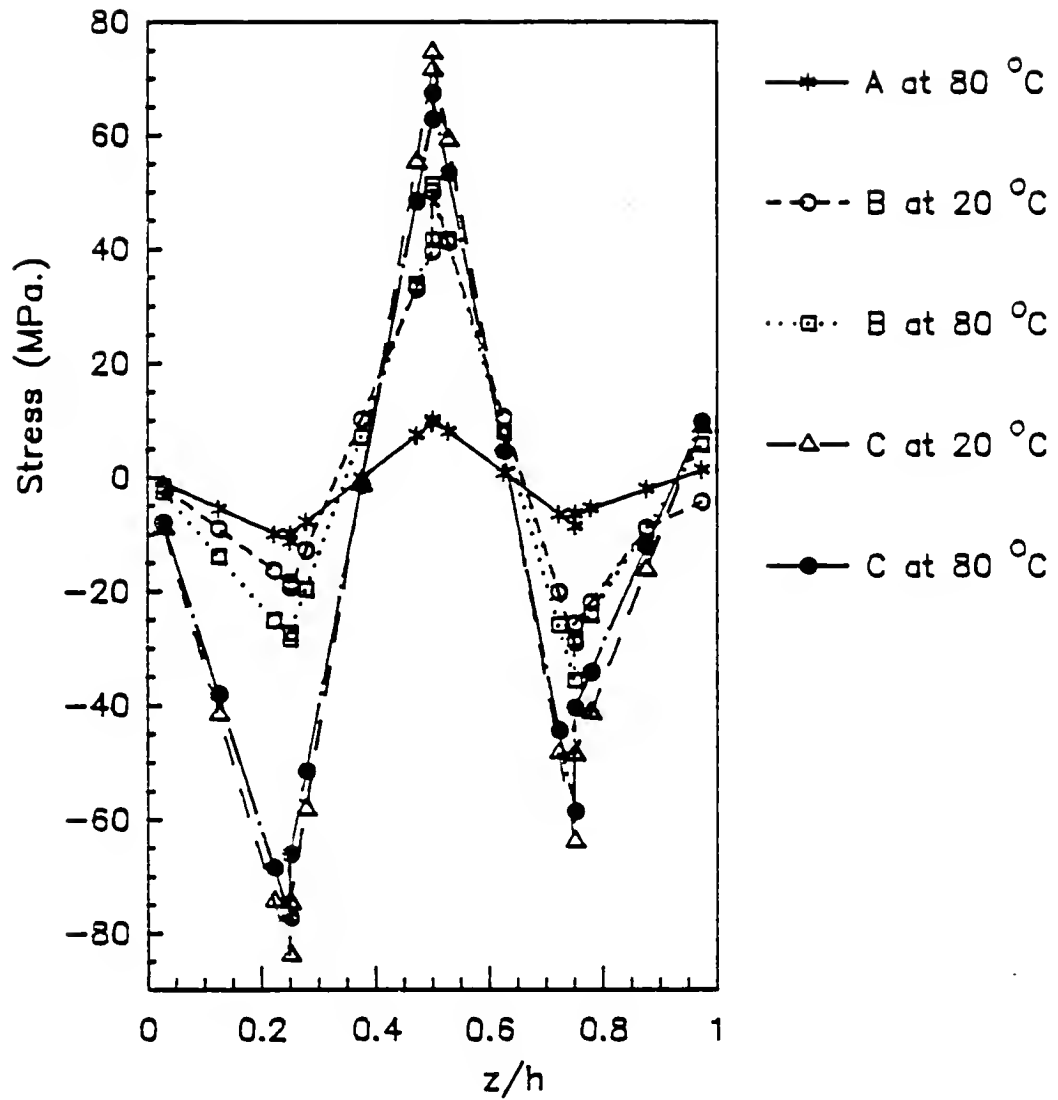


Fig. 9.6 Profile of the hygrothermal stress σ_{yz} across a $[(90/0)_2]_s$ Glass/Epoxy laminate at $y/b = 0.993$.

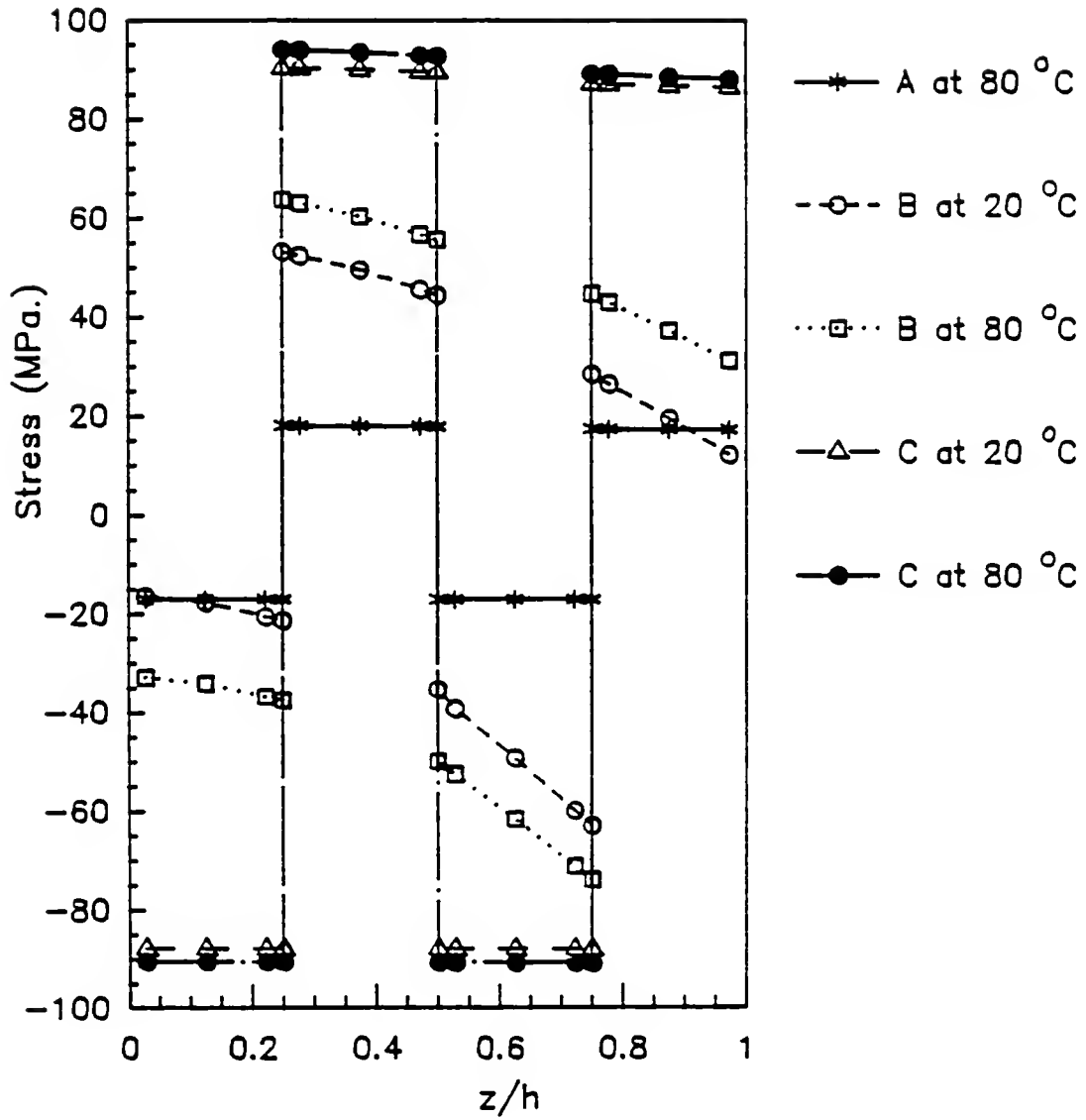


Fig. 9.7 Profile of the hygrothermal stress σ_y across a $[(90/0)_2]_s$ Graphite/Epoxy laminate at $y/b = 0.472$.

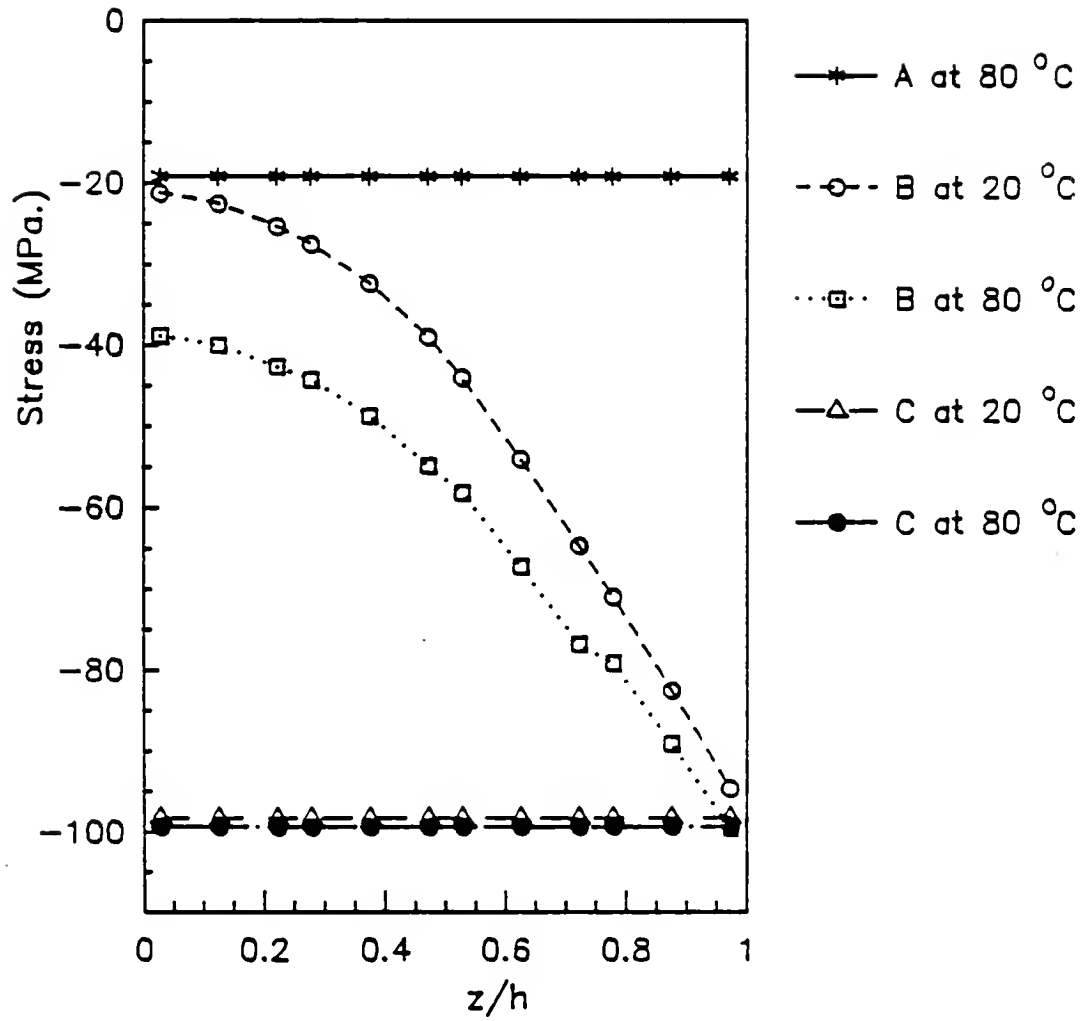


Fig. 9.8 Profile of the hygrothermal stress σ_z across a $[(90/0)_2]_s$ Graphite/Epoxy laminate at $y/b = 0.472$.

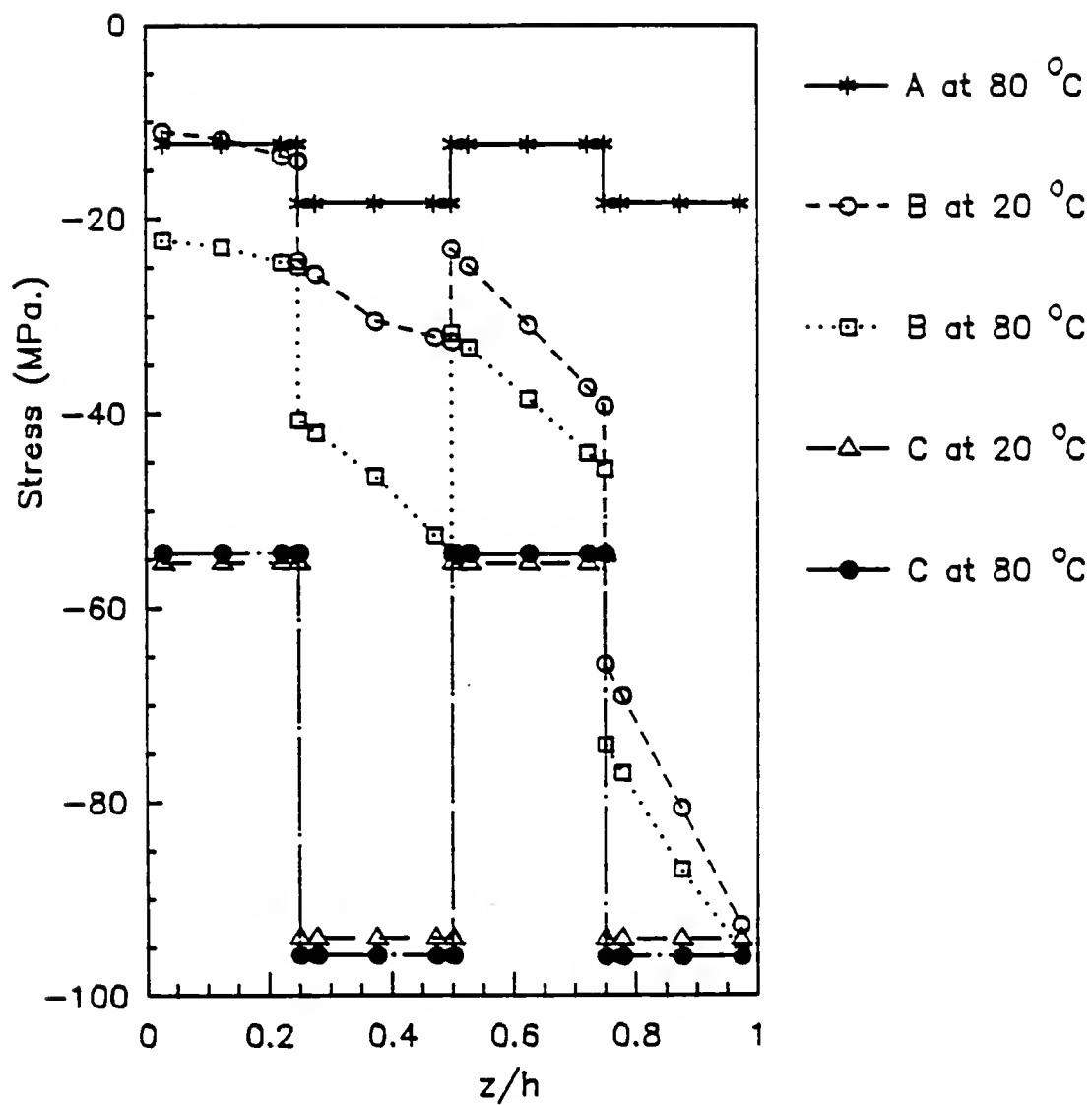


Fig. 9.9 Profile of the hygrothermal stress σ_x across a $[(90/0)_2]_s$ Graphite/Epoxy laminate at $y/b = 0.472$.

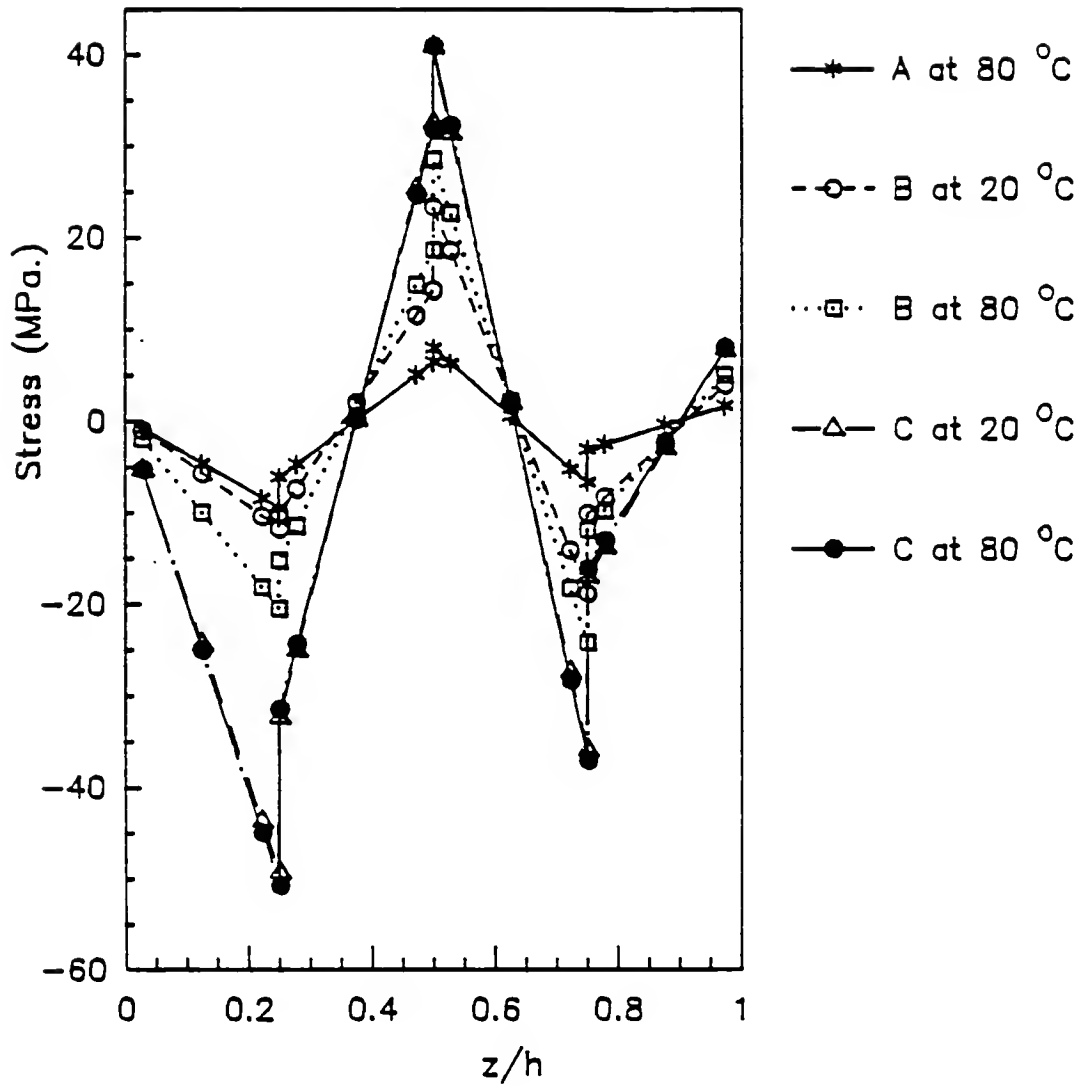


Fig. 9.10 Profile of the hygrothermal stress σ_{yz} across a $[(90/0)_2]_s$ Graphite/Epoxy laminate at $y/b = 0.993$.

CHAPTER 10 HYGROTHERMAL EFFECTS ON COMPLEX STIFFNESSES

10.1 Introduction

The hygrothermal effects on the in-plane (A_{ij}^*) and the bending (D_{ij}^*) complex stiffnesses of Glass/Epoxy and Graphite/Epoxy angle-ply $[(\pm\theta)_2]_S$ laminates are investigated. The applied moisture gradients are the cases A, B, and C that are given in section 9.2 and the uniform applied temperatures are 20°C and 80°C . The material properties in terms of moisture content and temperature have been determined in Chapter 8. The fibers properties are given in Table 7.2. The theoretical expressions of A_{ij}^* and D_{ij}^* in terms of the fibers and matrix properties have been developed in Chapter 5 and Appendix A.

10.2 Numerical Results and Discussion

10.2.1 Glass/Epoxy

The fiber volume fraction of the Glass/Epoxy is 0.5 and the equilibrium moisture content c_∞ is 0.025. Since

the fibers do not absorb any moisture, the equilibrium moisture concentration of the matrix is 0.05. The thickness of the laminate is 2.0 mm and A_{ij}^* and D_{ij}^* are normalized with respect to 75.86×10^6 N/m and 25.29 N.m, respectively.

The real part of the longitudinal in-plane complex stiffness, A'_{11} , and its corresponding damping, $I\eta_{11}$, are plotted in Figure 10.2. As the moisture gradients and the temperature change, the relative changes of A'_{11} vary from 6% (for $\pm\theta = 0^\circ$) to 33% (for $\pm\theta = 90^\circ$). The line style legend of the figures of this chapter is defined in Figure 10.1.

Similarly, A'_{12} and $I\eta_{12}$ are plotted in Figure 10.3 and A'_{66} and $I\eta_{66}$ in Figure 10.4. All these cases show that the hygrothermal effects on A_{ij}^* is matrix dominated.

The real part of the bending stiffnesses, D_{ij}^* , and their corresponding damping, $F\eta_{ij}$, are plotted in Figures 10.5-7. These results yield similar conclusions to those of A_{ij}^* .

10.2.2 Graphite/Epoxy

The volume fraction of the Graphite/Epoxy laminate is 0.7 and its equilibrium moisture concentration c_∞ is 0.015. Since all the moisture is absorbed by the matrix, c_∞ of the epoxy is 0.050. The laminate is 2.0 mm thick.

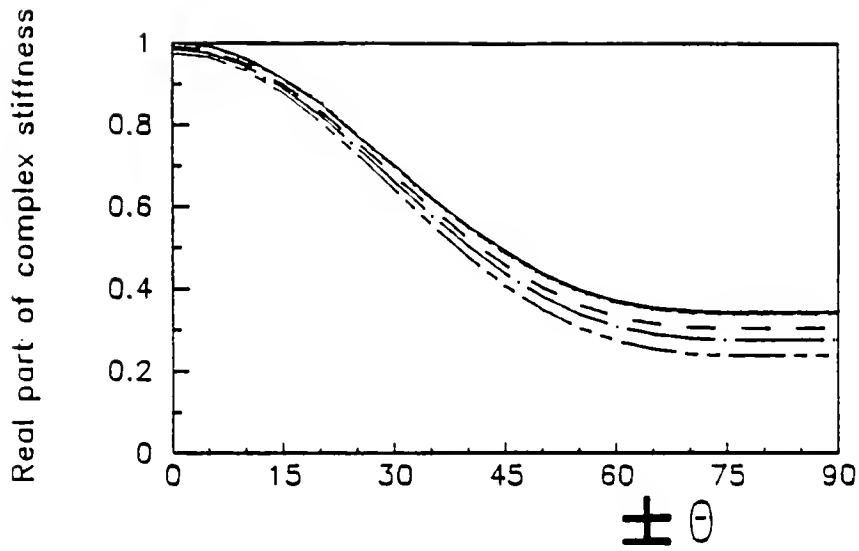
The real parts of the complex stiffnesses (A'_{ij} and D'_{ij}) and their corresponding damping ($I\eta_{ij}$ and $F\eta_{ij}$) are plotted in Figures 10.8-13. The terms A'_{ij} and D'_{ij} are normalized with respect to 311.3×10^6 N/m and 103.77 N.m, respectively. These results show the same tendency as those of Glass/Epoxy. Since the volume fraction and the longitudinal modulus of the graphite fibers are higher, the hygrothermal effects are less pronounced.

10.2.3 Summary

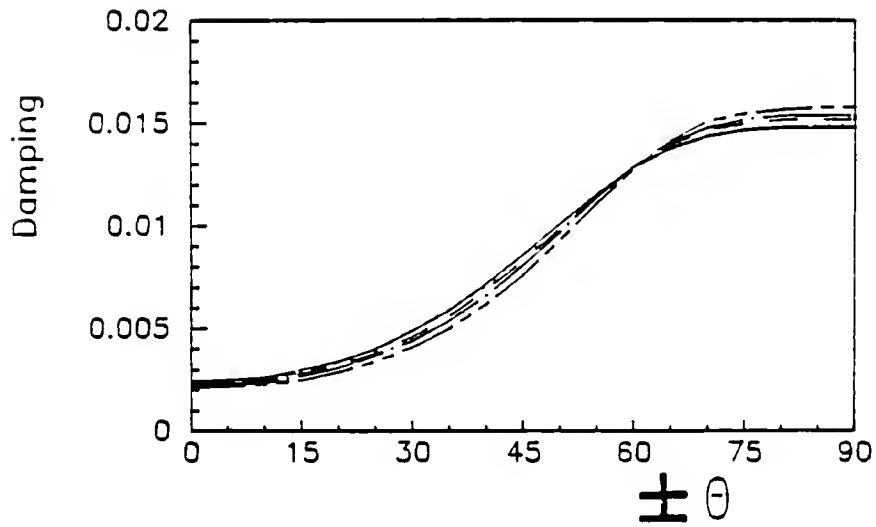
The effects of moisture on the stiffnesses A^*_{ij} 's and D^*_{ij} 's of composites at room temperature are negligible for all the considered cases. But, as temperature increases, the combined influence induces significant changes in the complex stiffnesses especially for the matrix dominated terms.

—————	Moisture gradient case A at 20°C
-----	Moisture gradient case B at 20°C
.....	Moisture gradient case C at 20°C
- - - - -	Moisture gradient case A at 80°C
——— · ———	Moisture gradient case B at 80°C
—— - - - ———	Moisture gradient case C at 80°C

Fig. 10.1 Line style legend of Figures 10.2-13.

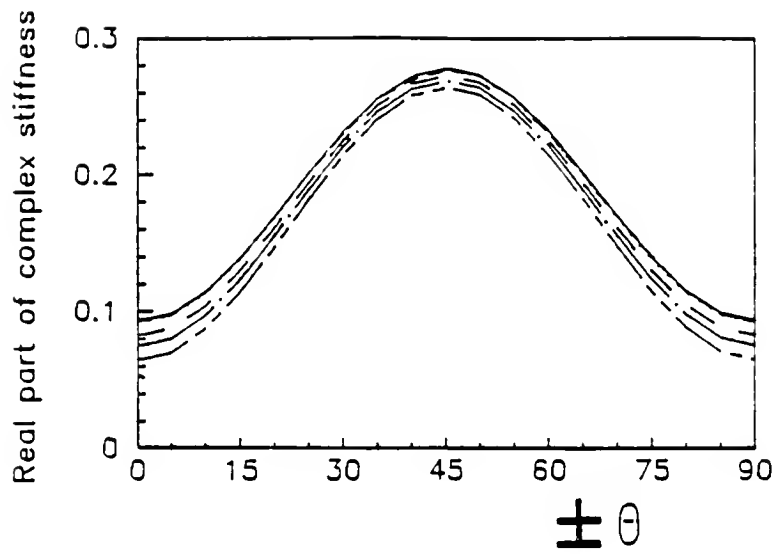


(a)

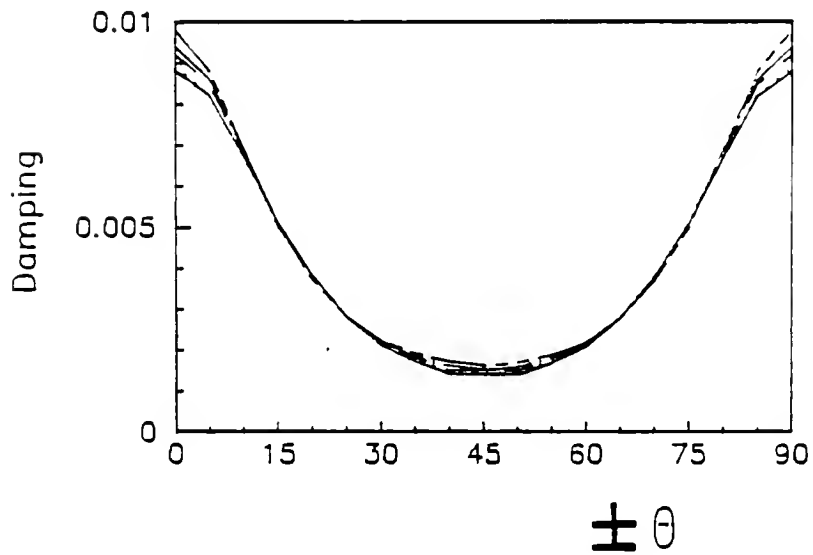


(b)

Fig. 10.2 Complex in-plane stiffness A_{11}^* of Glass/Epoxy.
 a) Non-dimensional Real part ; b) corresponding damping.

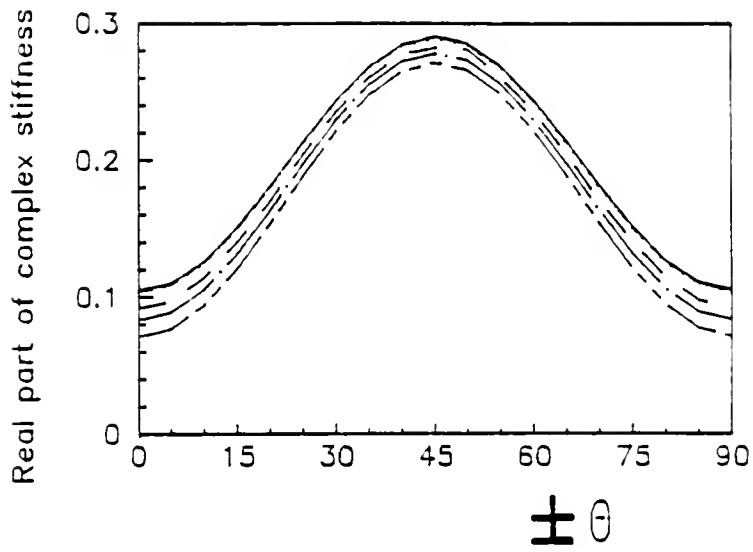


(a)

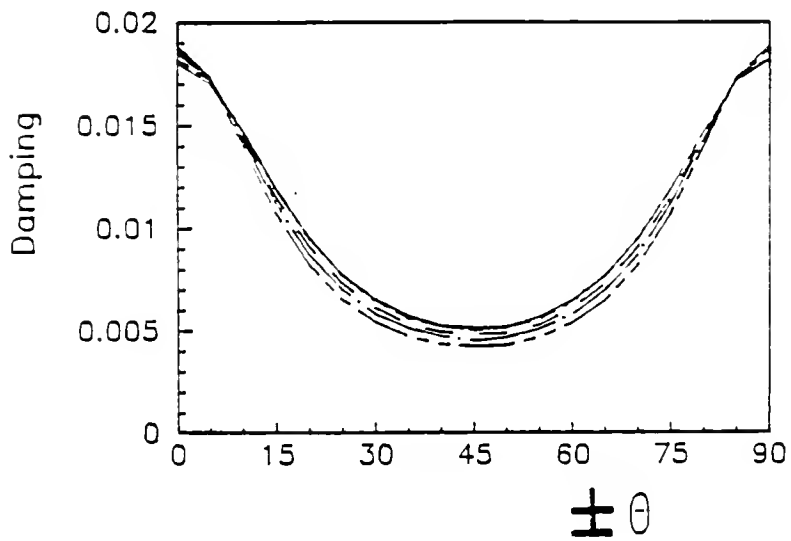


(b)

Fig. 10.3 Complex in-plane stiffness A_{12}^* of Glass/Epoxy.
 a) Non-dimensional Real part; b) corresponding damping.

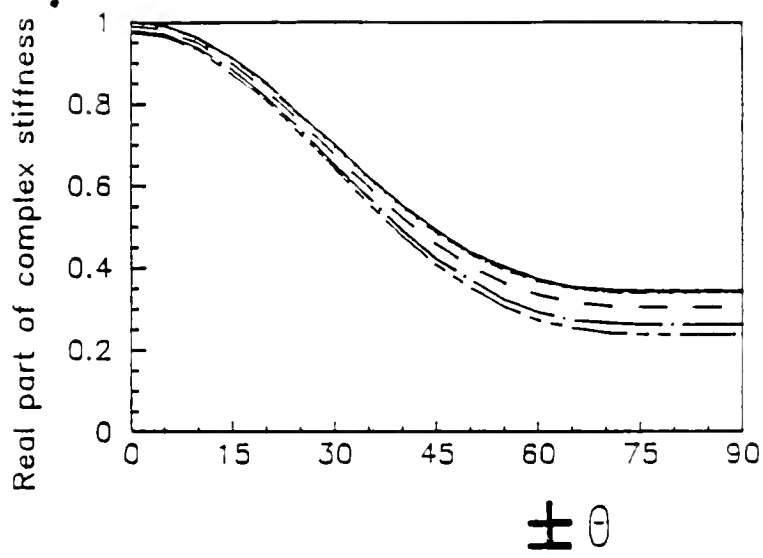


(a)

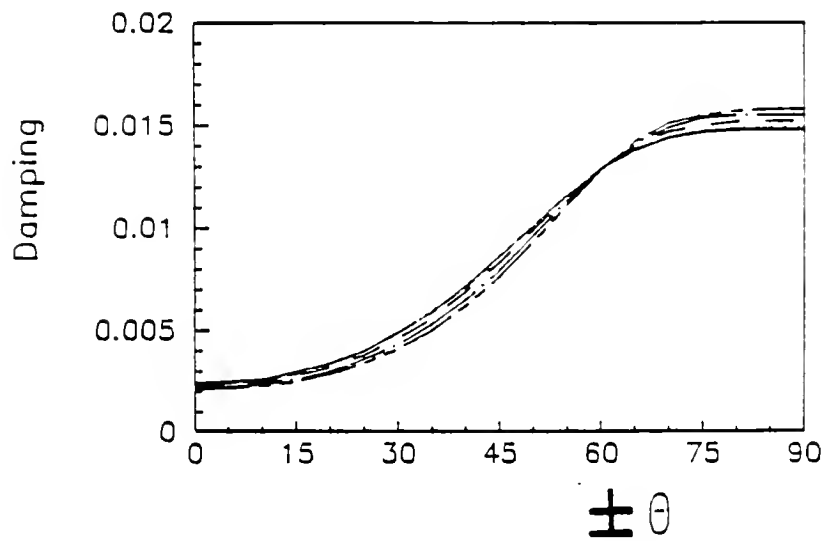


(b)

Fig. 10.4 Complex in-plane stiffness A_{66}^* of Glass/Epoxy.
 a) Non-dimensional Real part; b) corresponding damping.

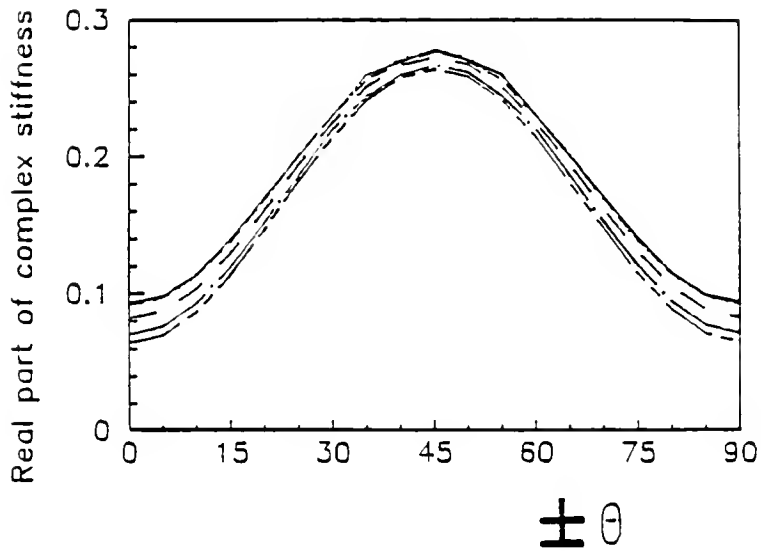


(a)

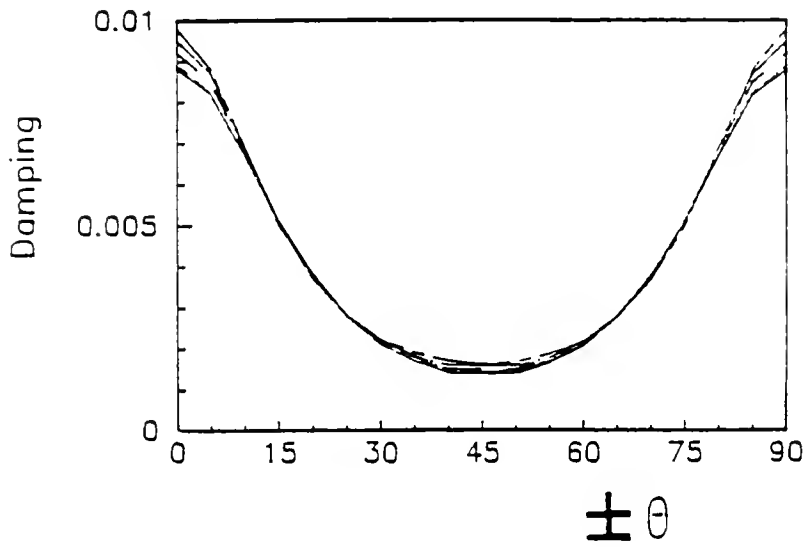


(b)

Fig. 10.5 Complex bending stiffness D_{11}^* of Glass/Epoxy.
 a) Non-dimensional Real part; b) corresponding damping.

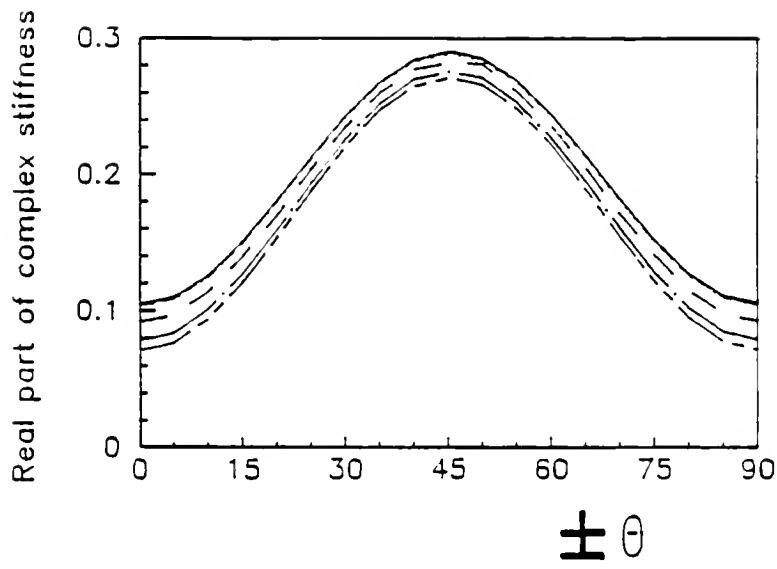


(a)

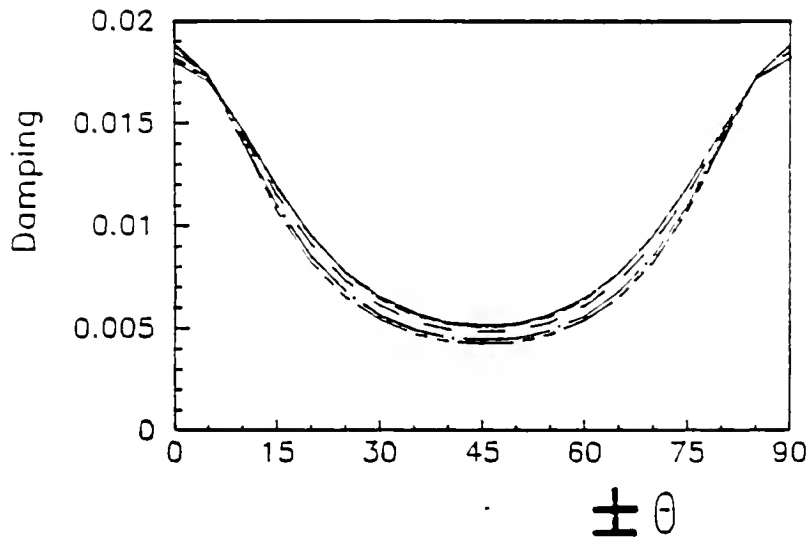


(b)

Fig. 10.6 Complex bending stiffness D_{12}^* of Glass/Epoxy.
 a) Non-dimensional Real part; b) corresponding damping.

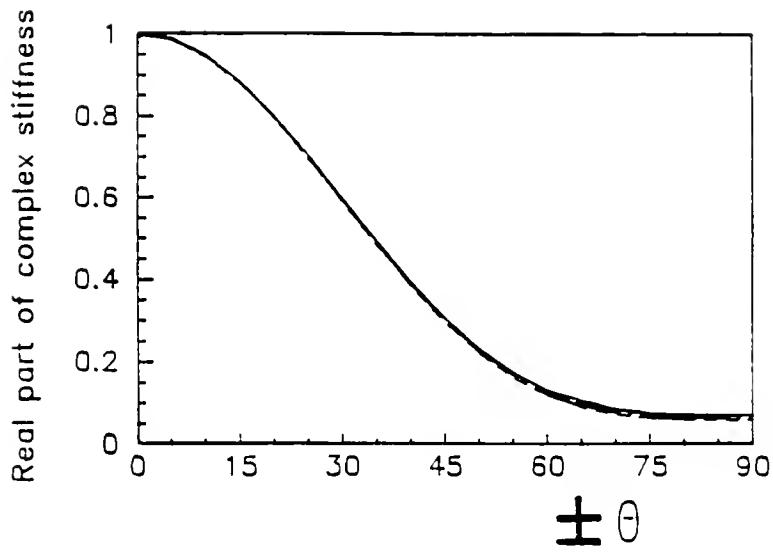


(a)

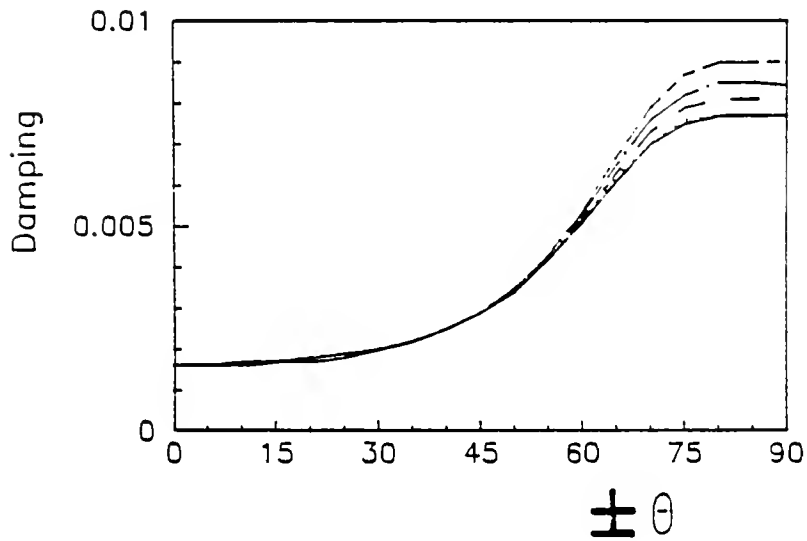


(b)

Fig. 10.7 Complex bending stiffness D_{66}^* of Glass/Epoxy.
 a) Non-dimensional Real part; b) corresponding damping.

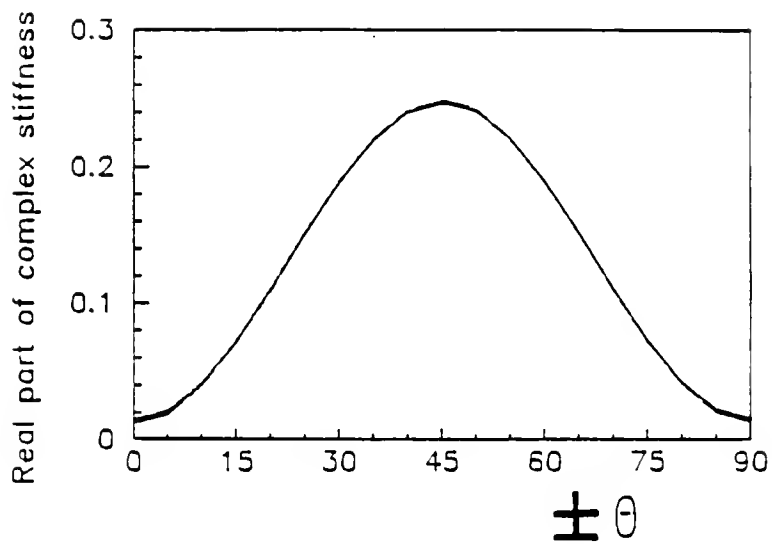


(a)

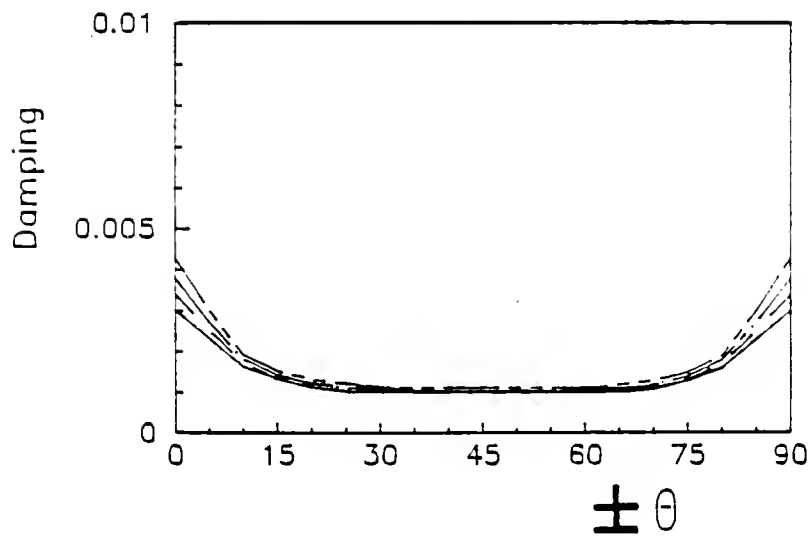


(b)

Fig. 10.8 Complex in-plane stiffness A_{11}^* of Graphite/Epoxy. a) Non-dimensional Real part; b) corresponding damping.

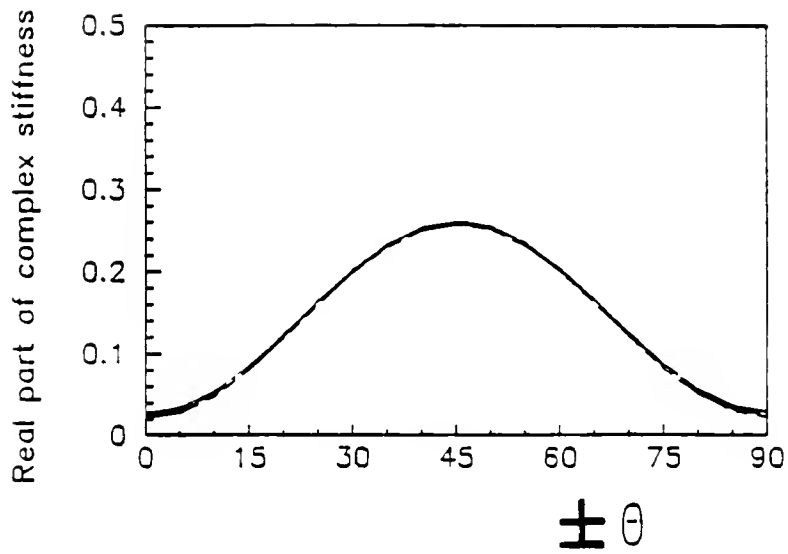


(a)

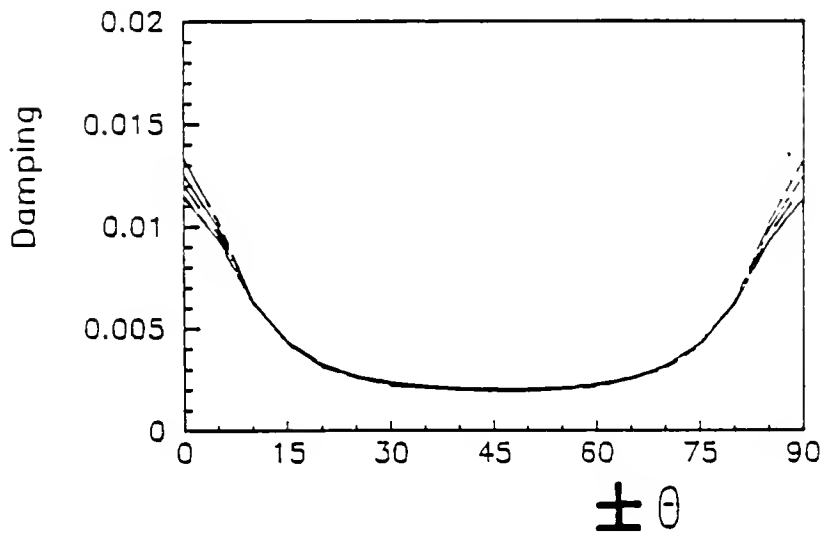


(b)

Fig. 10.9 Complex in-plane stiffness A_{12}^* of Graphite/Epoxy. a) Non-dimensional Real part; b) corresponding damping.

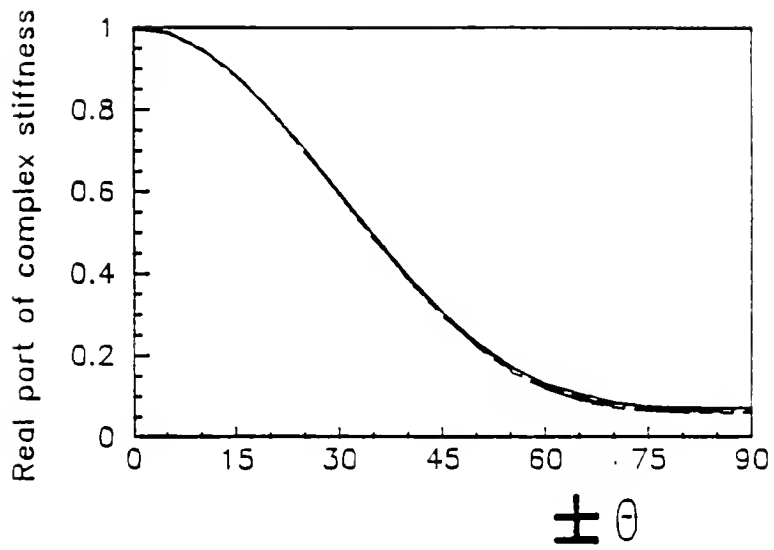


(a)

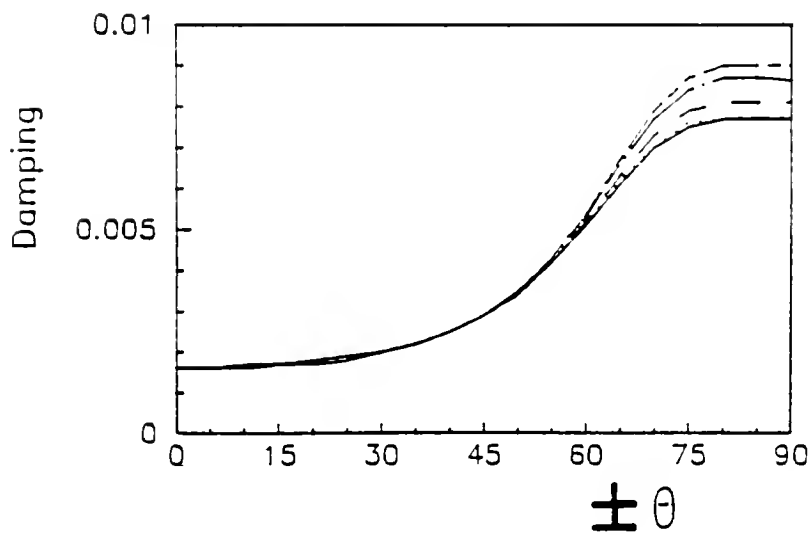


(b)

Fig. 10.10 Complex in-plane stiffness A_{66}^* of Graphite/Epoxy. a) Non-dimensional Real part; b) corresponding damping.

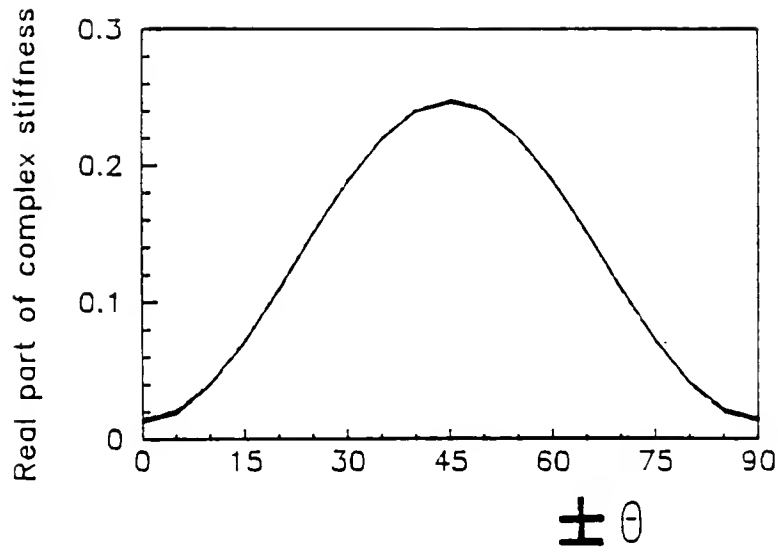


(a)

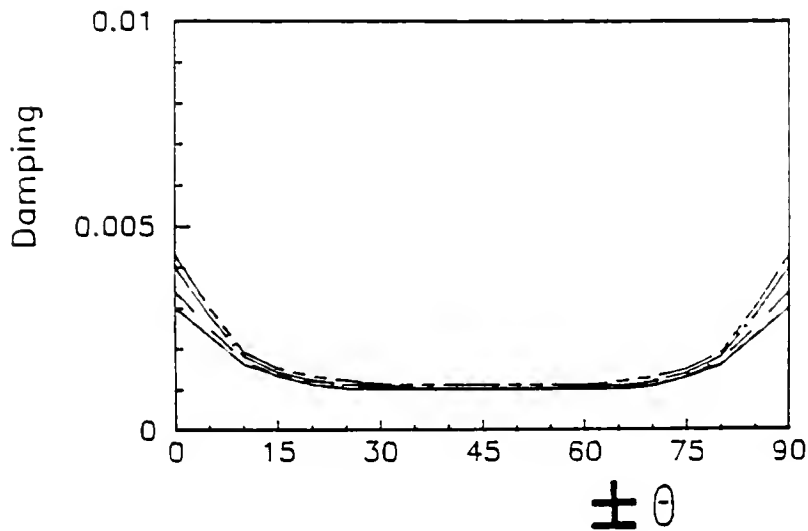


(b)

Fig. 10.11 Complex bending stiffness D_{11}^* of Graphite/Epoxy. a) Non-dimensional Real part; b) corresponding damping.

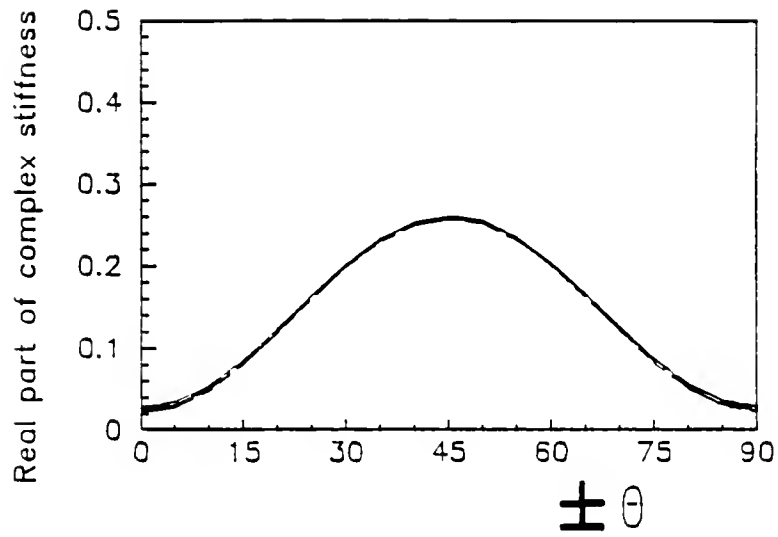


(a)

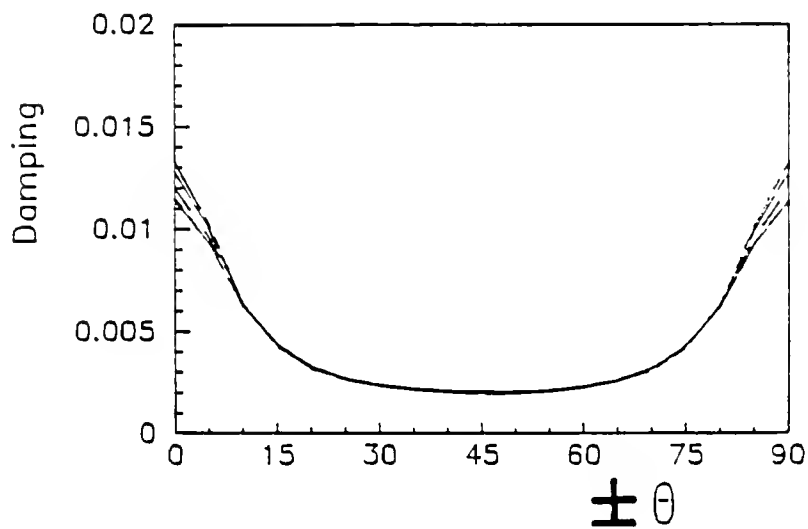


(b)

Fig. 10.12 Complex bending stiffness D_{12}^* of Graphite/Epoxy. a) Non-dimensional Real part; b) corresponding damping.



(a)



(b)

Fig. 10.13 Complex bending stiffness D_{66}^* of Graphite/Epoxy. a) Non-dimensional Real part; b) corresponding damping.

CHAPTER 11 CONCLUSION

Theoretical and experimental methods have been incorporated in order to determine the effects of temperature and absorbed moisture on the complex moduli of composite materials. The effects of hygrothermal loadings and of the changes of the complex moduli on the stress field and on the structural damping of composite laminates are also analyzed.

The Fickian theory of mass diffusion has been used for analyzing the diffusion of moisture. The Fickian diffusion is adequate for the experimental determination of moisture diffusion through unstressed test specimens. Therefore, theories that incorporate the coupling of moisture diffusion with stress, viscoelastic relaxation, entropy inequality, etc. [43-45], have not been included.

The complex moduli of unidirectional composites are expressed in terms of the constituent material properties in Chapter 3 by using the following steps:

- first, the elastic moduli of unidirectional composites in terms of the fibers and epoxy properties are

obtained by using the rule of mixture and the Halpin-Tsai equations,

- then, the correspondence principle is applied to determine the complex moduli.

Equations (3.20) show that in order to determine the hygrothermal effects on the complex moduli of composites, the effects on eight distinct parameters need to be assessed. But, these effects on the fibers properties are negligible. Hence, only three terms, $E'_m(T,c)$, $\eta_m(T,c)$ and $\nu'_m(T,c)$, have to be experimentally measured. The necessary test procedures are described in Chapter 6.

The complex moduli of epoxy in terms of temperature and moisture content are presented in Chapter 8. The storage moduli, E'_m , is strongly dependent on temperature and moisture content. But, η_m and ν'_m stay constant up to a moisture content $M = 4.5\%$ and a temperature $T = 80^\circ\text{C}$. More severe hygrothermal conditions could not be reached in the environmental chamber due to operating temperature limitations of the chamber and of the motion and force transducers used in the impulse hammer technique.

The experimental results of the epoxy properties in combination with the micromechanics formulas of Chapter 3 are used to determine the hygrothermal effects on the complex moduli of unidirectional Glass/Epoxy and Graphite/Epoxy laminates. It is shown that only the matrix

dominated terms (E'_{22} and G'_{12}) are strongly affected by temperature and/or moisture.

Hygrothermal conditions and changes in the complex moduli influence the stress field and the structural damping of laminated composites.

The stresses induced by hygrothermal conditions in Glass/Epoxy and Graphite/Epoxy cross-ply laminates are illustrated in Chapter 9. The $[(90/0)_2]_S$ lay-ups are chosen since they display the highest hygroscopic stresses. The induced stresses in the 90° layers are of the same order of magnitude as the strengths. Hence, high loadings induced by temperature and moisture content can lead to failure.

The complex stiffnesses and structural damping of $[(\pm\theta)_2]_S$ Glass/Epoxy and Graphite/Epoxy laminates are analyzed in Chapter 10. These results display the same general trend as those of the complex moduli of unidirectional composites. That is, only the matrix dominated terms are strongly affected by moisture and/or temperature.

The important conclusions of this investigations are:

- hygrothermal effects are very significant for the matrix dominated properties only;
- for certain laminates, severe hygrothermal stresses alone can lead to failure. Therefore, hygrothermal effects need to be taken into account when designing composite structures that are subjected to moisture and/or temperature.

Recommendations and additional remarks that arose from this investigation are listed below.

- The results and conclusions could vary among different material systems. Hence, it might be necessary to repeat the tests and the methodology for different materials.

- The experimental results are valid up to a 80°C temperature and a 4.5% moisture content. In order to determine the properties of epoxy through a wider range of temperature (from - 50°C to 200°C) and moisture content, an environmental chamber and transducers that can operate under more severe hygrothermal conditions need to be used.

APPENDIX A
COMPLEX STIFFNESSES OF COMPOSITES

A.1 Elastic Stiffnesses

The in-plane, coupling and bending stiffnesses of a general laminated elastic composite plate (Figure A.1) are given by

$$\begin{aligned} A_{ij} &= \int_{-h/2}^{+h/2} \bar{Q}_{ij} \, dz \\ B_{ij} &= \int_{-h/2}^{+h/2} z \bar{Q}_{ij} \, dz \\ D_{ij} &= \int_{-h/2}^{+h/2} z^2 \bar{Q}_{ij} \, dz \end{aligned} \tag{A.1}$$

where the components of the transformed matrix

$$[\bar{Q}] = \begin{bmatrix} \bar{Q}_{11} & \bar{Q}_{12} & \bar{Q}_{16} \\ \bar{Q}_{12} & \bar{Q}_{22} & \bar{Q}_{26} \\ \bar{Q}_{16} & \bar{Q}_{26} & \bar{Q}_{66} \end{bmatrix} \tag{A.2}$$

are given by

$$\begin{aligned}
 \bar{Q}_{11} &= Q_{11}m^4 + 2(Q_{12} + 2Q_{66})m^2n^2 + Q_{22}n^4 \\
 \bar{Q}_{12} &= (Q_{11} + Q_{22} - 4Q_{66})m^2n^2 + Q_{12}(m^4 + n^4) \\
 \bar{Q}_{22} &= Q_{11}n^4 + 2(Q_{12} + 2Q_{66})m^2n^2 + Q_{22}m^4 \\
 \bar{Q}_{16} &= (Q_{11} - Q_{12})m^3n + (Q_{12} - Q_{22})mn^3 + 2Q_{66}(m^2 - n^2)mn \\
 Q_{26} &= (Q_{11} - Q_{12})mn^3 + (Q_{12} - Q_{22})m^3n + 2Q_{66}(m^2 - n^2)mn \\
 \bar{Q}_{66} &= (Q_{11} + Q_{22} - 2Q_{12} - 2Q_{66})m^2n^2 + Q_{66}(m^4 - n^4)
 \end{aligned} \tag{A.3}$$

and

$$m = \cos \theta$$

$$n = \sin \theta$$

The angle θ represents the fibers orientation of the lamina under consideration.

The parameters Q_{ij} 's can be expressed in terms of the longitudinal (E_{11}) and transverse (E_{22}) Young modulus, the shear modulus (G_{12}) and the major Poisson's ratio (ν_{12})

$$Q_{11} = E_{11}/(1 - \nu_{12}\nu_{21})$$

$$Q_{12} = \nu_{12}E_{11}/(1 - \nu_{12}\nu_{21})$$

$$Q_{22} = E_{22}/(1 - \nu_{12}\nu_{21}) \quad (A.4)$$

$$Q_{66} = G_{12}$$

$$\nu_{21} = \nu_{12}E_{22}/E_{11}$$

The parameters E_{11} , E_{22} , G_{12} and ν_{12} are obtained as functions of the properties of the constituent materials (fibers and matrix) by using Eqs. (3.5)-(3.10).

A.2 Complex Stiffnesses

The laminate complex stiffnesses are determined by carrying the following steps

i) The elastic-viscoelastic correspondence principle is applied to Eqs. (3.5)-(3.10)

ii) The resulting complex values replace their corresponding elastic modulus in Eqs. (A.4)

iii) Consequently, the complex stiffnesses Q_{ij}^* 's are obtained and substituted for their corresponding elastic stiffnesses in Eqs. (A.3)

iv) Finally, the complex transformed stiffnesses Q_{ij}^* 's are substituted in Eqs. (5.1).

This procedure is easily executed with a FORTRAN program.

APPENDIX B DEVELOPMENT OF THE FINITE ELEMENT METHOD

The finite element displacement method used to derive the stress field in the cases of Chapter 9 is presented in this Appendix. The F.E.M presented below is used only to give a first approximation of the hygrothermal stress magnitudes in laminated composites. In order to obtain more accurate results, another method that takes into account the zero-stress boundary conditions on the free surfaces should be applied.

B.1 Equilibrium Equations

The stress-strain relation of a linear elastic solid continuum undergoing any type of loading can be written in the form

$$\{\sigma\} = [D](\{\epsilon\} - \{\epsilon^0\}) + \{\sigma^0\} \quad (B.1)$$

where $[D]$ is the elasticity matrix, $\{\epsilon\}$ is the strain vector, $\{\epsilon^0\}$ is the hygrothermal and/or initial strain vector, $\{\sigma^0\}$ is any initial stress vector.

In this method, it is assumed that the displacements have unknown values only at the nodal points. The displacements are

$$\{\delta\} = [N]\{\delta^e\} = \sum_{i=1}^n [N_i]\{\delta_i\} \quad (\text{B.2})$$

where

$$[N] = [N_1, N_2, \dots, N_n]$$

$$[N_i] = N_i[I]$$

and n is the number of variables per node and $[I]$ is the identity matrix.

The strains in terms of the displacements are given by the following expression

$$\begin{aligned} \{\epsilon\} &= \begin{Bmatrix} \epsilon_y \\ \epsilon_z \\ \gamma_{yz} \end{Bmatrix} = \begin{Bmatrix} \frac{\partial v}{\partial y} \\ \frac{\partial w}{\partial z} \\ \frac{\partial v}{\partial z} + \frac{\partial w}{\partial y} \end{Bmatrix} \\ &= [B]\{\delta^e\} = \sum_{i=1}^n [B_i]\{\delta_i\} \end{aligned} \quad (\text{B.3})$$

where the strain matrix is defined as

$$[B_i] = \begin{bmatrix} \frac{\partial N_i}{\partial y} & 0 \\ 0 & \frac{\partial N_i}{\partial z} \\ \frac{\partial N_i}{\partial z} & \frac{\partial N_i}{\partial y} \end{bmatrix} \quad (B.4)$$

The set of functions N_i are called the shape functions and are subsequently defined.

The continuum is subdivided into a finite number of elements. Consider an element that is acted upon by nodal forces $\{F^e\}$ and body forces $\{p\}$. Then, application of the virtual work principle to an element e yields

$$[\delta^e]^T \{F^e\} + \int_{V_e} [\delta]^T \{p\} dV = \int_{V_e} [\epsilon]^T \{\sigma\} dV \quad (B.5)$$

Substitution of Eqs. (B.1)-(B.4) into Eq. (B.5) results in

$$\begin{aligned} \{F^e\} + \int_{V_e} [N]^T \{p\} dV &= \left[\int_{V_e} [B]^T [D] [B] dV \right] \{\delta^e\} \\ &\quad - \int_{V_e} [B]^T [D] \{\epsilon^0\} dV + \int_{V_e} [B]^T \{\sigma^0\} dV \end{aligned} \quad (B.6)$$

or

$$\{F^e\} + \{F_p^e\} + \{F_{\epsilon^0}^e\} + \{F_{\sigma^0}^e\} = [K^e] \{\delta^e\} \quad (B.7a)$$

where

$$[K^e] = \int_{V_e} [B]^T [D] [B] dV = \text{element stiffness matrix}$$

$$\{F_p^e\} = \int_{V_e} [N]^T \{p\} dV = \text{equivalent nodal body force}$$

$$\{F_{\epsilon_o}^e\} = \int_{V_e} [B]^T [D] \{\epsilon^o\} dV = \text{hygrothermal or initial strain loading}$$

$$\{F_{\sigma_o}\} = - \int_{V_e} [B]^T \{\sigma\} dV = \text{initial stress loading}$$

These equations are valid for one element only. For the complete structure, Eq. (B.6) should be summed over all elements. It is noted that if an element is subjected to surface traction forces, $\{t\}$, then the additional equivalent nodal force

$$\{F_t^e\} = \int_{S_e} [N]^T \{t\} dS \quad (B.7b)$$

should be added to the left hand side of Eq. (B.7a)

B.2 Program Organization

Hinton and Owen [42] have developed a detailed F.E.M. code to solve isotropic beam, plane stress/strain and plate bending problems. Their procedure for the plane stress/strain has been modified so that it is adapted to

composite laminates that have nonconstant material properties and undergo thermal and moisture induced expansion.

The F.E.M. operations are performed by modular subroutines. The general organization of these programs is shown in Figure B.1.

B.3 Shape Functions, Jacobian and Strain Matrix

Eight node isoparametric elements are used in the F.E.M. code. In this case, the shape functions are used to approximate both the geometry and the displacement field. The coordinates of any point of the element shown in Figure B.2 are

$$y(\xi, \eta) = \sum_{i=1}^8 N_i(\xi, \eta) y_i \quad (B.8)$$

$$z(\xi, \eta) = \sum_{i=1}^8 N_i(\xi, \eta) z_i$$

where (y_i, z_i) are the coordinates of the node i and the quadratic shape functions are defined as

$$N_1 = - (1 - \xi)(1 - \eta)(1 + \xi + \eta)/4$$

$$N_2 = (1 - \xi^2)(1 - \eta)/2$$

$$N_3 = (1 + \xi)(1 - \eta)(\xi - \eta - 1)/4$$

$$N_4 = (1 + \xi)(1 - \eta^2)/2 \quad (\text{B.9})$$

$$N_5 = (1 + \xi)(1 + \eta)(\xi + \eta - 1)/4$$

$$N_6 = (1 - \xi^2)(1 + \eta)/2$$

$$N_7 = (1 - \xi)(1 + \eta)(-\xi + \eta - 1)/4$$

$$N_8 = (1 - \xi)(1 - \eta^2)/2$$

The direction of the local curvilinear coordinates ξ and η are given in Figure B.2. The displacements at any point are expressed as

$$v(\xi, \eta) = \sum_{i=1}^8 N_i(\xi, \eta) v_i \quad (\text{B.10})$$

$$w(\xi, \eta) = \sum_{i=1}^8 N_i(\xi, \eta) w_i$$

The Jacobian matrix $[J(\xi, \eta)]$ is necessary to derive the elemental volume dV , and area dS . It is defined as follows

$$[J] = \begin{bmatrix} \frac{\partial y}{\partial \xi} & \frac{\partial z}{\partial \xi} \\ \frac{\partial y}{\partial \eta} & \frac{\partial z}{\partial \eta} \end{bmatrix} = \sum_{i=1}^8 \begin{bmatrix} \frac{\partial N_i}{\partial \xi} y_i & \frac{\partial N_i}{\partial \xi} z_i \\ \frac{\partial N_i}{\partial \eta} y_i & \frac{\partial N_i}{\partial \eta} z_i \end{bmatrix} \quad (B.11)$$

Then the elemental area dS is given by

$$dS = dy \, dz = \det[J] \, d\xi \, d\eta$$

Once the shape functions are chosen, the strains can be written in terms of N_i and δ_i (Eq. (B.3)).

B.4 Elasticity Matrix

The stress-strain relation of an orthotropic lamina is given by

$$\begin{Bmatrix} \sigma_x \\ \sigma_y \\ \sigma_z \\ \sigma_{yz} \\ \sigma_{xz} \\ \sigma_{xy} \end{Bmatrix} = \begin{bmatrix} \bar{Q}_{11} & \bar{Q}_{12} & \bar{Q}_{13} & 0 & 0 & \bar{Q}_{16} \\ \bar{Q}_{12} & \bar{Q}_{22} & \bar{Q}_{23} & 0 & 0 & \bar{Q}_{26} \\ \bar{Q}_{13} & \bar{Q}_{23} & \bar{Q}_{33} & 0 & 0 & \bar{Q}_{36} \\ 0 & 0 & 0 & \bar{Q}_{44} & \bar{Q}_{45} & 0 \\ 0 & 0 & 0 & \bar{Q}_{45} & \bar{Q}_{55} & 0 \\ \bar{Q}_{16} & \bar{Q}_{26} & \bar{Q}_{36} & 0 & 0 & \bar{Q}_{66} \end{bmatrix} \cdot \begin{Bmatrix} \epsilon_x - \alpha_x \Delta T - \beta_x c \\ \epsilon_y - \alpha_y \Delta T - \beta_y c \\ \epsilon_z - \alpha_z \Delta T - \beta_z c \\ \gamma_{yz} \\ \gamma_{xz} \\ \gamma_{xy} - \alpha_{xy} \Delta T - \beta_{xy} c \end{Bmatrix} \quad (B.12)$$

where the transformed stiffnesses that have not been defined in Appendix A are expressed as

$$\bar{Q}_{13} = Q_{13}m^2 + Q_{23}n^2$$

$$\bar{Q}_{23} = Q_{13}n^2 + Q_{23}m^2$$

$$\bar{Q}_{33} = Q_{33} \quad (\text{B.13})$$

$$\bar{Q}_{36} = (Q_{13} - Q_{23})mn$$

$$\bar{Q}_{44} = G_{23}m^2 + G_{12}n^2$$

$$\bar{Q}_{45} = (G_{12} - G_{23})mn$$

$$\bar{Q}_{55} = G_{12}m^2 + G_{23}n^2$$

The stiffnesses Q_{ij} 's are

$$Q_{13} = \nu_{21}(1 + \nu_{12})E_{11}/Q$$

$$Q_{23} = \nu_{12}(1 + \nu_{21})E_{22}/Q$$

$$Q_{33} = (1 - \nu_{12}\nu_{21})E_{22}/Q$$

$$Q = 1 - 2\nu_{12}\nu_{21}(1 + 2\nu_{23}) - \nu_{23}^2$$

where

$$\frac{1}{G_{23}} = \frac{1}{v_f + \eta_4 v_m} \left[\frac{v_f}{G_{f12}} + \eta_4 \frac{v_m}{G_m} \right]$$

$$\eta_4 = \frac{3 - 4v_m + G_m/G_{12}}{4(1 - v_m)}$$

$$v_{23} = v_m$$

For the case of Chapter 9, Eq. (B.12) can be reduced to

$$\{\sigma\} = \begin{Bmatrix} \sigma_y \\ \sigma_z \\ \sigma_{yz} \end{Bmatrix} = \begin{bmatrix} \bar{Q}_{22} & \bar{Q}_{23} & 0 \\ \bar{Q}_{23} & \bar{Q}_{33} & 0 \\ 0 & 0 & \bar{Q}_{44} \end{bmatrix} \begin{Bmatrix} \epsilon_y \\ \epsilon_z \\ \gamma_{yz} \end{Bmatrix} - \begin{bmatrix} \bar{Q}_{12} & \bar{Q}_{22} & \bar{Q}_{23} & \bar{Q}_{26} \\ \bar{Q}_{13} & \bar{Q}_{23} & \bar{Q}_{33} & \bar{Q}_{36} \\ 0 & 0 & 0 & 0 \end{bmatrix} \begin{Bmatrix} \alpha_x \Delta T + \beta_x c \\ \alpha_y \Delta T + \beta_y c \\ \alpha_z \Delta T + \beta_z c \\ \alpha_{xy} \Delta T + \beta_{xy} c \end{Bmatrix} \quad (B.15)$$

or

$$\{\sigma\} = [D_1]\{\epsilon\} - [D_2]\{\epsilon^0\}$$

The last equation is a reduced form of Eq. (B.1) with the initial stresses left out.

The through the thickness stress is given by

$$\begin{aligned} \sigma_x = & \bar{Q}_{11}(-\alpha_x \Delta T - \beta_x c) + \bar{Q}_{12}(\epsilon_y - \alpha_y \Delta T - \beta_y c) \\ & + \bar{Q}_{13}(\epsilon_z - \alpha_z \Delta T - \beta_z c) + \bar{Q}_{16}(-\alpha_{xy} \Delta T - \beta_{xy} c) \quad (B.16) \end{aligned}$$

B.5 Element Stiffness Matrix

A submatrix of the element stiffness matrix $[K^e]$ linking nodes i and j is evaluated from the expression

$$[K^e]_{ij} = \int_{-1}^{+1} \int_{-1}^{+1} [B_i]^T [D] [B_j] t \det[J] d\xi d\eta \quad (B.17)$$

where t is the thickness of the element under consideration. The integration is done by using a 3-point Gauss integration rule.

B.6 Equivalent Nodal Loadings

B.6.1 Element Edge loadings

An element edge might have both tangential and normal distributed load per unit length. Every edge of the isoparametric element has three nodal points. The values of the normal and tangential loads at each nodal point are called $(p_n)_i$ and $(p_t)_i$. Then, the distributed loads at any point along the edge are given by

$$\begin{Bmatrix} p_n \\ p_t \end{Bmatrix} = \sum_{i=1}^3 N_i \begin{Bmatrix} (p_n)_i \\ (p_t)_i \end{Bmatrix} \quad (B.18)$$

It can be shown that the equivalent nodal forces are expressed as

$$P_{y_i} = \int_{S_e} N_i (p_t \frac{\partial y}{\partial \xi} - p_n \frac{\partial z}{\partial \xi}) d\xi$$

$$P_{z_i} = \int_{S_e} N_i (p_n \frac{\partial y}{\partial \xi} + p_t \frac{\partial z}{\partial \xi}) d\xi$$
(B.19)

if the loads are applied on an edge parallel to the curvilinear coordinate ξ . The Gaussian numerical integration is used to derive Eqs. (B.19) which are a form of Eq. (B.7b).

B.6.2 Hygrothermal Loadings

The equivalent nodal loadings due to hygrothermal strains are given in matrix form as

$$\begin{Bmatrix} F_{y_i} \\ F_{z_i} \end{Bmatrix} = \int_{V_e} [B_i]^T ([D_2] \{\epsilon^0\}) dv$$
(B.20)

where the matrices $[D_2]$ and $\{\epsilon^0\}$ are defined in Eq. (B.15).

B.7 Element Displacements and Stresses

The global stiffness matrix as well as the equivalent nodal loading matrix are assembled. Then, the displacements are computed by a frontal solution method. Once the displacements are known, the strains and the stresses can be deduced

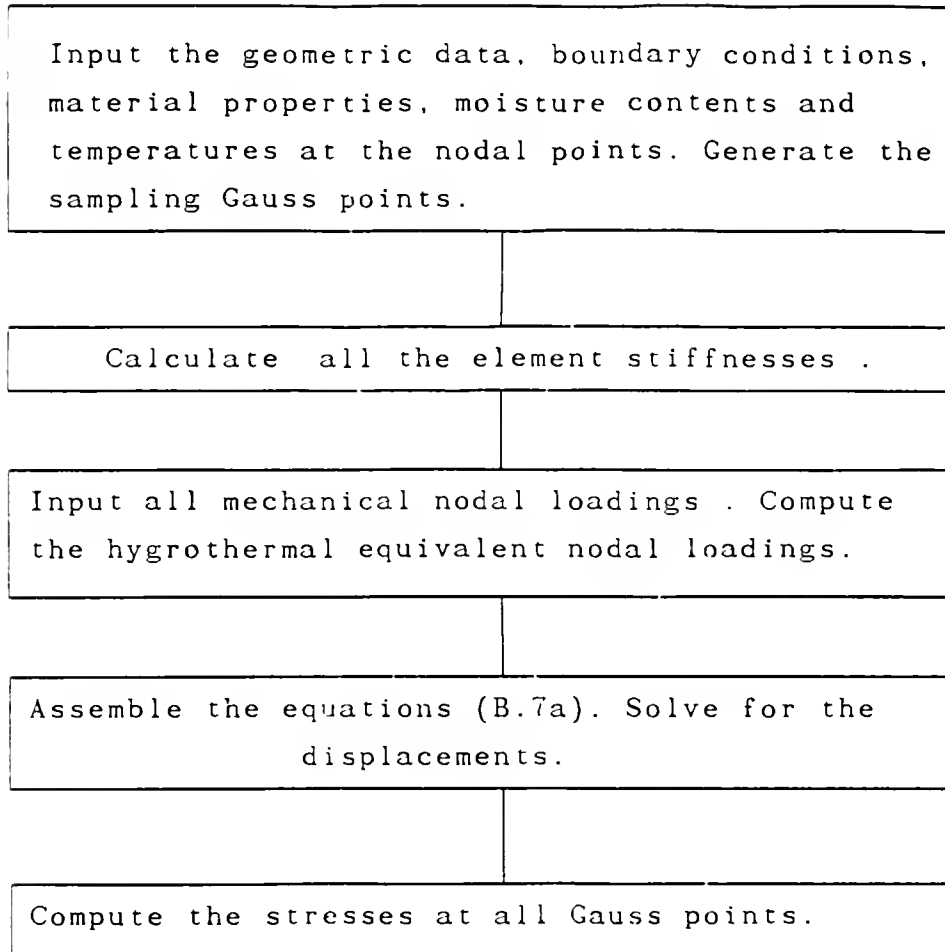


Fig. B.1 Organization of the F.E.M. program.

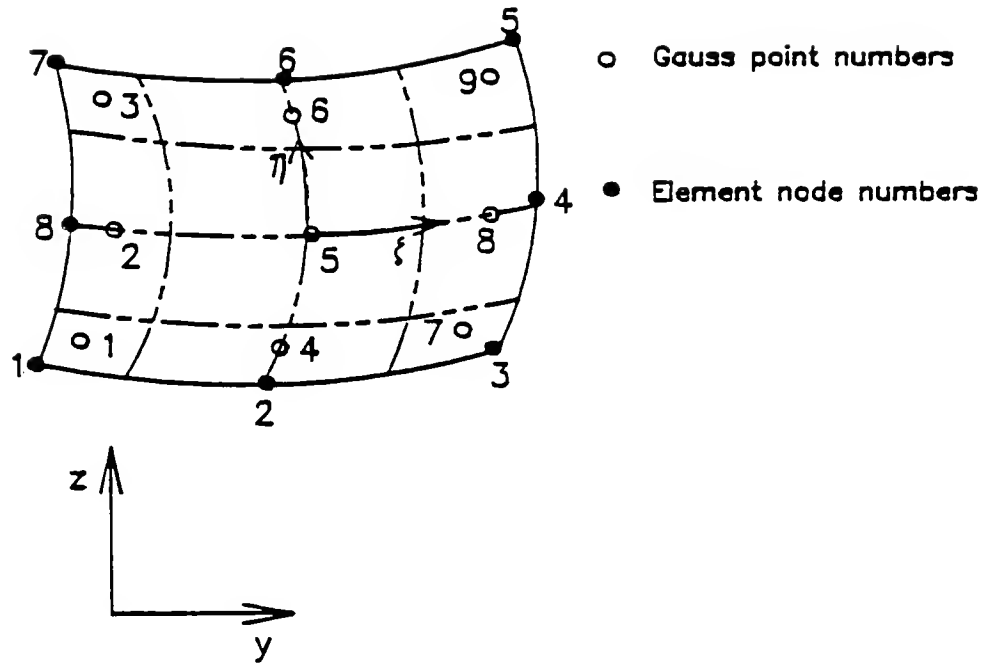


Fig. B.2 Local axes ξ and η , Gauss point numbers and local node numbers of an eight-point isoparametric element.

REFERENCES

1. Broutman, L. J. and Krock, R. H., COMPOSITE MATERIALS, Vols. 1-8, Academic Press, New York, 1974.
2. Jones, R. M., MECHANICS OF COMPOSITE MATERIALS, McGraw-Hill Book Company, Washington, D. C., 1975.
3. Fried, N., "Degradation of Composite Materials: The effects of water on Glass-Reinforced Plastics," in MECHANICS OF COMPOSITES, Proceedings of the 5th symposium on Naval Structural Mechanics, Pergamon Press, Philadelphia, Pennsylvania, 1967, p. 813-837
4. Shen, C.-H. and Springer, G. S., "Moisture Absorption and Desorption of Composite Materials," Journal of Composite Materials, Vol. 10, January 1976, p. 2-20.
5. Whitney, J. M., "Moisture Diffusion in Fiber Reinforced Composites," Proceedings of the 1978 International Conference on Composite Materials, Toronto, Canada, 1978, p. 1584-1601.
6. DeIasi, R. and Whiteside, J. B., "Effects of Moisture on Epoxy Resins and Composites," ASTM-STP 658, 1978, p. 2-20.
7. Shirrel, C. D., "Diffusion of Water vapor in Graphite/Epoxy Composites," ASTM-STP 658, 1978, p. 21-42.
8. Whitney, J. M. and Browning, C. E., "Some Anomalies Associated with Moisture Diffusion in Epoxy Matrix Composite Materials," ASTM-STP 658, 1978, p. 43-60.
9. Blikstad, M., Sjoblom, P. O. W., and Johannesson, T. R., "Long-Term Moisture Absorptin in Graphite/Epoxy AnglePly Laminates," Journal of Composite Materials, Vol. 18, January 1984, p. 32-46.
10. Springer, G. S., ENVIRONMENTAL EFFECTS ON COMPOSITE MATERIALS, Technomic Publishing Company, Westport, Connecticut, 1981.
11. Springer, G. S. "Environmental Effects on Epoxy Matrix Composites," ASTM-STP 674, 1979, p. 291-312.

12. Shen, C.-H and Springer, G. S., "Environmental Effects on the Elastic Moduli of Composite Materials," Journal of Composite Materials, Vol. 11, July 1977, p. 250-264.
13. Shen, C.-H. and Springer, G. S., "Effects of moisture and Temperature on the Tensile Strength of Composite Materials," Journal of Composite Materials, Vol. 11, January 1977, p. 2-16.
14. Lee, B. L., Lewis, R. W. and Sacher, R. E., "Environmental Effects on the Mechanical Properties of GlassFiber/Epoxy Resin," Proceedings of the 1978 International Conference on Composite Materials, Toronto, Canada, 1978, p. 1560-1583.
15. Phillips, D. C., Scott, J. M. and Buckley, N., "The Effects of Moisture on the Shear Fatigue of Fibre Composites," Proceedings of the 1978 International Conference on Composite Materials, 1978, Toronto, Canada, p. 1544-1559.
16. Watanabe, M, "Effects of Water Environment on Fatigue Behavior of Fiberglass Reinforced Plastics," ASTM-STP 674, 1979, p. 345-367.
17. Chamis, C. C. and Sinclair J. H., "Durability/Life of Fiber Composites in Hygrothermal Environments," ASTM-STP 787, 1982, p. 498-367.
18. Browning, C. E., "The Mechanisms of Elevated Temperature Property Losses in High Performance Structural Epoxy Resin Matrix Materials After Exposure to High Humidity Environments," Proceedings of the 1978 International Conference on Composite Materials, Toronto, Canada, 1978, p. 1527-1543.
19. Crossman, F. W., Mauri, R. E. and Warren, W. J., "Moisture Altered Viscoelastic Response of Graphite/Epoxy Composites," ASTM-STP 658, 1978, p. 105-220.
20. Flaggs, D. L. and Crossman, F. W., "Analysis of the Viscoelastic Response of Composite of Composite Laminates During Hygrothermal Exposure," Journal of Composite Materials, Vol. 15, January 1981, p. 21-39.
21. Hahn, H. T. and Kim, R. Y., "Swelling of Composite laminates," ASTM-STP 658, 1978, p. 98-120.

22. Maymon, G., Briley, R. P. and Rehfield, L. W., "Influence of Moisture Absorption and Elevated Temperature on the Dynamic Behavior of Resin Matrix Composites: Preliminary Results," ASTM-STP 658, 1978, p. 221-233.
23. Carter, H. G., Kiber, K. G. and Reynolds, J. D., "Fundamental and Operational Glass Temperature of Composite Resins and Adhesives," ASTM-STP 658, 1978, p. 84-97.
24. Crank, J., THE MATHEMATICS OF DIFFUSION, Oxford University Press, Oxford, 1957.
25. Jost, W., DIFFUSION IN SOLIDS, LIQUIDS, GASES, Academic Press, New York, 1952.
26. Hahn, H. T., "Hygrothermal Damage in Graphite/Epoxy Laminates," presented at the ASME, Winter Annual Meeting, Miami Beach, Fl., November 16-21, 1985.
27. Hashin, Z., "Complex Moduli of Viscoelastic Composites -I. General Theory and Application to Particulate Composites," International Journal of Solids and Structures, Vol. 6, 1970, p. 539-552.
28. Gibson, R. F. and Plunkett, R., "Dynamic Behavior of Fiber Reinforced Composites: Measurement and Analysis," Journal of Composite Materials, Vol. 10, 1976, p. 325-341.
29. Hashin, Z., "Complex Moduli of Viscoelastic Composites -II. Fiber Reinforced Materials," International Journal of Solids and Structures, Vol. 6, 1970, p. 797-807.
30. Nashif, Z. D., Jones, D. I. G. and Henderson, J. P., VIBRATION DAMPING, John Wiley and Sons, New York, 1985.
31. Whitney, J. M., Browning, C. E. and Mair, A., "Analysis of the Flexure Test for Laminated Composite Materials," ASTM-STP 546, 1974, p. 30-45.
32. Halvorsen, W. G. and Brown, D. L., "Impulse Technique for Structural Frequency Response Testing," Sound and Vibration, November 1977, p. 8-20.
33. Thomson, W. T., THEORY OF VIBRATION WITH APPLICATIONS, Prentice-Hall, Englewood Cliff, New Jersey, 1981.

34. Lee, B. T., "Measurements of Damping for Nondestructively Assessing the Integrity of Fiber Reinforced Composites," Ph.D. dissertation, University of Florida, 1985.
35. Whitney, J. M., Daniel, I. M. and Pipes, R. B., EXPERIMENTAL MECHANICS OF FIBER REINFORCED COMPOSITES MATERIALS, Prentice-Hall, 1982.
36. Tsai, S. W. and Hahn, H. T., INTRODUCTION TO COMPOSITE MATERIALS, Technomic, Westport, Connecticut, 1980.
37. Lo, S. Y. and Hahn, H. T., "Swelling of Kevlar49/Epoxy and S2-Glass/Epoxy Composites," Proceedings of the 4th International Conference on Composite Materials, T. Hayashi, Ed., Tokyo, 1982, p. 987.
38. Putter, S., Buchanan, D. L. and Rehfield, L. W., "Influence of Frequency and Environmental Conditions on Dynamic Behavior of Graphite/Epoxy Composites," ASTM-STP 787, 1982, p. 414-424.
39. Malvern, L. E., INTRODUCTION TO THE MECHANICS OF A CONTINUOUS MEDIUM, Prentice-Hall, Englewood Cliff, New Jersey, 1969.
40. McKague, L., "Environmental Synergism and Simulation in Resin Matrix Composites," ASTM-STP 658, J. R. Vinson, Ed., 1978, p. 193-204.
41. Aklonis, J. J., MacKnight, W. J. and Shen, M., INTRODUCTION TO POLYMER VISCOELASTICITY, John Wiley & Sons, New York, 1972.
42. Hinton, E. and Owen, D. R. J., FINITE ELEMENT PROGRAMMING, Academic Press, London, 1977.
43. Aifantis, E. C. and Gerberich, W. W., "Gaseous Diffusion in a stressed-Thermoelastic Solid. I: The Thermomechanical Formulation," Acta Mechanica 28, 1977, p. 1-24.
44. Nowacki, W., "Certain Problems of Thermodiffusion in Solids," Archives of Mechanics 23, 6, 1971, p. 731-755.
45. Weitsman, Y., "Coupling of Moisture and Damage in Composites," in TWELFTH ANNUAL MECHANICS OF COMPOSITES REVIEW, Mueller, D. C., Ed., Bal Harbour, Florida, October 1987, p 50-57.

BIOGRAPHICAL SKETCH

Hacene Bouadi was born in Algeria in August 12, 1954. After graduating from high school in 1972, he attended the Ecole Polytechnique d'Alger (Polytechnic Institute of Algiers). He obtained a bachelor's degree in mechanical engineering in 1977.

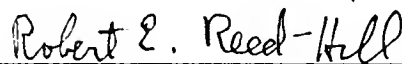
He was awarded a graduate scholarship by the Algerian Government which allowed him to obtain a Master of Science degree in 1979 and the Degree of Engineer in 1982 from the Aeronautics and Astronautics Department of Stanford University. Thereafter, he continued his studies toward the doctorate degree at the University of Florida. He completed his Ph.D. in December 1987 in the field of aerospace engineering.

I certify that I have read this study and that in my opinion it conforms to acceptable standards of scholarly presentation and is fully adequate, in scope and quality, as a dissertation for the degree of Doctor of Philosophy.



Charles E. Taylor
Professor of Engineering Sciences

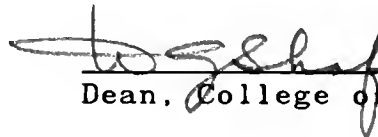
I certify that I have read this study and that in my opinion it conforms to acceptable standards of scholarly presentation and is fully adequate, in scope and quality, as a dissertation for the degree of Doctor of Philosophy.



Robert E. Reed-Hill
Professor Emeritus of Material
Sciences and Engineering

This dissertation was submitted to the Graduate Faculty of the College of Engineering and to the Graduate School and was accepted as partial fulfillment of the requirements for the degree of Doctor of Philosophy.

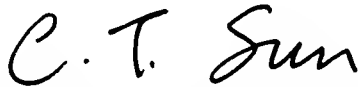
April 1988



Dean, College of Engineering

Dean, Graduate School

I certify that I have read this study and that in my opinion it conforms to acceptable standards of scholarly presentation and is fully adequate, in scope and quality, as a dissertation for the degree of Doctor of Philosophy.



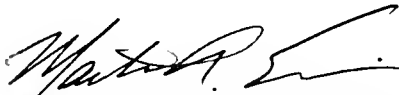
Chang-T. Sun, Chairman
Professor of Engineering Sciences

I certify that I have read this study and that in my opinion it conforms to acceptable standards of scholarly presentation and is fully adequate, in scope and quality, as a dissertation for the degree of Doctor of Philosophy.



Lawrence E. Malvern
Professor of Engineering Sciences

I certify that I have read this study and that in my opinion it conforms to acceptable standards of scholarly presentation and is fully adequate, in scope and quality, as a dissertation for the degree of Doctor of Philosophy.



Martin A. Eisenberg
Professor of Engineering Sciences

UNIVERSITY OF FLORIDA



3 1262 08556 7880